Doctoral Thesis

Morphological and Topochemical Study on Woody Biomass Treated with Ionic Liquid

by

Toru KANBAYASHI

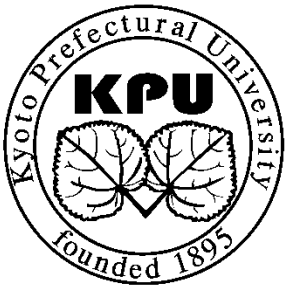

Laboratory of Forest Resource Circulatory System
Division of Environmental Sciences
Graduate School of Life and Environmental Sciences
Kyoto Prefectural University

September 2016

Table of Contents

List of Publications……1

List of Abbreviations……2

List of Figures……3

List of Tables……11

CHAPTER 1 General Introduction

1.1 Preface……12

1.2 Tissue structure and chemical composition of woody biomass……12

1.2.1 Tissue structure……12

1.2.2 Chemical composition and distribution……15

1.3 Woody biomass conversion technology……17

1.4 Ionic liquid……19

1.4.1 What is ionic liquid?……19

1.4.2 Reaction behavior of woody biomass in ionic liquid……19

1.5 Objectives of this work……23

CHAPTER 2 Microscopic Study on Woody Biomass after Treatment with the Ionic Liquid, 1-Ethyl-3-methylimidazolium Chloride ([C2mim][Cl])

2.1 Introduction……25

2.2 Materials and methods……27

2.2.1 Samples and chemicals……27

2.2.2 Treatment with [C2mim][Cl] for light microscopy analysis……27

2.2.3 Treatment with [C2mim][Cl] for SEM observation……27

2.2.4 Treatment with [C2mim][Cl] for confocal Raman microscopy analysis……29

2.3 Results and discussion……30
2.3.1 Morphological changes of *Fagus crenata* treated with [C2mim][Cl]……..30
2.3.2 Comparative study on morphological changes in hardwoods treated with [C2mim][Cl]…….…….…….39
2.3.3 Raman microscopic analysis of *Cryptomeria japonica* after treatment with [C2mim][Cl]……..…….50
2.3.3.1 Point analysis…….55
2.3.3.2 Raman mapping analysis…….....61
2.3.3.3 Line analysis……..63
2.3.4 Raman microscopic analysis of *Fagus crenata* after treatment with [C2mim][Cl]……...63
2.3.4.1 Point analysis……..……...63
2.3.4.2 Raman mapping analysis……..….73
2.4 Conclusions……...75

CHAPTER 3 Microscopic Study on Woody Biomass after Treatment with the Ionic Liquid, 1-Ethylpyridinium Bromide ([EtPy][Br])

3.1 Introduction……..76
3.2 Materials and methods…….77
3.2.1 Samples and chemicals……...……..77
3.2.2 Treatment with [EtPy][Br] for light microscopy analysis……..……..77
3.2.3 Treatment with [EtPy][Br] for SEM observation……..…...78
3.2.4 Treatment with [EtPy][Br] for confocal Raman microscopy analysis……..78
3.3 Results and discussion……..…...79
3.3.1 Morphological and topochemical study on *Cryptomeria japonica* cell walls treated with [EtPy][Br]…….....79
3.3.1.1 Morphological observation using light microscopy and SEM…….….79
3.3.1.2 Topochemical analysis using confocal Raman microscopy……..84
3.3.1.2.1 Point analysis…….……..85

3.3.1.2.2 Raman mapping analysis……..91
3.3.2 Morphological and topochemical study on *Fagus crenata* cell walls treated with [EtPy][Br]……..…….……94
3.3.2.1 Morphological observation using light microscopy and SEM……..94
3.3.2.2 Topochemical analysis using confocal Raman microscopy……104
3.3.2.2.1 Point analysis…….……104
3.3.2.2.2 Raman mapping analysis……106
3.4 Conclusions……108

CHAPTER 4 Microscopic Study on Reaction Wood Treated with Ionic Liquid

4.1 Introduction……110
4.2 Materials and methods……...111
4.2.1 Samples and chemicals……...111
4.2.2 Ionic liquid treatment for light microscopy analysis……..111
4.2.3 Ionic liquid treatment for SEM observation……...112
4.2.4 Ionic liquid treatment for confocal Raman microscopy analysis……112
4.3 Results and discussion……...113
4.3.1 Effect of ionic liquid treatment on morphological and topochemical features of compression wood in *Cryptomeria japonica*……..113
4.3.1.1 Compression wood……113
4.3.1.2 Opposite wood……...122
4.3.2 Effect of ionic liquid treatment on morphological and topochemical features of tension wood in *Fagus crenata*……...……124
4.4 Conclusions……133

CHAPTER 5 General Conclusions……..134

References……136
Acknowledgements……..152

List of publications

The present study is based on the following original publications.

1. **Kanbayashi T**, Miyafuji H (2013) Morphological changes of Japanese beech treated with the ionic liquid, 1-ethyl-3-methylimidazolium chloride. Journal of Wood Science 59:410-418.
2. **Kanbayashi T**, Miyafuji H (2014) Comparative study of morphological changes in hardwoods treated with the ionic liquid, 1-ethyl-3-methylimidazolium chloride. Journal of Wood Science 60:152-159.
3. **Kanbayashi T**, Miyafuji H (2015) Raman microscopic analysis of wood after treatment with the ionic liquid, 1-ethyl-3-methylimidazolium chloride. Holzforschung 69:273-279.
4. **Kanbayashi T**, Miyafuji H (2015) Topochemical and morphological characterization of wood cell wall treated with the ionic liquid, 1-ethylpyridinium bromide. Planta 242:509-518.
5. **Kanbayashi T**, Miyafuji H (2015) Anatomical and topochemical aspects of Japanese beech (*Fagus crenata*) cell walls after treatment with the ionic liquid, 1-ethylpyridinium bromide. Microscopy and Microanalysis 21:1562-1572.
6. **Kanbayashi T**, Miyafuji H (2016) Raman microscopic study of Japanese beech (*Fagus crenata*) as treated with the ionic liquid, 1-ethyl-3-methylimidazolium chloride. Journal of Wood Chemistry and Technology 36:224-234.
7. **Kanbayashi T**, Miyafuji H (2016) Microscopic characterization of tension wood cell walls of Japanese beech (*Fagus crenata*) treated with ionic liquids. Micron 88:24-29.
8. **Kanbayashi T**, Miyafuji H (2016) Effect of ionic liquid treatment on the ultrastructural and topochemical features of compression wood in Japanese cedar (*Cryptomeria japonica*). Scientific Reports 6:30147.

List of Abbreviations

CC	Cell corner
CML	Compound middle lamella
[C2mim][Cl]	1-Ethyl-3-methylimidazolium chloride
DMSO	Dimethylsulfoxide
[EtPy][Br]	1-Ethylpyridinium bromide
P	Primary wall
S_1	Outer layer of secondary wall
S_2	Middle layer of secondary wall
S_3	Inner layer of secondary wall
SEM	Scanning electron microscopy
WF_{CC}	Cell corner of wood fiber
WF_{CML}	Compound middle lamella of wood fiber
WF_{SW}	Secondary wall of wood fiber

List of Figures

1.1 Schematic diagram of cell wall organization (Walker 1993). *M*: middle lamella, *P*: primary wall, S_1, S_2, S_3: layers of secondary wall, *W*: warty layer.…….....14

1.2 Distribution of the main chemical component in the cell wall (Panshin and Zeeuw 1970). S_1, S_2, S_3: layers of secondary wall.....16

1.3 The typical cations and anions for ionic liquids (Kanbayashi and Miyafuji 2016b). *R*: represents alkyl groups…….20

1.4 Structural formula of the ionic liquids, (a) 1-ethyl-3-methylimidazolium chloride ([C2mim][Cl]) and (b) 1-ethylpyridinium bromide ([EtPy][Br])……22

2.1 Definition of cell lumen area, cell wall area and total of cell lumen area + cell wall area……..……28

2.2 Light microscopy images of transverse sections before and after treatment with [C2mim][Cl] at 120°C for (a, c, e) 0 h and (b, d, f) 72 h. (a, b) Around annual ring boundary. (c, d) Magnified view of earlywood. (e, f) Magnified view of latewood. *V*: vessel, *arrow*: wood fiber….……..……...31

2.3 Changes in cell wall area, cell lumen area and total of cell lumen area + cell wall area for (a) wood fiber and (b) vessel of *Fagus crenata* during [C2mim][Cl] treatment……..33

2.4 Light microscopy images of parenchyma cells before and after treatment with [C2mim][Cl] at 120°C for (a, c, e) 0 h and (b, d, f) 72 h. (a, b) Ray parenchyma in radial section. (c, d) Ray parenchyma in tangential section. (e, f) Axial parenchyma……..……35

2.5 SEM images of transverse section before and after treatment with [C2mim][Cl] at 120°C for (a, c, e) 0 h and (b, d, f) 72 h. (a, b) Boundary of earlywood and latewood. (c, d) Earlywood. (b, d, f) Latewood. *arrow*: crack……...36

2.6 SEM images of vessel perforations before and after treatment with [C2mim][Cl] at 120°C for (a, c) 0 h and (b, d) 72 h. (a, b) Perforation

rim. (c, d) Scalariform perforation plate……..……..37
2.7 SEM images of parenchyma before and after treatment with [C2mim][Cl] at 120°C for (a, c, e) 0 h and (b, d, f) 72 h. (a, b) Ray parenchyma in radial section. (c, d) Ray parenchyma in tangential section. (e, f) Axial parenchyma……38
2.8 SEM images of vessel pits treated with [C2mim][Cl] at 120°C for (a, c, e) 0 h and (b, d, f) 72 h. (a, b) Intervascular pits. (c, d) Intervascular pits of small vessel. (e, f) Ray-vessel pits…….……40
2.9 Light microscopy images of transverse sections before and after treatment with [C2mim][Cl] at 120°C for (a–c, A–C) 0 h and (d–f, D–F) 72 h. (a–f) Around annual ring boundary. (A–F) Magnified view of (a–f). *V*: vessel, *open arrowhead*: annual ring boundary, *open arrow*: wood fiber, *asterisk*: tracheid, *filled arrow*: crack……...41
2.10 Changes in cell wall area, cell lumen area, and total of cell lumen area + cell wall area for wood fiber of (a) *Quercus glauca*, (b) *Quercus mongolica*, (c) *Fagus crenata*, and tracheid of (d) *Trochodendron aralioides* in earlywood during [C2mim][Cl] treatment. *Refer to data in Fig. 2.3a……...……..…….43
2.11 Changes in cell wall area, cell lumen area, and total of cell lumen area + cell wall area for wood fiber of (a) *Quercus glauca*, (b) *Quercus mongolica*, (c) *Fagus crenata*, and tracheid of (d) *Trochodendron aralioides* in latewood during [C2mim][Cl] treatment. *Refer to data in Fig. 2.3a……..……44
2.12 SEM images of transverse section before and after treatment with [C2mim][Cl] at 120°C for (a, c, e) 0 h and (b, d, f) 72 h. (a, b) *Quercus glauca*. (c, d) *Quercus mongolica*. (e, f) *Trochodendron aralioides*. *open arrow*: axial parenchyma cell…….46
2.13 Light microscopy images of ray parenchyma before and after treatment with [C2mim][Cl] at 120°C for (a, c, e) 0 h and (b, d, f) 72 h. (a, b) *Quercus glauca*. (c, d) *Quercus mongolica*……..……..48

2.14 SEM images of various pits before and after treatment with [C2mim][Cl] at 120°C for (a, c, e) 0 h and (b, d, f) 72 h. (a, b) Ray-vessel pits of *Quercus glauca*. (c, d) Ray-vessel pits of *Quercus mongolica*. (e, f) Ray-ray pits of *Quercus glauca*…….……51
2.15 Raman spectra for (a) S_2, (b) CML, and (c) CC of tracheids before and after treatment with [C2mim][Cl] at 120°C for 0 h, 24 h, and 72 h; enlargement of the region from 350 to 1050 cm^{-1}…….……52
2.16 Raman spectra for (a) S_2, (b) CML, and (c) CC of tracheids before and after treatment with [C2mim][Cl] at 120°C for 0 h, 24 h, and 72 h; enlargement of the region from 1050 to 1550 cm^{-1}……...53
2.17 Raman spectra for (a) S_2, (b) CML, and (c) CC of tracheids before and after treatment with [C2mim][Cl] at 120°C for 0 h, 24 h, and 72 h; enlargement of the region from 2750 to 3150 cm^{-1}……..…….54
2.18 Raman spectra for (a) CML of tracheids and (b) ray parenchyma cells before and after treatment with [C2mim][Cl] at 120°C for 0 h, 24 h, and 72 h; enlargement of the region from 1540 to 1710 cm^{-1}……..56
2.19 Pictures of the wood samples before and after treatment with [C2mim][Cl] at 120°C for (a, d) 0 h, (b, e, g) 24 h, and (c, f, h) 72 h. (a−c) Light microscopy images and (d−f, g, h) polarized light microscopy images. (e, f) Before washing with water and (g, h) after washing with water……..……..57
2.20 Raman mapping on transverse sections of tracheids before and after treatment with [C2mim][Cl] at 120°C for (a, d, g) 0 h, (b, e, h) 24 h, and (c, f, i) 72 h. (a−c) Bright field images of the measured position. (d−f) Distribution of lignin (1591–1613 cm^{-1}). (g−i) Distribution of polysaccharides (2884–2905 cm^{-1}). Bright regions indicate high concentrations of specific chemical compositions, dark regions indicate low concentrations…….62
2.21 Line analysis on the double cell wall of tracheids on transverse section (lines shown in Fig. 2.20) before and after treatment with [C2mim][Cl] at 120°C for various times: (a) distribution of lignin (1586−1607 cm^{-1}) and

(b) distribution of polysaccharides (2884−2894 cm^{-1})……..64
2.22 Raman spectra for (a) WF_{SW}, (b) WF_{CC}, (c) vessel, and (d) axial parenchyma cell before and after treatment with [C2mim][Cl] at 120°C for 0 h, 24 h, and 72 h; enlargement of the region of 300–950 cm^{-1}…….……65
2.23 Raman spectra for (a) WF_{SW}, (b) WF_{CC}, (c) vessel, and (d) axial parenchyma cell before and after treatment with [C2mim][Cl] at 120°C for 0 h, 24 h, and 72 h; enlargement of the region of 950–1750 cm^{-1}……..…….66
2.24 Raman spectra for (a, a') WF_{SW}, (b, b') WF_{CC}, (c, c') vessel, and (d, d') axial parenchyma cell before and after treatment with [C2mim][Cl] at 120°C for 0 h, 24 h, and 72 h; enlargement of the region of 1520–1710 cm^{-1}. (a'−d') All spectra overlapped to clarify broadening of the peaks……...67
2.25 Raman spectra for (a) WF_{SW}, (b) WF_{CC}, (c) vessel, and (d) axial parenchyma cell before and after treatment with [C2mim][Cl] at 120°C for 0 h, 24 h, and 72 h; enlargement of the region of 2750–3150 cm^{-1}……..…...68
2.26 Raman mapping on transverse sections of wood fibers before and after treatment with [C2mim][Cl] at 120°C for (a, d, g) 0 h, (b, e, h) 24 h, and (c, f, i) 72 h. (a−c) Bright field images of the measured position. (d−f) Distribution of lignin (1581–1613 cm^{-1}). (g−i) Distribution of polysaccharides (2884–2905 cm^{-1}). Bright regions indicate high concentrations of specific chemical compositions, dark regions indicate low concentrations…….....74
3.1 Light microscopy and polarized light microscopy images of transverse sections before and after treatment with [EtPy][Br] at 120°C for (a–d) 0 h and (e–h) 72 h. (a, e) Around annual ring boundary. (b, f) Polarized light micrographs of (a) and (e). (c, g) Magnified view of earlywood. (d, h) Magnified view of latewood. *Filled arrow*: ray parenchyma cell, *open arrow*: axial parenchyma cell…….....80
3.2 Changes in cell wall area, cell lumen area and total of cell lumen area + cell wall area for tracheids of *Cryptomeria japonica* during [EtPy][Br] treatment…….....82

3.3 SEM images of various tissues before and after treatment with [EtPy][Br] at 120°C for (a, c, e, g, i) 0 h and (b, d, f, h, j) 72 h. (a, b) Around annual ring boundary. (c, d) Magnified view of earlywood. (e, f) Magnified view of latewood. (g, h) Bordered pits. (i, j) Taxodioid pits……...83
3.4 Raman spectra for (a) S_2, (b) CML, and (c) CC of tracheids before and after treatment with [EtPy][Br] at 120°C for 0 h, 24 h, and 72 h; enlargement of the region from 350 to 1050 cm^{-1}……...……..86
3.5 Raman spectra for (a) S_2, (b) CML, and (c) CC of tracheids before and after treatment with [EtPy][Br] at 120°C for 0 h, 24 h, and 72 h; enlargement of the region from 1050 to 1540 cm^{-1}……..…….87
3.6 Raman spectra for CML of tracheids before and after treatment with [EtPy][Br] at 120°C for 0 h, 24 h, and 72 h; enlargement of the region from 1540 to 1710 cm^{-1}…….88
3.7 Raman spectra for (a) S_2, (b) CML, and (c) CC of tracheids before and after treatment with [EtPy][Br] at 120°C for 0 h, 24 h, and 72 h; enlargement of the region from 2750 to 3150 cm^{-1}……..…….89
3.8 Raman mapping on transverse sections of tracheids before and after treatment with [C2mim][Cl] at 120°C for (a, d, g) 0 h, (b, e, h) 24 h, and (c, f, i) 72 h. (a−c) Bright field images of the measured position. (d−f) Distribution of lignin (1591–1613 cm^{-1}). (g−i) Distribution of polysaccharides (2884–2905 cm^{-1}). Bright regions indicate high concentrations of specific chemical compositions, dark regions indicate low concentrations…….……..…..92
3.9 Light microscopy and polarized light microscopy images of transverse sections before and after treatment with [EtPy][Br] at 120°C for (a, c) 0 h and (b, d) 72 h. (c, d) Polarized light micrographs of (a) and (b). *V*: vessel, *arrow* wood fiber……95
3.10 Changes in cell wall area, cell lumen area and total of cell lumen area + cell wall area for (a) wood fiber and (b) vessel of *Fagus crenata* during [EtPy][Br] treatment……...……96

3.11 Light microscopy images of tangential sections of ray parenchyma before and after treatment with [EtPy][Br] at 120°C for (a) 0 h and (b) 72 h……97

3.12 SEM images of transverse sections before and after treatment with [EtPy][Br] at 120°C for (a, c) 0 h and (b, d) 72 h. (c, d) Magnified view of wood fibers……99

3.13 SEM images of parenchyma before and after treatment with [EtPy][Br] at 120°C for (a, c, e) 0 h and (b, d, f) 72 h. (a, b) Ray parenchyma in tangential sections. (c, d) Ray parenchyma in radial sections. (e, f) Axial parenchyma cells……..101

3.14 SEM images of parenchyma before and after treatment with [EtPy][Br] at 120°C for (a, c) 0 h and (b, d) 72 h. (a, b) Perforation rim. (c, d) Scalariform perforation plate……...102

3.15 SEM images of vessel pits before and after treatment with [EtPy][Br] at 120°C for (a, c) 0 h and (b, d) 72 h. (a, b) Ray-vessel pits. (c, d) Intervascular pits……..103

3.16 Raman spectra for (a) S_2 and (b) CC of wood fibers before and after treatment with [EtPy][Br] at 120°C for 0 h, 24 h, and 72 h. *solid lines*: lignin, *dashed lines*: polysaccharides……105

3.17 Raman mapping on transverse sections of wood fibers before and after treatment with [EtPy][Br] at 120°C for (a, d, g) 0 h, (b, e, h) 24 h, and (c, f, i) 72 h. (a−c) Bright field images of the measured position. (d−f) Distribution of lignin (1580–1622 cm^{-1}). (g−i) Distribution of polysaccharides (2871–2897 cm^{-1}). Bright regions indicate high concentrations of specific chemical compositions, dark regions indicate low concentrations……...107

4.1 Light microscopy images of transverse sections in compression wood (a, b) before and after treatment with (c) [C2mim][Cl] and (d) [EtPy][Br] at 120°C for 72 h……..114

4.2 Polarized light microscopy images of transverse sections in compression

wood (a, b) before and after treatment with (c) [C2mim][Cl] and (d) [EtPy][Br] at 120°C for 72 h……..……...116
4.3 Changes in cell wall area, cell lumen area and total of cell lumen area + cell wall area for compression wood tracheids of *Fagus crenata* in (a, b) earlywood and (c, d) latewood during (a, c) [C2mim][Cl] and (b, d) [EtPy][Br] treatment…….117
4.4 SEM images of compression wood tracheids (a–c) before and after treatment with (d–f) [C2mim][Cl] and (g–i) [EtPy][Br] at 120°C for 72 h. (a, d, g) Transverse view of earlywood. (b, e, h) Transverse view of latewood. (c, f, i) Radial view of earlywood. Arrows, dissociated S_2; arrowheads, ruptured S_1 and CML……...119
4.5 Raman mapping on transverse sections of compression wood tracheids (a–c, g–i) before and after treatment with (d–f) [C2mim][Cl] and (j–l) [EtPy][Br] at 120°C for 72 h. (a, d, g, j) Bright field images of the measured position. (b, e, h, k) Distribution of lignin (1,585−1,606 cm^{-1}). (c, f, i, l) Distribution of polysaccharides (2,876−2,902 cm^{-1}). Bright regions represent high concentrations of specific chemical compositions, whereas dark regions represent low concentrations. Arrows, S_2(L); arrowheads, CML…….121
4.6 Light microscopy images of transverse sections in opposite wood treated with (a) [C2mim][Cl] and (b) [EtPy][Br] at 120 °C for various time periods. In lower panels, changes in cell wall area, cell lumen area and total of cell lumen + cell wall area for tracheids during ionic liquid treatment are presented. *EW*: earlywood, *LW*: latewood…….…….123
4.7 SEM images of opposite wood tracheids (a, d, g) before and after treatment with (b, e, h) [C2mim][Cl] and (c, f, i) [EtPy][Br] at 120°C for 72 h. (a–c) Earlywood. (d–f) Latewood. (g–i)Bordered pits. *S_2*: middle layer of secondary wall, *S_3*: inner layer of secondary wall, *CML*: compound middle lamella, *T*: torus……..125
4.8 Bright-field microscopy and polarized light microscopy images of

transverse sections in tension wood (a, b, e, f) before and after treatment with (c, d) [C2mim][Cl] and (g, h) [EtPy][Br] at 120°C for 72 h. *large arrow*: gelatinous fiber, *small arrow*: ray parenchyma cell, *arrow head*: axial parenchyma cell, *V*: vessel……..126

4.9 Changes in cell wall area, cell lumen area and total of cell lumen area + cell wall area for gelatinous fiber during (a) [C2mim][Cl] and (b) [EtPy][Br] treatment at 120°C……..……...128

4.10 SEM images of transverse sections in tension wood (a, b) before and after treatment with (c, d) [C2mim][Cl] and (e, f) [EtPy][Br] at 120°C for 72 h. (a, c, e) Around annual ring boundary. (b, d, f) Magnified view of gelatinous fibers. *arrow*: gelatinous layer, *arrow head*: annual ring boundary……...130

4.11 Raman spectra for gelatinous layer (a) before and after treatment with (b) [C2mim][Cl] at 120°C for 24 h and (c) [EtPy][Br] at 120°C for 72 h. *solid lines*: lignin, *dashed lines*: polysaccharides……..……..132

List of Tables

2.1 Swelling ratio of cell wall area and thickness of ray parenchyma cells after treatment for 72 h with [C2mim][Cl] at 120°C…….....49

2.2 Raman bands used for the analysis, and their assignment to lignin and polysaccharides…….....58

CHAPTER 1

General Introduction

1.1 Preface

Remarkable developments in science and technology since the industrial revolution have given us great benefits and a comfortable life. However, energy and environmental problems such as global warming from greenhouse gas emissions and exhaustion of nonrenewable fossil resources are of concern.

The use of lignocelluloses, which are renewable and carbon neutral, is expected to reduce our dependence on fossil resources. To try to solve some of the energy and environmental problems caused by the global mass consumption of fossil resources, efficient conversion technology of lignocelluloses to bio-fuels, bio-plastics and bio-based composites has been researched (Howard et al. 2003). Above all, because woody biomass is abundantly stockpiled on the earth and does not compete with food supply, it is regarded as one of the most promising sustainable resources (Sannigrahi et al. 2010; Zhu and Pan 2010). In order to use the woody biomass in many of the processes where fossil resources are currently applied, it is necessary to perform chemical, physical, physicochemical, and other treatments. However, effective techniques that enable substitution of woody biomass for fossil resources have not yet been established. Thus, further improvement and development of the conversion technologies is an urgent subject to date.

1.2 Tissue structure and chemical composition of woody biomass

1.2.1 Tissue structure

Woody plant is aggregate of xylem cells made from the cambium cell and takes complicated tissue structure. Softwood is mainly constituted by tracheid, axial parenchyma cell, and ray parenchyma cell, and the tissue structures of softwood lack in

variety compared to that of hardwood (Panshin and Zeeuw 1970; Tsoumis 1991). Pits exist on the surface of all woody cells, and the form of pit varies according to the cell type. There is bordered pit between tracheids, and the pit membrane is generally comprised of so-called torus and margo. In addition, cross-field pit exists between tracheid and parenchyma cell, and single pit appears between parenchyma cells. The cross-field pits are classified into six types of category: window-like, pinoid, cupressoid, taxodioid, piceoid, and araucarioid (Richter et al. 2004). In softwood, axial parenchyma is not always present in all species.

Hardwood has diverse tissue structures, and it is mainly constructed by vessel, wood fiber, axial parenchyma cell, and ray parenchyma cell (Panshin and Zeeuw 1970; Tsoumis 1991). Wood fiber can be classified into four kinds of cells; libriform wood fiber, fiber-tracheid, vascular tracheid, and vasicentric tracheid (Carlquist 2001). Hardwood is mainly classified into various groups such as ring-porous wood, diffuse-porous wood, and radial-porous wood according to vessel arrangement. Vessel perforations are found in end-to-end connection of vessel elements, and the perforation shows various types, such as simple perforation, scalariform perforation, and foraminate perforation. In hardwood, axial parenchyma cell is seldom absent. In general, it is more abundant than in softwood, and its distribution is multifarious depend on the species (Panshin and Zeeuw 1970; Tsoumis 1991).

The cell walls of tracheid and wood fiber were composed of multilayer structure. The principal features are the middle lamellae, primary wall, and secondary wall. The orientation of the microfibril in the various layers is shown schematically (Fig. 1.1). In the primary wall (P) the microfibril orientation is random except for cell corner (CC) where they run axially along the length of the cell. In the secondary wall three distinct layers, the inner (S_1), middle (S_2) and outer (S_3) layers, are recognized according to the differences in microfibril angle. The orientation of microfibril across the secondary wall is S-Z-S in the S_1 (flat-helix), S_2 (steep-helix) and S_3 (flat-helix) layers respectively (Walker 1993). The microfibril angles of S_1, S_2 and S_3 are considered to be 50–70, 5–30 and 60–90°, respectively, depending on the source of the cell (Côté 1968; Parham and Gray 1984).

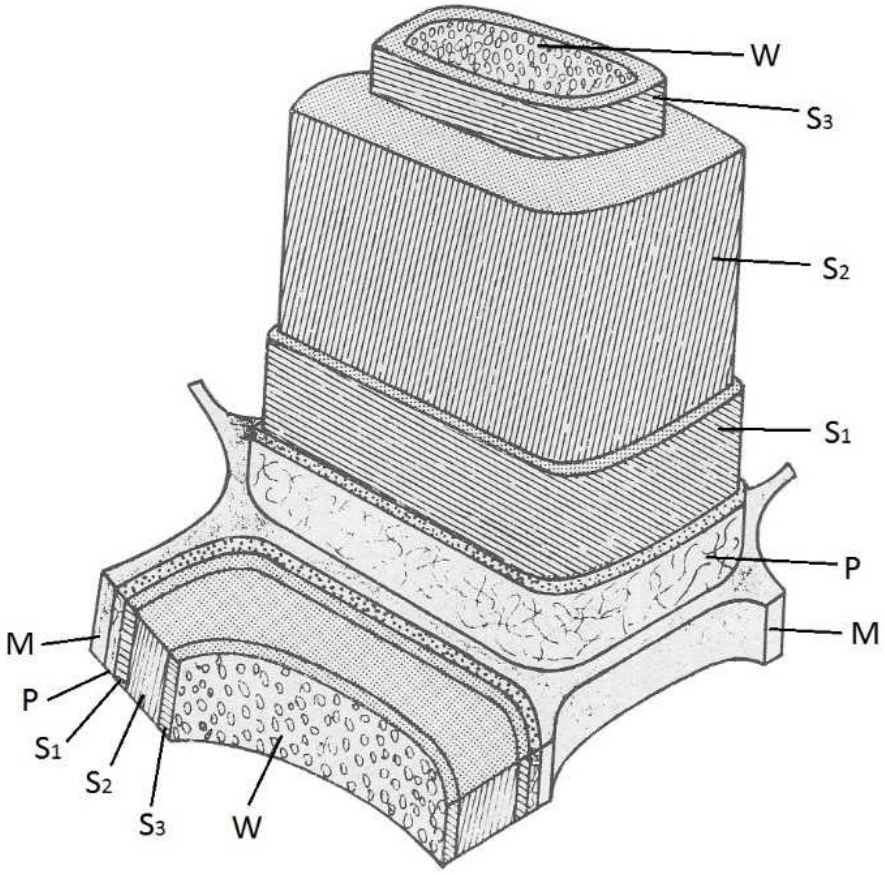

Fig. 1.1 Schematic diagram of cell wall organization (Walker 1993). *M*: middle lamella, *P*: primary wall, S_1, S_2, S_3: layers of secondary wall, *W*: warty layer.

1.2.2 Chemical composition and distribution

Wood is composed principally of cellulose, hemicellulose, lignin, and small amount of pectic substance. The proportions of cellulose, hemicellulose, and lignin are approximately as follows; cellulose, 40–50% (about the same in softwood and hardwood); hemicellulose, 20% in softwood and15–35% in hardwood; lignin, 25–35% in softwood and 17–25% in hardwood (Pettersen 1984; Tsoumis 1991). The distribution of chemical composition in wood cell wall is shown in Fig. 1.2 (Panshin and Zeeuw 1970).

Cellulose is one of the most abundant organic substances on the earth. It is a liner polymer containing thousands of β-D-glucose units linked by glucosidic linkages at C1 and C4 positions. In the wood cell wall, the cellulose microfibril is composed of a bundle of cellulose molecules. As seen in Fig. 1.2, the S_2 of secondary wall is predominantly composed of cellulose.

Hemicellulose is the general term of polysaccharides which can be dissolved in alkaline aqueous solution such as sodium and potassium hydroxide, whereas it cannot be extracted by hot water and ammonium oxalate. The main compositions of hemicellulose are as follows; galactoglucomannan and arabinoglucuronoxylan in softwood; glucuronoxylan and small amount of glucomannan in hardwood. The distribution of hemicellulose on wood cell walls have been mainly studied by some types of immunomicrscopic methods (Altaner et al. 2007; Awano et al. 1998; Baba et al. 1994; Kim et al. 2010a). In wood cell walls, xylan and glucomannan are localized at the secondary wall (Awano et al. 1998; Baba et al. 1994).

Lignin is a complex and high molecular weight three-dimensional polymer built upon phenylpropane units, linked together by C–O–C and C–C linkages. The main composition of lignin differs between softwoods and hardwoods, and also varies among different wood species, cell type, and morphological region (Tsoumis 1991). The distribution of lignin on wood cell walls have been investigated by various microscopy techniques, such as interference microscopy (Boutelje 1972; Donaldson 1987), ultraviolet (UV) microscopy (Fergus et al. 1969; Fergus and Goring 1970; Scott et al. 1969), scanning and transmission electron microscopy coupled with an energy dispersive X-ray analysis (SEM- and TEM-

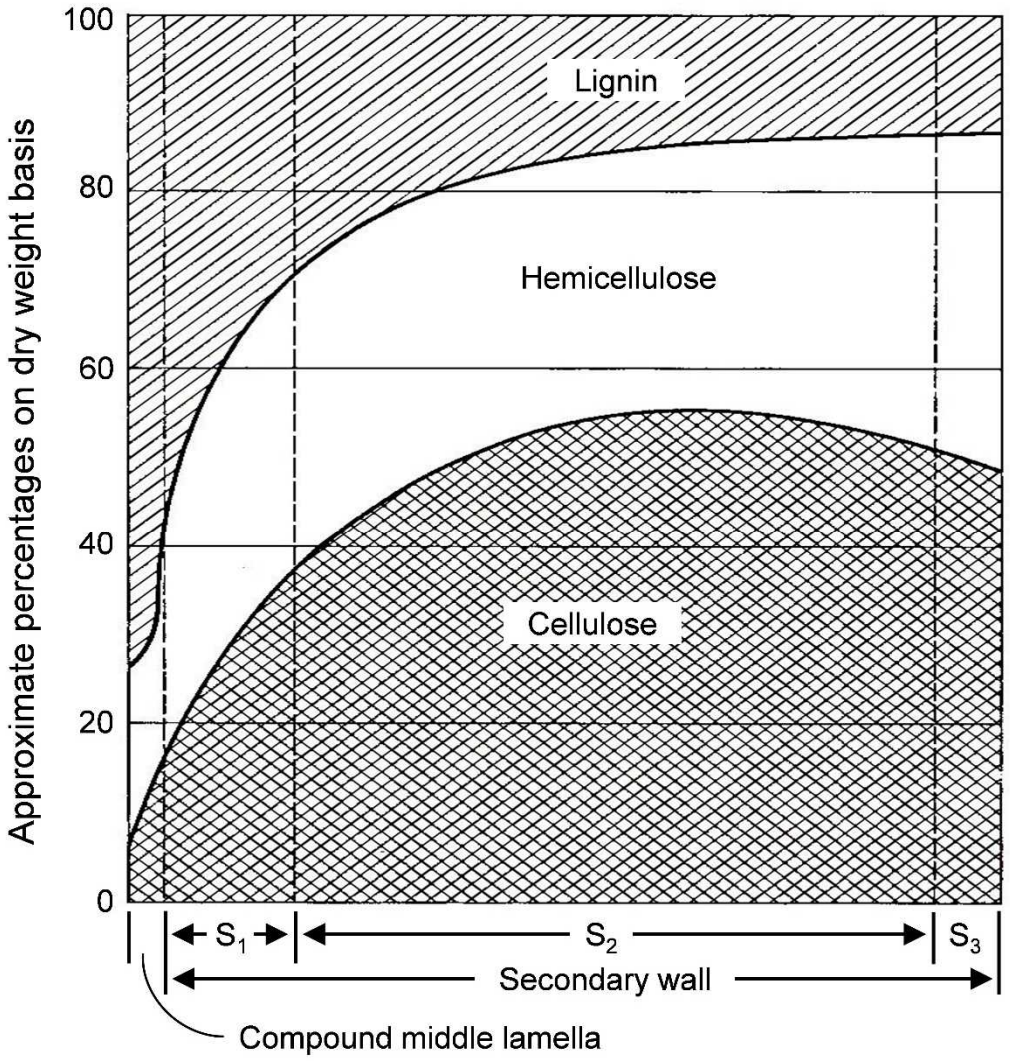

Fig. 1.2 Distribution of the main chemical component in the cell wall (Panshin and Zeeuw 1970). *S1, S2, S3*: layers of secondary wall.

EDXA) (Eriksson et al. 1988; Saka and Goring 1988; Saka and Thomas 1982a, b; Westermark et al. 1988), autoradiography (Terashima and Fukushima 1988), immunomicroscopy (Joseleau and Ruel 2007; Kim et al. 2010b), and confocal Raman microscopy (Agarwal 2006; Gierlinger and Schwanninger 2006; Ma et al. 2011, 2013; Röder et al. 2004; Schmidt et al. 2009; Zhang et al. 2012). The concentration of lignin is about 3 times higher in CC than in the secondary wall. In addition, the cell walls of the vessels and the ray parenchyma cells are almost equal in lignin concentration and had about 1.5–1.6 times higher concentration than the secondary wall of the wood fibers (Eriksson et al. 1988). Softwood lignin is predominantly composed of guaiacylpropane units, whereas hardwood lignin contains a mixture of guaiacylpropane and syringylpropane units. In hardwood, the secondary walls of wood fibers and vessel contains syringylpropane units, whereas the CML of wood fibers and parenchyma cells contains a mixture of guaiacylpropane and syringylpropane units (Fergus and Goring 1970; Fujii et al. 1987; Musha and Goring 1975; Saka and Goring 1988). In addition, the CML of softwood tracheids is composed of approximately 40% of *p*-hydroxyphenyl units (Terashima and Fukushima 1988; Whiting and Goring 1982).

1.3 Woody biomass conversion technology

Woody biomass has been one of the most promising alternative to fossil resources. To break down its complicated and recalcitrant cell wall structure, physical and/or chemical treatments are required, and many conversion methods have been investigated. Examples of such treatments or conversion technologies, including acid hydrolysis (Goldstein 1980; Parisi 1989; Taherzadeh et al. 1997), enzymatic hydrolysis (Chang and Holtzapple 2000; Zhao et al. 2008), pyrolysis (Bridgwater et al. 1999; Oasmaa et al. 2010; Piskorz et al. 1988), and supercritical fluid treatment (Xu and Etcheverry 2008; Yamazaki et al. 2006; Yoshida et al. 2005) have been studied.

The methods, acid and enzymatic hydrolysis, are the major saccharification techniques. Cellulose is hydrolyzed to glucose followed by converting glucose into ethanol according to the fermentation. However, each method has specific advantage and

disadvantage. Although acid hydrolysis is a relatively short time and high yield method, excessive decomposition and generation of by-products which hinder the growth of yeast occur. In addition, it is difficult to collect and recycle the acid solution, and need a thermal, pressure and acid resistant reactor. On the other hand, although enzymatic hydrolysis does not need a large scale reactor and a great deal of energy and does not generate by-products, longer time processing is needed compared with the acid hydrolysis. In addition, to increase the enzyme accessibility improving digestibility of cellulose, some sort of pretreatments which destroy the rigid structure of wood cell walls are necessary. For instance, milling (Matsumura et al. 1977), steam explosion (Brownell and Saddler 1987), microwave irradiation (Tsubaki and Azuma 2011), delignification with acid (Sudo et al. 1976), alkaline (Chang et al. 2001), ozone (Hayashi et al. 1989; Sugimoto et al. 2009), organic solvent (Zhao et al. 2009), and wood-decay fungus (Mes-Hartree et al. 1987). Recently, research on a novel pretreatment method using ionic liquid has proceeded (Dadi et al. 2007; Lee et al. 2009).

Pyrolysis is a method in which biomass is heated at high temperature in the absence of oxygen and can directly produce a bio-oil and bio-gas (Bridgwater 2012). The products of pyrolysis can be used for fuels and chemicals. However, the reaction process is complex and the quantity and quality of the products vary according to the reaction condition, such as treatment time, temperature, heating and cooling speed, and atmosphere. In addition, the energy content of the biomass is greatly lost in the processing.

Supercritical fluid treatment has been thought to be an attractive method of thermal biomass conversion. Lignocelluloses are able to be decomposed in supercritical water (>374°C, >22.1 MPa), methanol (>239°C, >8.09 MPa), and ethanol (>243°C, >6.38 MPa) (Yamazaki et al. 2006; Yoshida et al. 2005). The supercritical fluid treatment has been applied to obtain bioethanol and valuable chemicals from polysaccharides (cellulose and hemicellulose) and lignin in lignocelluloses, respectively (Saka 2006). However, a large amount of cost and energy consumption need to make high-temperature and high-pressure conditions.

As stated above, various conversion methods have been investigated; nevertheless, effective techniques that enable substitution of woody biomass for fossil resources have

not yet been established.

1.4 Ionic liquid

1.4.1 What is ionic liquid?

Ionic liquids have been the subject of intense study in many fields since the discovery of air and water-stable ionic liquids (Wilkes and Zaworotko 1992). Ionic liquids are the general term for any organic salts that are liquid around or below 100°C, and they are strong solvents for a wide range of organic, inorganic, and organometallic compounds (Sheldon 2001). Compared with conventional, volatile organic solvents, ionic liquids have many attractive characteristics: no effective vapor pressure, chemical and thermal stability, non-flammability, and reusability (Earle and Seddon 2000; Rogers and Seddon 2003; Seddon 1997; Sheldon 2001). For that reason, they have been regarded as environmental friendly solvents.

There are many types of ionic liquids, such as imidazolium, pyridinium, pyrrolidinium, piperidinium, phosphonium, and ammonium-based ones. Figure 1.3 shows the typical cations and anions found in ionic liquids. There are an infinite number of combinations of cations and anions and their physical properties, such as melting point, viscosity and dissolving power, can be easily changed by altering the combination. Therefore, they can be thought of as “designer solvents” (Freemantle 1998). In addition, the high solubility and reusability of ionic liquids are very attractive properties from the point of view of green chemistry and, therefore, ionic liquids show great promise as new reaction solvents (Earle and Seddon 2000). Recently, ionic liquid treatment has been investigated as a woody biomass conversion technology (Miyafuji 2015; Muhammad et al. 2012).

1.4.2 Reaction behavior of woody biomass in ionic liquid

Since it was reported that certain imidazolium-based ionic liquids can dissolve cellulose (Swatloski et al. 2002), many studies on application of ionic liquids to cellulose have been

Cations

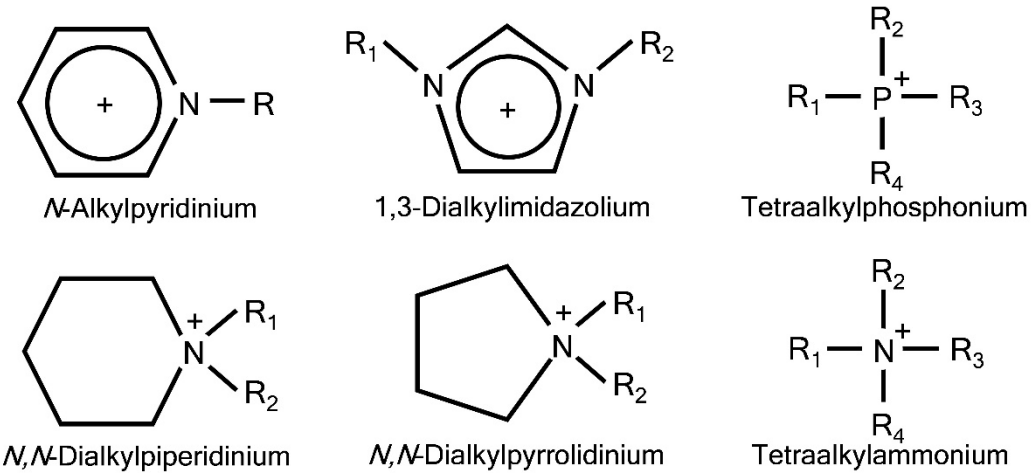

Anions

Cl^-	$C(CN)_3^-$	PF_6^-	NO_3^-
Br^-	CH_3COO^-	$N(SO_2F)_2^-$	$HCOO^-$
I^-	$(CF_3SO_2)_2N^-$	$CF_3SO_3^-$	$AlCl_4^-$
BF_4^-	$(CF_3SO_2)_3C^-$		

Fig. 1.3 The typical cations and anions for ionic liquids (Kanbayashi and Miyafuji 2016b). *R*: represents alkyl groups.

carried out (Fukaya et al. 2008; Kosan et al. 2008; Miyata and Miyafuji 2014; Ohno and Miyafuji 2013, 2014; Zhang et al. 2005; Zhu et al. 2006). It has been also reported that wood can be liquefied in some ionic liquids (Abe et al. 2014; Brandt et al. 2010; Fort et al. 2007; Honglu and Tiejun 2006; Kilpeläinen et al. 2007; Li et al. 2010; Miyafuji et al. 2009; Nakamura et al. 2010a; Sun et al. 2009; Yokoo and Miyafuji 2014).

To establish effective conversion methods for woody biomass using ionic liquids, fundamental investigations of the reaction behaviors of wood in ionic liquid have been performed. The main wood components, such as cellulose, hemicellulose and lignin, are reported to be liquefied during treatment with the ionic liquid, 1-ethyl-3-methylimidazolium chloride ([C2mim][Cl]). The structural formula of [C2mim][Cl] is described in Fig. 1.4a. This ionic liquid can decompose these carbohydrates into low molecular weight compounds such as glucose (Fort et al. 2007; Miyafuji et al. 2009), and the crystalline structures of cellulose are destroyed as the reaction proceeds (Miyafuji et al. 2009). Sun et al. (2009) reported that the dissolution rate of wood in ionic liquids is not only affected by particle size and the initial wood concentration. In addition, softwood and hardwood show different liquefaction behavior in ionic liquid because of their differences in the lignin chemical structure (Nakamura et al. 2010a). For instance, Japanese beech (*Fagus crenata*) is more readily liquefied than Western red cedar (*Thuja plicata*). The reaction atmosphere is also a key factor; an oxidative atmosphere accelerates the liquefaction of wood (Nakamura et al. 2010b). The interaction of wood with ionic liquids is different for the types of ionic liquids. Although two ionic liquids, [C2mim][Cl] and 1-ethypyridinium bromide ([EtPy][Br]), are able to liquefy wood, [C2mim][Cl] preferentially dissolves cellulose (Miyafuji et al. 2009; Nakamura et al. 2010a), whereas [EtPy][Br] preferentially dissolves lignin (Yokoo and Miyafuji 2014). The structural formula of [EtPy][Br] is shown in Fig. 1.4b. In this way, the reaction mechanism of wood in ionic liquid has been in the process of revealing gradually from the chemical viewpoint.

Several studies on the effects of ionic liquid treatment on wood cell walls have been also conducted from the point of view of morphology (Çetinkol et al. 2010; Lucas et al. 2010, 2011; Miyafuji and Suzuki 2011, 2012; Viell and Marquardt 2011). Laser scanning fluorescence microscopy clarified that the cell walls of poplar (*Populus tremuloides*)

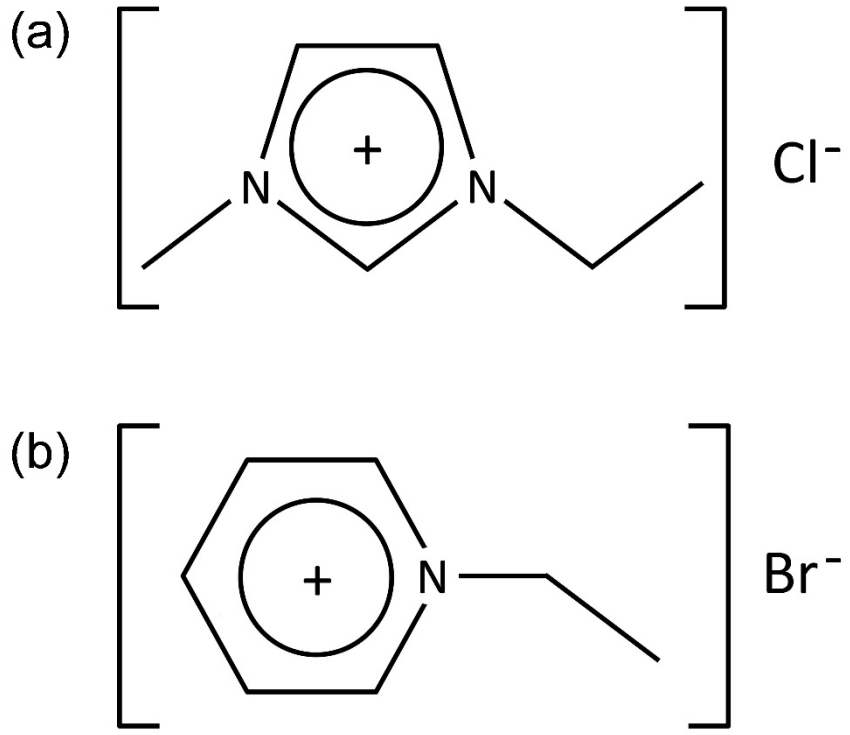

Fig. 1.4 Structural formula of the ionic liquids, (a) 1-ethyl-3-methylimidazolium chloride ([C2mim][Cl]) and (b) 1-ethylpyridinium bromide ([EtPy][Br]).

mainly swell toward the lumen side during ionic liquid 1-*n*-ethyl-3-methylimidazolium acetate treatment at room temperature (Lucas et al. 2010, 2011). In the study using polarized light microscopy, [C2mim][Cl] was found to destroy the crystalline structure of cellulose in wood with treatment time although the wood tissue shape was retained (Miyafuji and Suzuki 2012). Light microscopy and scanning electron microscopy (SEM) studies have shown that the wood tissue of the latewood of *Cryptomeria japonica* became distorted and dissociated significantly compared with those in earlywood (Miyafuji and Suzuki 2011, 2012). Furthermore, the morphological changes in wood after ionic liquid treatment were different between softwood and hardwood (Viell and Marquardt 2011). Topochemical studies revealed that the interaction of wood with the ionic liquid, 1-ethyl-3-methylimidazolium acetate, was different for various locations on the wood cell wall: secondary wall, compound middle lamella (CML) and CC; lignin in CML and CC have high recalcitrance to degradation with the ionic liquid (Zhang et al. 2014). The reaction mechanism of wood in ionic liquids has been in the process of revealing by degrees.

1.5 Objectives of this work

Using ionic liquids as the solvent to process woody biomass, many fundamental studies on the reaction behavior of wood in ionic liquids have been carried out focusing on the chemical processes. However, woody biomass is a very inhomogeneous composite at the cell level. Wood comprises various types of tissues such as the tracheids, wood fibers, vessels, and parenchyma. In addition, wood cell walls consist of several layers: P, S_1, S_2, S_3, and CML. The chemical components and distribution vary depending on the wood species, types of tissues and cell wall layers. Therefore, to improve the chemical conversion process using ionic liquids, a better understanding of the effects of ionic liquid treatment of wood, such as the interaction of wood with ionic liquids at the cellular level and the deconstruction behavior of various types of tissues in ionic liquids, are required.

In the present work, the morphological and topochemical features on the liquefaction of wood in ionic liquids, especially [C2mim][Cl] and [EtPy][Br], were investigated using various microscopy techniques. [C2mim][Cl] and [EtPy][Br] are known as the ionic

liquids which can preferentially liquefy cellulose (Miyafuji et al. 2009; Nakamura et al. 2010a) and lignin (Yokoo and Miyafuji 2014), respectively. Bright-field microscopy and polarized light microscopy were employed to determine the swelling and decomposition behaviors of wood cell walls and the state of cellulose crystallinity during ionic liquids treatment. SEM was used to observe the detailed ultrastructural changes in various wood tissues treated with ionic liquids. Confocal Raman microscopy was employed to examine the changes in chemical components including polysaccharides and lignin at the cellular level and to visualize their distribution on the cell walls during ionic liquids treatment.

CHAPTER 2

Microscopic Study on Woody Biomass after Treatment with the Ionic Liquid, 1-Ethyl-3-methylimidazolium Chloride ([C2mim][Cl])

2.1 Introduction

The application of the ionic liquids for the field of biomass conversion has been the subject of intensive study since the first report on dissolution of cellulose in some sort of ionic liquids by Swatloski et al. (2002). The liquefaction of woody biomass in ionic liquids has been subsequently demonstrated by a number of investigators (Abe et al. 2014; Brandt et al. 2010; Fort et al. 2007; Honglu and Tiejun 2006; Kilpeläinen et al. 2007; Li et al. 2010; Miyafuji et al. 2009; Sun et al. 2009). Many fundamental studies of the reactivity of wood in ionic liquids have been conducted to facilitate the use of ionic liquids as solvents for processing woody biomass.

[C2mim][Cl] is one of the most acknowledged imidazolium-based ionic liquid. It has been reported that [C2mim][Cl] has the ability to dissolve cellulose (Kosan et al. 2008; Ohno and Miyafuji 2013, 2014) and even wood (Miyafuji et al. 2009; Nakamura et al. 2010a). The main wood components, such as cellulose, hemicellulose and lignin, are liquefied during [C2mim][Cl], with preferential liquefaction of cellulose and hemicellulose (Miyafuji et al. 2009; Nakamura et al. 2010a). The crystalline structures of cellulose are destroyed as the reaction proceeds in [C2mim][Cl] (Miyafuji et al. 2009). In addition, the reaction behavior of wood in [C2mim][Cl] is different for each wood species. Japanese cedar (*Cryptomeria japonica*) is more readily liquefied than Western red cedar (*Thuja plicata*) (Nakamura et al. 2010a). A study on the influence of oxygen and humidity enhances wood liquiefaction (Nakamura et al. 2010b).

Previous observations (using light microscopy and SEM) of morphological changes

in wood after [C2mim][Cl] treatment showed that wood tissues in latewood of *Cryptomeria japonica* were distorted and dissociated but tissues in earlywood were not (Miyafuji and Suzuki 2011, 2012). However, morphological changes of wood tissues from species other than *Cryptomeria japonica* upon treatment with [C2mim][Cl] have not yet been studied. Hardwood is anatomically quite different from softwood. Although the former has various tissues such as wood fibers, vessels and parenchyma cells, the latter is mainly composed of tracheids (Tsoumis 1991). These cells vary not only in size and shape, but also in their chemical composition: vessel and parenchyma cells have higher proportion of lignin than wood fibers (Eriksson et al. 1988; Fergus and Goring 1970). These differences are expected to influence the reactions of [C2mim][Cl] with the wood. In this study, therefore, detailed morphological changes in wood tissues of various species with characteristic tissue forms after treatment with [C2mim][Cl] were investigated using light microscopy and SEM.

Confocal Raman microscopy can obtain molecular information from plant cell walls with a high spatial resolution and without any pretreatment (Fackler and Thygesen 2013; Gierlinger and Schwanninger 2007; Lupoi et al. 2014). It has been reported that confocal Raman microscopy is an effective tool to investigate chemical composition of woody biomass (Röder et al. 2004). Several studies on the visualization of the distribution of cellulose and lignin in wood cell walls were carried out (Agarwal 2006; Gierlinger et al. 2010; Gierlinger and Burgert 2006; Gierlinger and Schwanninger 2006; Ji et al. 2013; Lehringer et al. 2008; Ma et al. 2011; Schmidt et al. 2009; Sun et al. 2011; Tirumalai et al. 1996). Furthermore, this technique can be also applied to study chemical changes in wood cell walls at the cellular level after physical and chemical treatment (Chunilall et al. 2012; Ji et al. 2014a, b; Ma et al. 2014; Zhang et al. 2014; Zhou et al. 2014). In this study, to study the effects of [C2mim][Cl] treatment on the chemical components of various fine morphological regions of softwood and hardwood, confocal Raman microscopy technique was applied.

2.2 Materials and Methods

2.2.1 Samples and chemicals

The woods used were: Japanese cedar (*Cryptomeria japonica*), Japanese beech (*Fagus crenata*), Japanese blue oak (*Quercus glauca*), Japanese oak (Q*uercus mongolica*), and Wheel tree (*Trochodendron aralioides*). They were cut into block samples [approximately 5(R) × 5(T) × 5(L) mm] that were extracted with ethanol/benzene (1:2, v/v) for 8 h in a Soxhlet apparatus. The extracted wood was oven dried at 105°C for 24 h prior to further treatment. The ionic liquid, [C2mim][Cl] (>97% purity), was purchased from Tokyo Chemical Industry Co., Ltd., Tokyo, Japan.

2.2.2 Treatment with [C2mim][Cl] for light microscopy analysis

The extracted wood samples were cut with a sliding microtome (TU-213, Yamato Kohki Industrial Co., Ltd., Saitama, Japan) into 15-μm-thick sections and mounted in a 20-μm-deep hemocytometer (Sunlead Glass Corp., Saitama, Japan). Each mounted section was dried for 2 h at 105°C, then 100 μL of [C2mim][Cl], heated to 120°C, was dropped onto the mounted section. The hemocytometer was immediately closed with a glass cover; this was designated as the beginning of the treatment. The hemocytometer was placed in an oven at 120°C for various time periods, and then removed from the oven to examine the anatomical changes in the wood section using light microscopy (BH-2, Olympus, Tokyo, Japan). Three areas (cell lumen area, cell wall area, and total of cell lumen area + cell wall area; defined as shown in Fig. 2.1) were measured for five neighboring cells in both latewood and earlywood, using image analysis software (Motic Image Plus 2.2S, Shimadzu Rika Corporation, Tokyo, Japan) and the average was calculated for each area.

2.2.3 Treatment with [C2mim][Cl] for SEM observation

Extracted wood samples were surfaced with a sliding microtome. The surfaced samples were dried for 24 h at 105°C and the surfaced area was then treated by dipping into [C2mim][Cl] and heating to 120°C for various periods of time. During the dipping

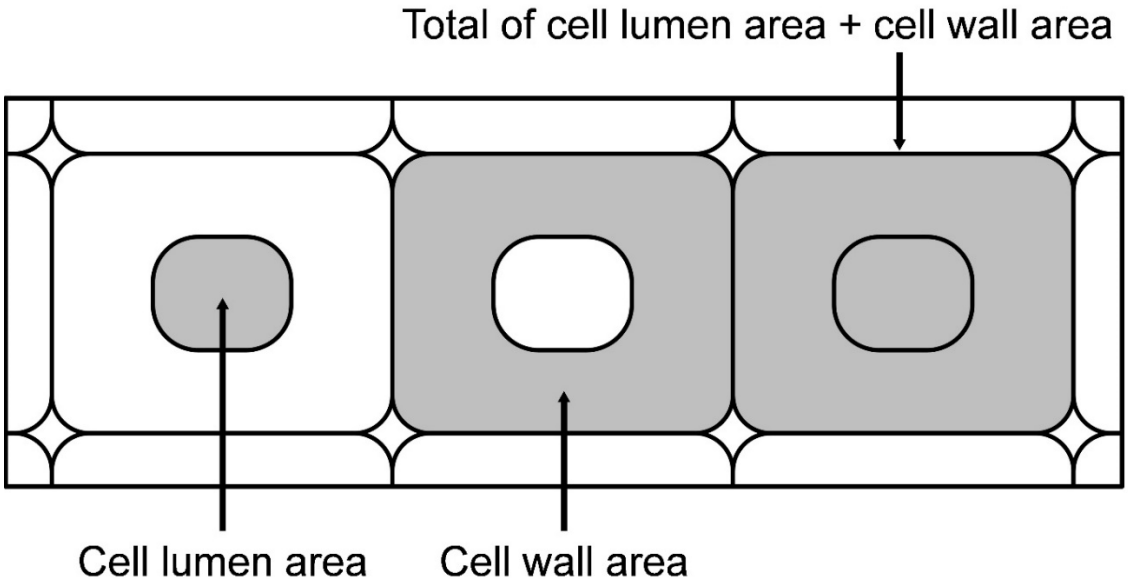

Fig. 2.1 Definition of cell lumen area, cell wall area and total of cell lumen area + cell wall area.

treatment, the [C2mim][Cl] was stirred gently with a magnetic stirrer. The treated specimens were dipped into dimethylsulfoxide (DMSO) to remove [C2mim][Cl] and then washed with distilled water to remove DMSO. After drying for 24 h at 105°C, each specimen was mounted on a specimen holder using carbon tape and sputter-coated with Au using a JEOL JFC-1600 auto fine coater (Tokyo, Japan). The exposed surface was examined by SEM (JSM-5510LV, JEOL) at beam accelerating voltages from 10 to 25 kV. Morphological changes in the wood cells resulting from these high accelerating voltages were not observed.

2.2.4 Treatment with [C2mim][Cl] for confocal Raman microscopy analysis

For Raman microscopy the [C2mim][Cl] treatment was the same as that for light microscopy. To perform analysis on the same cell wall area with respect to Raman mapping and line analysis, 15-μm-thick serial sections were prepared. After a specific treatment time, a large amount of distilled water was poured into the hemocytometer from its lateral direction, and then the hemocytometer was placed in a Petri dish filled with distilled water for 24 h at room temperature to completely remove [C2mim][Cl].

Raman analyses were performed with a confocal microRaman system (LabRAM ARAMIS, Horiba Jobin Yvon, Longjumeau, France) equipped with a confocal microscope (BX41, Olympus) and a motorized x, y stage. To ensure high spatial resolution, the measurements were conducted with a high numerical aperture (NA=1.40) oil immersion microscope objective (UPLSAPO 100XO, Olympus), and a 532 nm diode-pumped solid state laser (Ventus VIS 532, Laser Quantum, Cheshire, UK). Immersion oil was used as the medium between the objective and the glass cover. The theoretical lateral resolution on the sample was about 0.23 μm (0.61λ/NA), where λ is the wavelength of the laser and NA is the numerical aperture of the microscope objective. The incident laser power on the sample was approximately 10 mW. Scattered Raman light was detected by a charge-coupled device (CCD) detector behind either a 300 or 1800 lines/mm grating. A confocal pinhole diameter of 300 μm was used for all experiments.

To obtain high-quality spectra and avoid damaging the wood samples with the heat

from the laser during the point analysis, the Raman spectra were measured in 10 cycles, with each cycle consisting of a 1-s integration time for one spot. 10 spectra were obtained and averaged, and the averaged spectra from 10 different locations were again averaged. The grating used in the point analysis was 1800 lines/mm. For line analysis, measurements were conducted in 0.3 μm steps and the spectra were obtained by averaging 4 cycles, each with a 0.3 s integration time. For mapping analysis, measurements were conducted every 0.4 μm steps and the spectra were obtained by averaging 4 cycles, each with a 0.2 s integration time. The grating used for line analysis and mapping was 300 lines/mm.

The data acquisition and analysis was done by means of LabSpec5 software (Horiba Jobin Yvon). To remove the background from fluorescence, the raw spectral data were baseline-corrected. The smoothing to reduce spectral noise was performed with the Savitzky-Golay algorithm. In the point analysis, to clarify differences in the spectra after [C2mim][Cl] treatment, the spectra were normalized using an internal reference band. In this study, the strong band of an aromatic ring around 1600 cm^{-1}, which has superior chemical stability under the present ionic liquid treatment conditions, was selected.

2.3 Results and discussion

2.3.1 Morphological changes of *Fagus crenata* treated with [C2mim][Cl]

Figure 2.2 shows the light micrographs of the transverse sections treated with [C2mim][Cl] at 120°C for 0 and 72 h. Significant morphological changes such as dissociation and collapse of wood cells were not observed after 72 h of treatment (Fig. 2.2b). In the previous study on liquefaction of *Fagus crenata* by [C2mim][Cl] treatment, 95% of wood were found to be liquefied after treatment at 120°C for 24 h (Miyafuji et al. 2009). Although the reaction was processed by stirring in the previous experiment, the samples in this study were only soaked in [C2mim][Cl] without stirring. This is reason why wood cells were not liquefied completely as shown in Fig. 2.2 even after 72 h of treatment. In the previous study on morphological changes produced by [C2mim][Cl] treatment of wood tissues of *Cryptomeria japonica* (Miyafuji and Suzuki 2012), wood

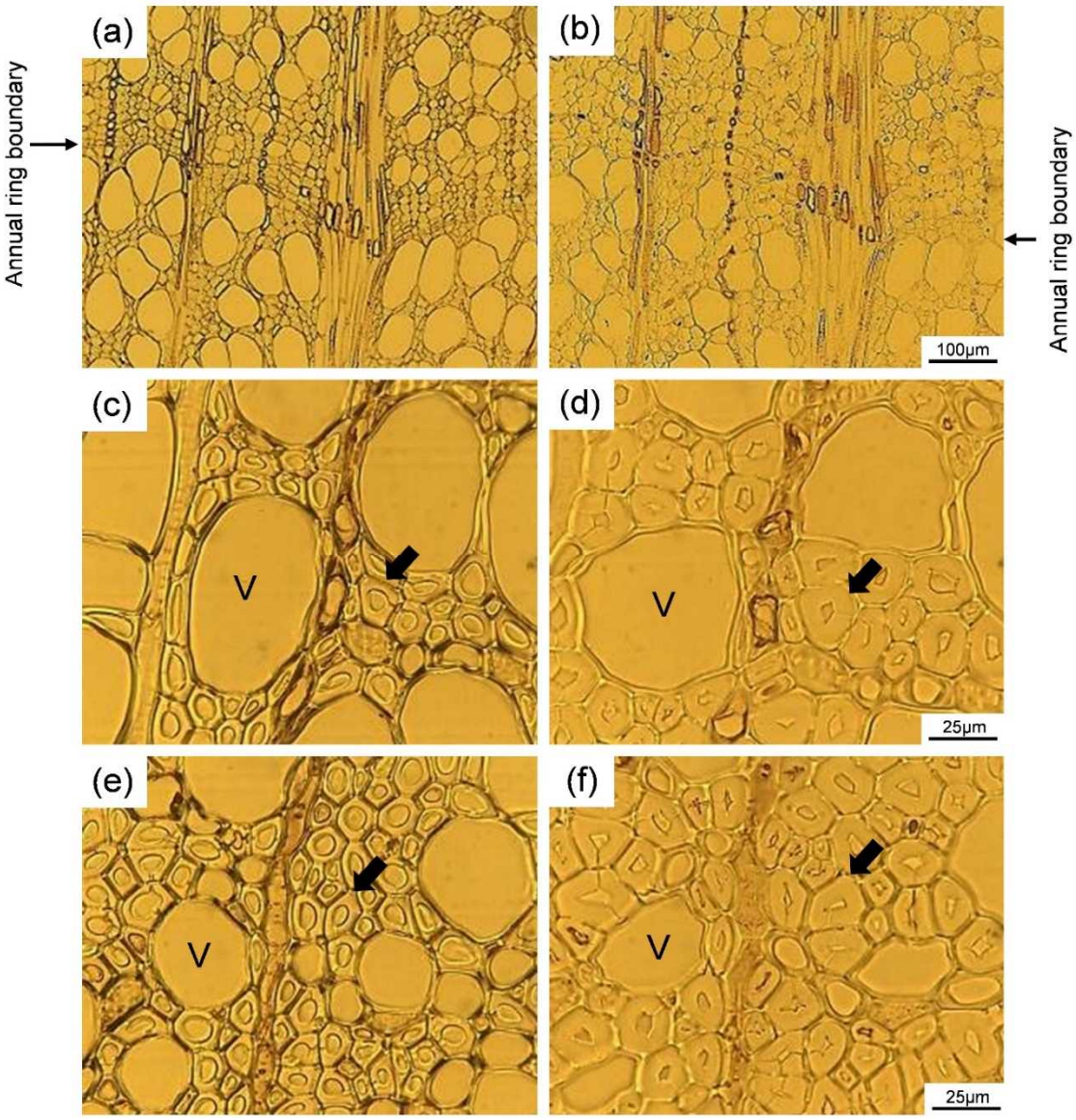

Fig. 2.2 Light microscopy images of transverse sections before and after treatment with [C2mim][Cl] at 120°C for (a, c, e) 0 h and (b, d, f) 72 h. (a, b) Around annual ring boundary. (c, d) Magnified view of earlywood. (e, f) Magnified view of latewood. *V*: vessel, *arrow*: wood fiber.

cells in latewood were dissociated, while such dissociation was not seen in earlywood. Thus the morphological changes of wood cells are different for each wood species. Closer investigation shows that, for *Fagus crenata*, the cell walls of wood fibers in both latewood and earlywood (indicated by arrows) swelled significantly (Fig. 2.2d, f). Although the cell walls of vessels in both latewood and earlywood (indicated by V) were round in shape at 0 h (Fig. 2.2c, e), they became distorted after treatment (Fig. 2.2d, f), but did not show the significant swelling observed for wood fibers. The vessels were compressed by many other swollen tissues, such as the surrounding wood fibers.

To study the swelling behavior of wood fibers and vessels upon [C2mim][Cl] treatment in detail, the author used image analysis software to determine the cell lumen area, cell wall area, and total of cell lumen area + cell wall area (defined in Fig. 2.1). The results obtained are shown in Fig. 2.3. In both latewood and earlywood, the cell lumen area of wood fibers decreases sharply to nearly zero. The cell wall area and the total of cell lumen area + cell wall area increase significantly in the initial stages of [C2mim][Cl] treatment (Fig. 2.3a). After these changes, the cell wall area and the total of cell lumen area + cell wall area increase much more gradually with prolonged treatment time. At the same time, the cell lumen area increased slightly. After 72 h of treatment, the cell wall areas in both latewood and earlywood had increased by a factor of approximately 4.

For vessels in earlywood, the cell lumen area and the total of cell lumen area + cell wall area initially decrease, while cell wall area increases, during [C2mim][Cl] treatment (Fig. 2.3b). After these initial changes, both the cell lumen area and the total of cell lumen area + cell wall area decrease gradually during further [C2mim][Cl] treatment. Meanwhile, the cell wall area increases gradually. These results indicate that cell walls of vessels in earlywood swelled towards the cell lumen without swelling outwards. Similar trends are observed for swelling of vessels in latewood, although the areas are smaller than those for vessels in earlywood. That is, the cell walls swelled toward the cell lumen, and the vessels were compressed by surrounding swollen tissues.

Overall, wood fibers swell much more than vessels. The increase in the total of cell lumen area + cell wall area of wood fibers counterbalances the decrease in the total cell lumen area + cell wall area of vessels that are distributed between wood fibers. This

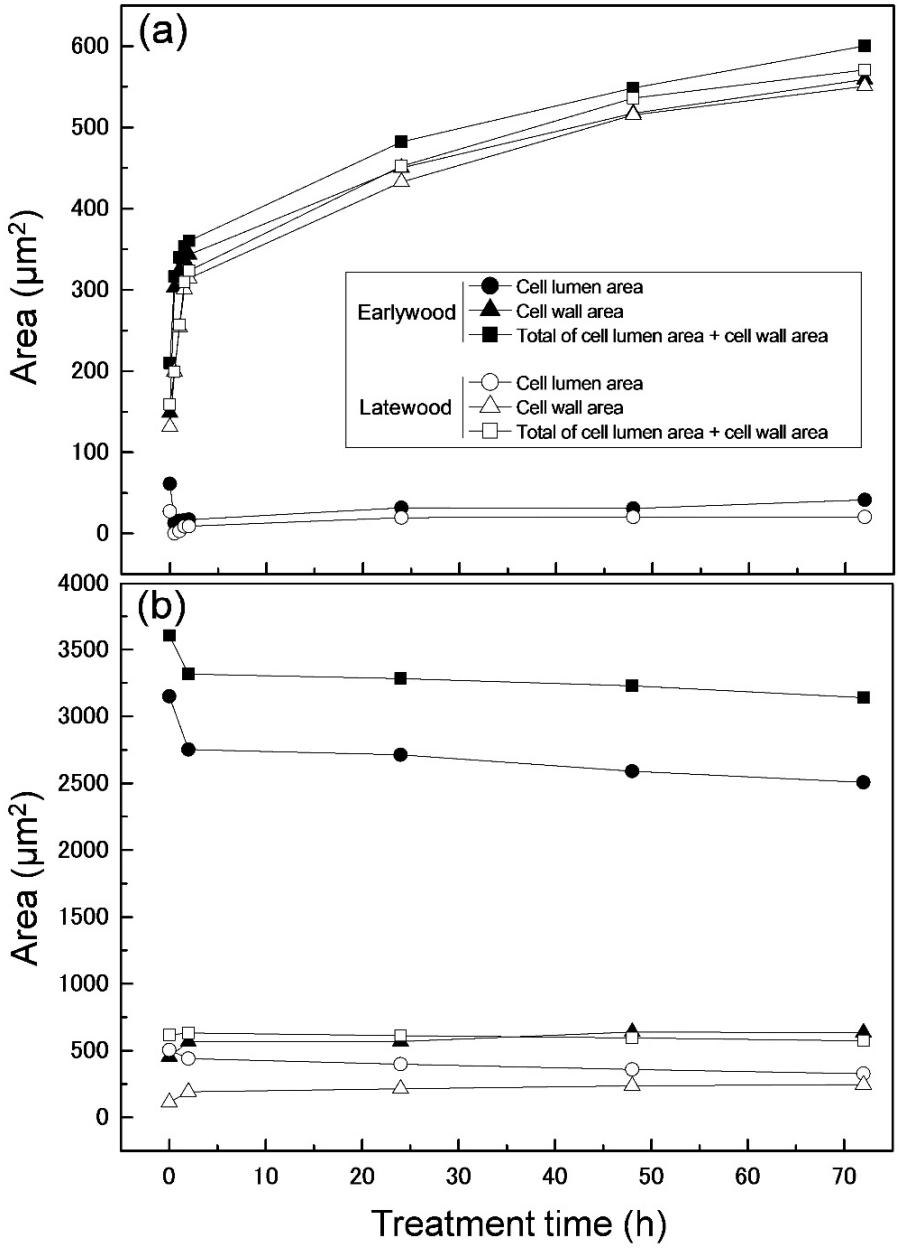

Fig. 2.3 Changes in cell wall area, cell lumen area and total of cell lumen area + cell wall area for (a) wood fiber and (b) vessel of *Fagus crenata* during [C2mim][Cl] treatment.

balance prevents dissociation and collapse of wood tissues.

Figure 2.4 shows light micrographs of ray parenchyma cells (a–d) and axial parenchyma cells (e, f) before and after treatment with [C2mim][Cl] at 120°C for 72 h. It was found that parenchyma cells swelled towards the cell lumen. After 72 h of treatment, the cell wall area of parenchyma cells increased by a factor of no more than 1.5, whereas the cell wall area of wood fibers increased by a factor of 4. Therefore, compared with the wood fibers shown in Fig. 2.2b, d, the degree of swelling for parenchyma cells was slight. After 72 h of treatment, the cell wall thickness along fiber direction increased by 2 times, whereas the cell wall thickness along tangential direction increased by 1.4 times. Thus, ray parenchyma cell walls (as observed from the tangential section) greatly swelled along the fiber direction (Fig. 2.4d). Compared with the wood fibers shown in Fig. 2.2b, d, the degree of swelling was slight. In addition, ray parenchyma cell walls (as observed from the tangential section) greatly swelled along the fiber direction (Fig. 2.4d). Some resinoids in the parenchyma cells can still be seen after treatment with [C2mim][Cl]. Thus, these resinoids are not dissolved in [C2mim][Cl].

Figure 2.5 shows SEM images of transverse sections before and after treatment with [C2mim][Cl] at 120°C for 72 h. Cracks are observed at the boundary of the annual ring and between ray parenchyma and peripheral tissues, as indicated by arrows (Fig. 2.5b), although such cracks were not seen in light microscope images of the transverse section (Fig. 2.2). This difference is most likely because the bonds between ray parenchyma and tissue adjacent to ray parenchyma, and at boundary of earlywood and latewood, were weakened by [C2mim][Cl] treatment, allowing significant cracking during the drying process required to prepare the samples for SEM. From the magnified views of earlywood and latewood, the author observed that the cell walls of various tissues are distorted after 72 h of treatment (Fig. 2.5d, f). As shown in Figs. 2.2, 2.3 and 2.5, there are no significant differences between the morphological changes of latewood and earlywood.

Figure 2.6 shows SEM images of vessel perforations before and after treatment with [C2mim][Cl]. Although the perforation rim was unchanged after 72 h of treatment (Fig. 2.6b), the scalariform perforation plate was distorted (Fig. 2.6d).

Figure 2.7 shows SEM images of two kinds of parenchyma cells before and after

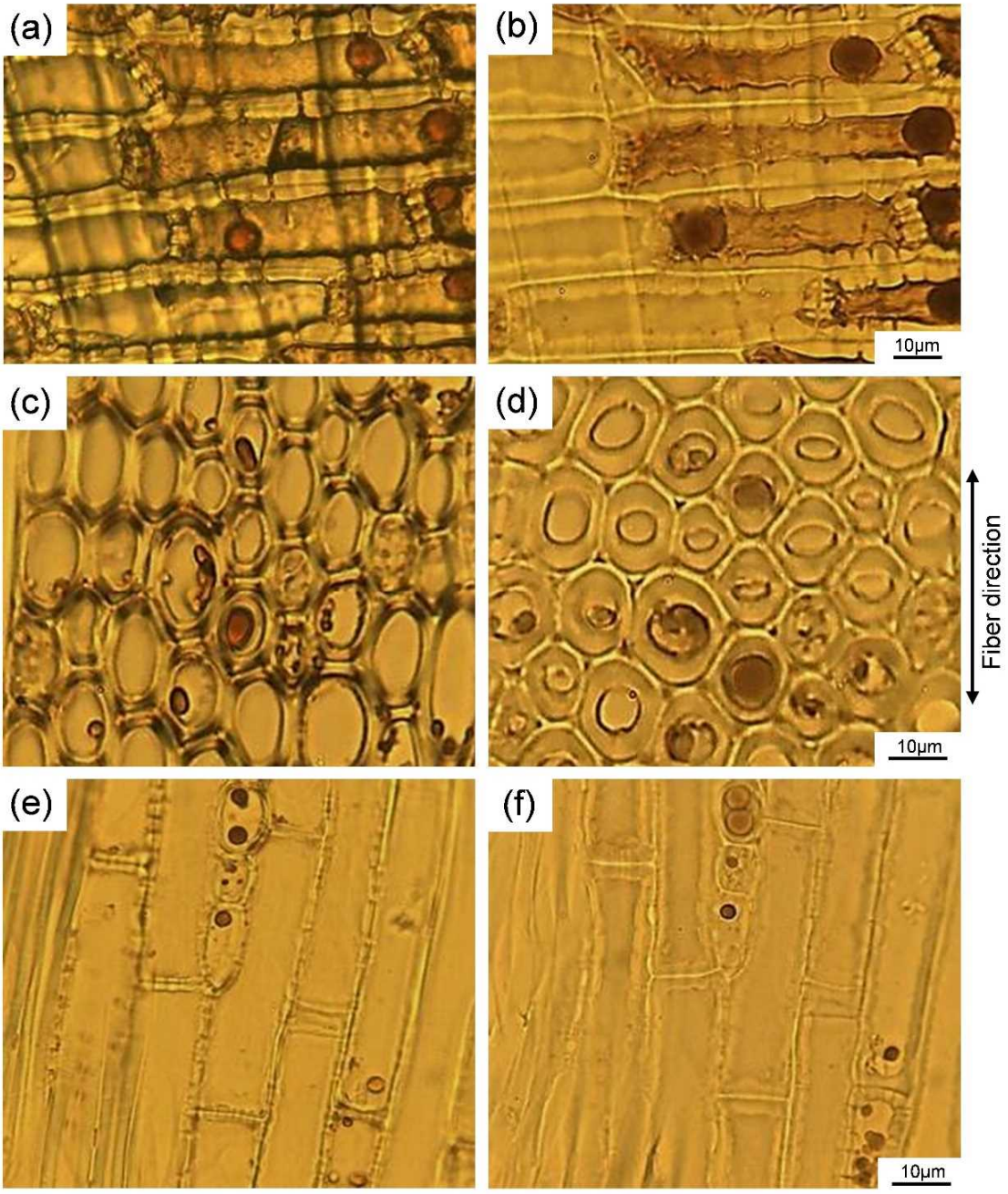

Fig. 2.4 Light microscopy images of parenchyma cells before and after treatment with [C2mim][Cl] at 120°C for (a, c, e) 0 h and (b, d, f) 72 h. (a, b) Ray parenchyma in radial section. (c, d) Ray parenchyma in tangential section. (e, f) Axial parenchyma.

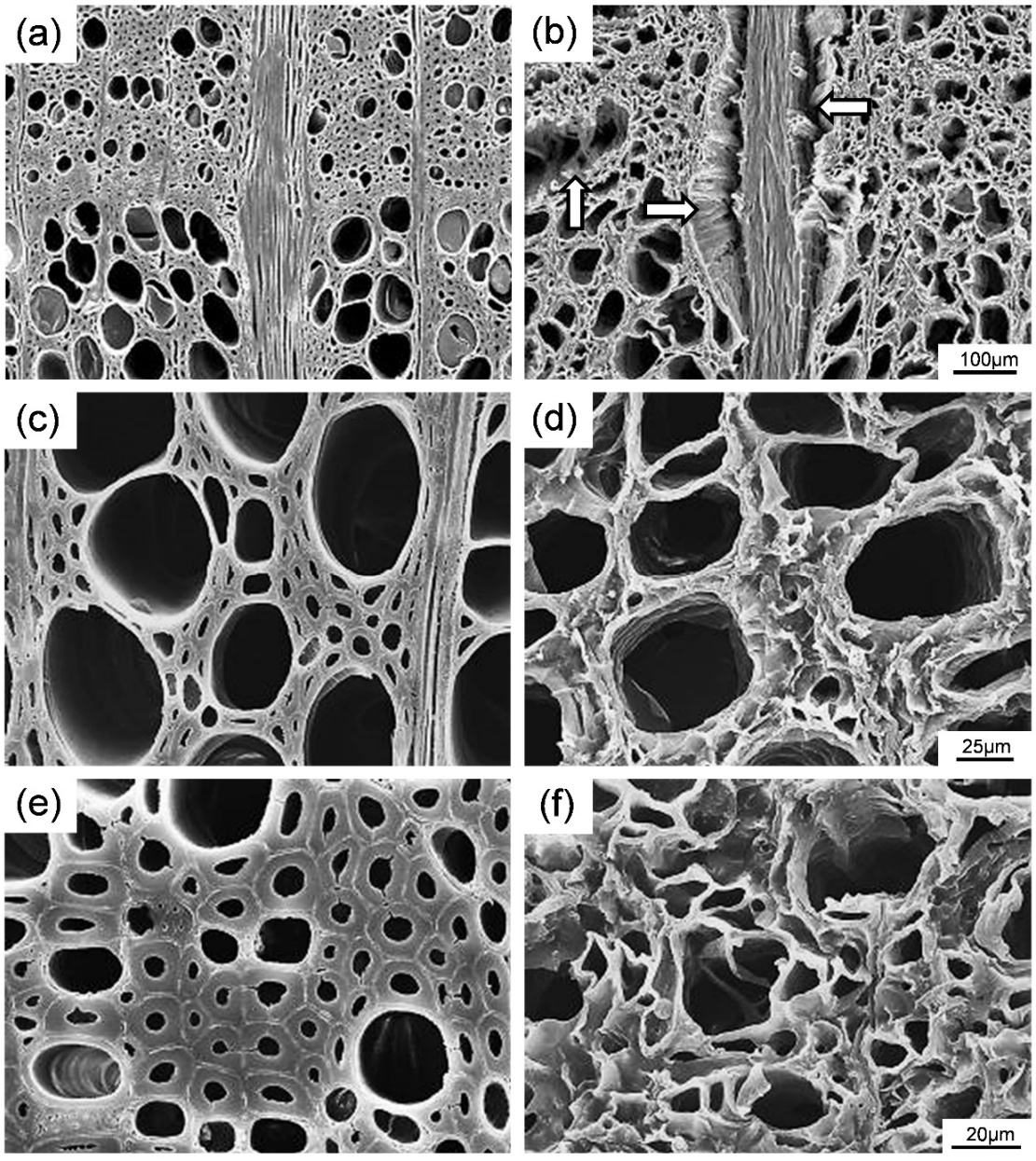

Fig. 2.5 SEM images of transverse section before and after treatment with [C2mim][Cl] at 120°C for (a, c, e) 0 h and (b, d, f) 72 h. (a, b) Boundary of earlywood and latewood. (c, d) Earlywood. (b, d, f) Latewood. *arrow*: crack.

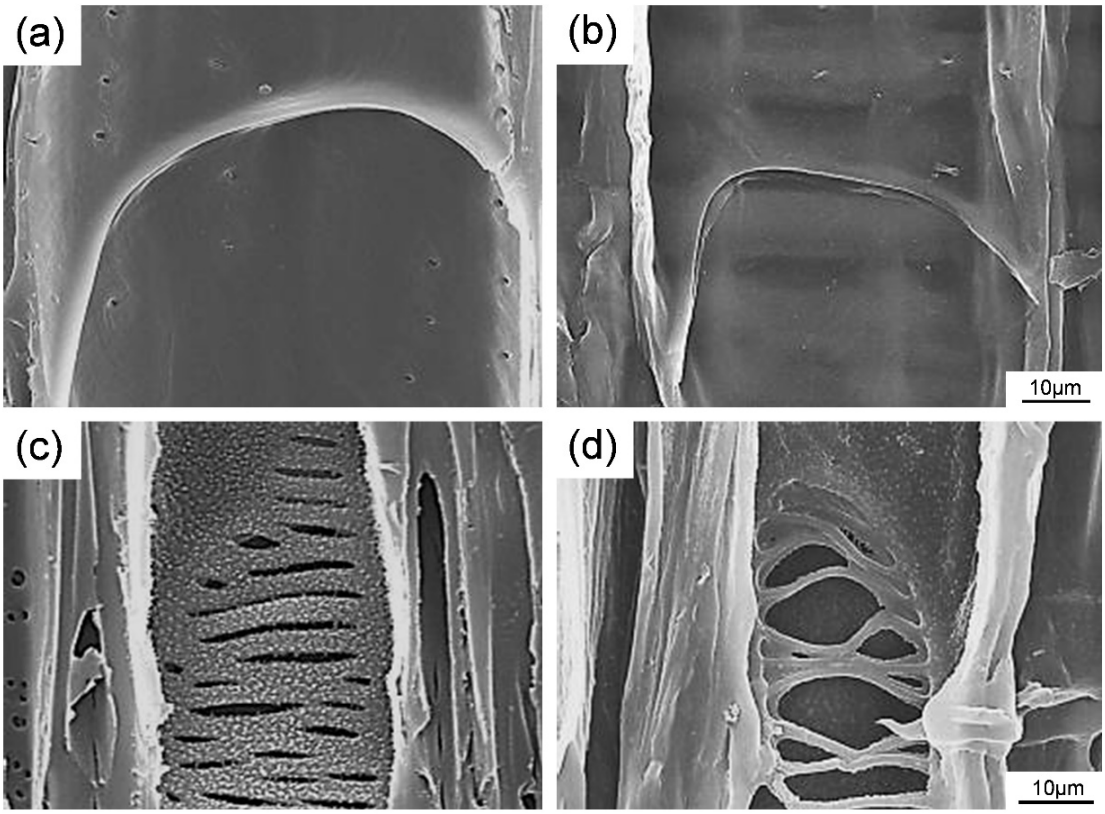

Fig. 2.6 SEM images of vessel perforations before and after treatment with [C2mim][Cl] at 120°C for (a, c) 0 h and (b, d) 72 h. (a, b) Perforation rim. (c, d) Scalariform perforation plate.

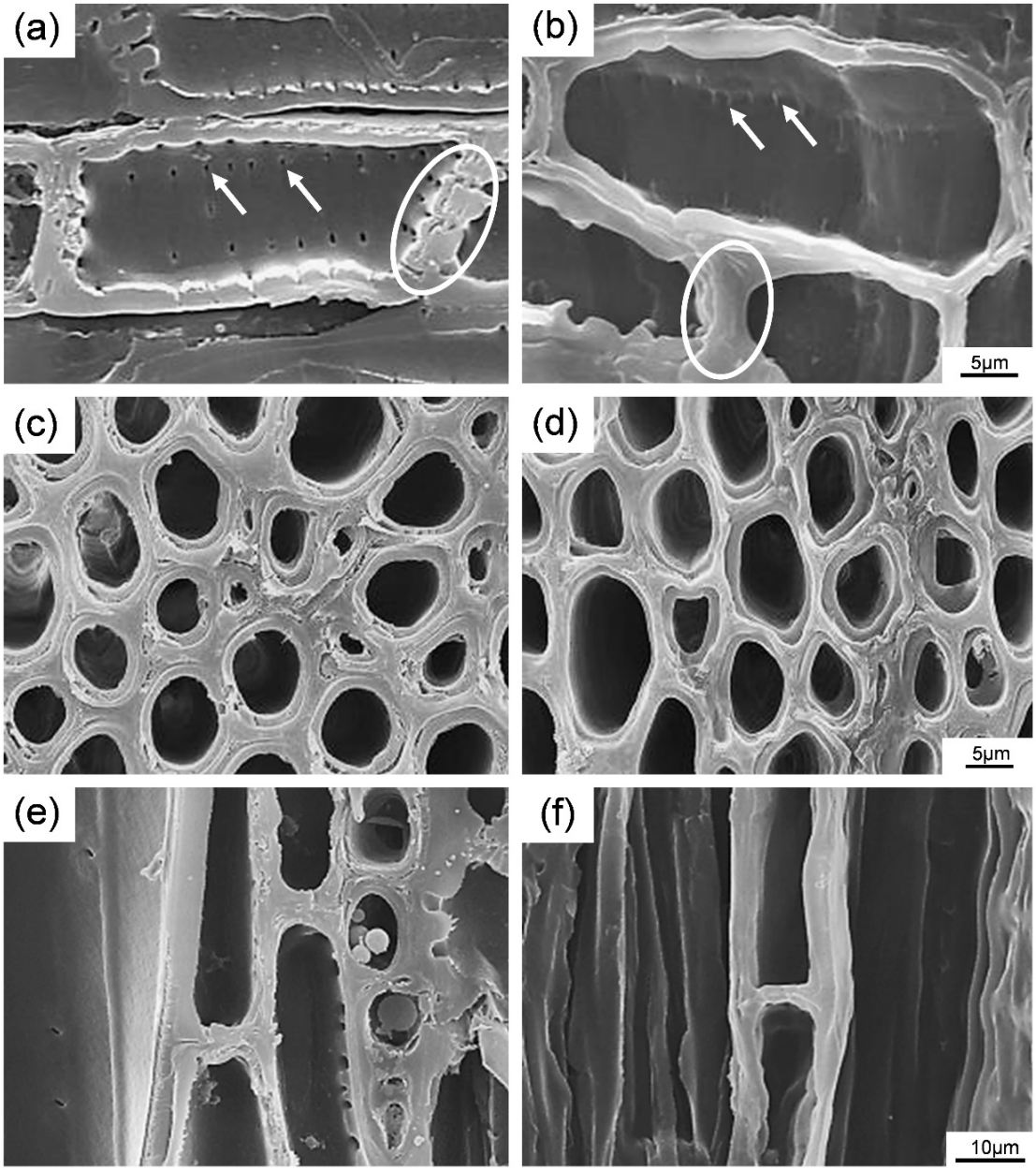

Fig. 2.7 SEM images of parenchyma before and after treatment with [C2mim][Cl] at 120°C for (a, c, e) 0 h and (b, d, f) 72 h. (a, b) Ray parenchyma in radial section. (c, d) Ray parenchyma in tangential section. (e, f) Axial parenchyma.

treatment with [C2mim][Cl]. As shown in Fig. 2.5, wood fibers were distorted by [C2mim][Cl] treatment. In contrast, ray and axial parenchyma cells retained their original shapes, although their surfaces were smoothed down (Fig. 2.7b, d, f). In addition, the pits of ray parenchyma cells were occluded after 72 h of treatment, as indicated by arrows and circles (Fig. 2.7b). These morphological changes occur because the parenchyma cells start to be liquefied by [C2mim][Cl] treatment.

Figure 2.8 shows SEM images of vessel pits. Intervascular pits of both vessels (Fig. 2.8b) and small vessels (Fig. 2.8d) were occluded after 72 h of treatment, as indicated by arrows. However, ray-vessel pits were not occluded; instead, large holes can be seen in ray-vessel pits because the pit membranes are broken after 72 h of treatment (Fig. 2.8f). These differences between the morphological changes of the two kinds of pits may be because of the difference in their diameters. The diameter of intervascular pits is smaller than that of ray-vessel pits. Small pits are thought to be easily occluded when wood cell walls are swollen during [C2mim][Cl] treatment. Simultaneously, they then become stuck shut by the liquefaction reaction with [C2mim][Cl]. However, large pits such as ray-vessel pits are not completely occluded, even after [C2mim][Cl] treatment. Instead, only the pit membranes were liquefied by [C2mim][Cl]. In the small vessels, many warts existed on the surface of cell lumen area; however, they became fewer and smaller after 72 h of treatment (Fig. 2.8d). In the previous paper on liquefaction of wood, lignin and hemicelluloses are found to be liquefied more slowly than cellulose (Miyafuji et al. 2009; Nakamura et al. 2010a). Because the warts consist of hemicelluloses and lignin (Jansen et al. 1998; Watanabe et al. 2006), they partly retain their original shapes after [C2mim][Cl] treatment, as shown in Fig. 2.8d.

2.3.2 Comparative study on morphological changes in hardwoods treated with [C2mim][Cl]

Light micrographs of the transverse sections treated with [C2mim][Cl] at 120°C for 0 and 72 h are shown in Fig. 2.9. The cell walls of all wood samples (indicated by open arrows or asterisks) swelled significantly after 72 h of treatment (Fig. 2.9D–F). The cell walls of

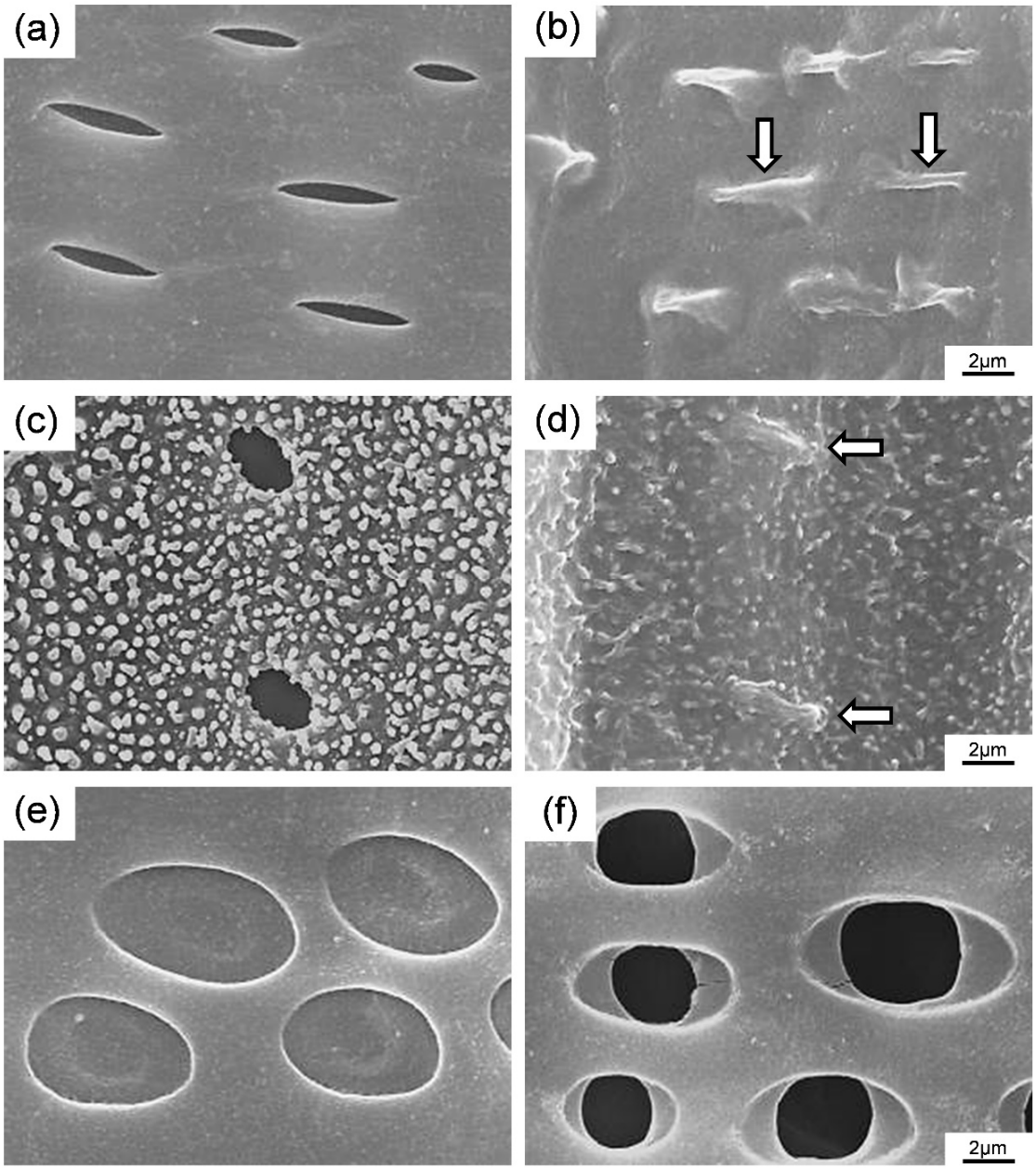

Fig. 2.8 SEM images of vessel pits treated with [C2mim][Cl] at 120°C for (a, c, e) 0 h and (b, d, f) 72 h. (a, b) Intervascular pits. (c, d) Intervascular pits of small vessel. (e, f) Ray-vessel pits.

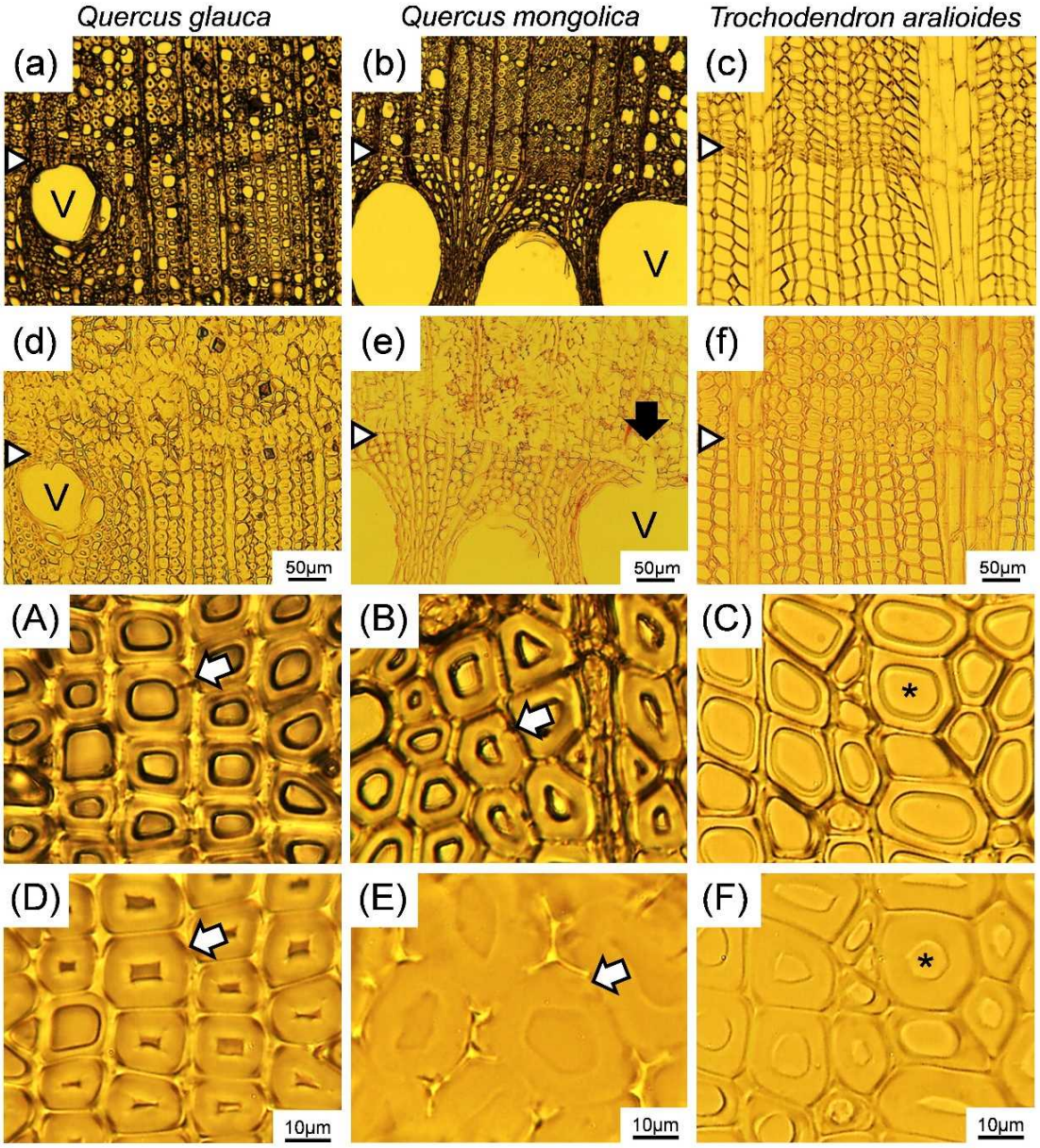

Fig. 2.9 Light microscopy images of transverse sections before and after treatment with [C2mim][Cl] at 120°C for (a–c, A–C) 0 h and (d–f, D–F) 72 h. (a–f) Around annual ring boundary. (A–F) Magnified view of (a–f). *V*: vessel, *open arrowhead*: annual ring boundary, *open arrow*: wood fiber, *asterisk*: tracheid, *filled arrow*: crack.

Quercus glauca and *Quercus mongolica* in latewood became slightly disordered and dissociated partially, but in earlywood, were well ordered after 72 h of treatment (Fig. 2.9d, e). Cracks (indicated by filled arrow) occurred in the vessels of *Quercus mongolica*. On the other hand, the cell walls of *Trochodendron aralioides* in both latewood and earlywood were well ordered after 72 h of treatment (Fig. 2.9f). In the previous studies on the morphological changes by [C2mim][Cl] treatment, the cell walls of the tracheids of *Cryptomeria japonica* that is softwood were dissociated in latewood but not in earlywood (Miyafuji and Suzuki 2011, 2012). Meanwhile, the wood fibers of *Fagus crenata* that is hardwood only swelled significantly and were not dissociated in both latewood and earlywood (Figs. 2.2, 2.3).

To analyze the swelling behavior of wood fibers during [C2mim][Cl] treatment in detail, the author used image analysis software to determine the cell lumen area, cell wall area, and total cell lumen area + cell wall area (defined in Fig. 2.1). Figures 2.10 and 2.11 show results obtained for earlywood and latewood, respectively (Figs. 2.10c and 2.11c refer to the data shown in Fig. 2.3). Because *Trochodendron aralioides* is composed of tracheid instead of wood fiber, Figs. 2.10d and 2.11d show tracheid swelling behavior. The cell lumen area of wood fibers of all species decreases rapidly, while the cell wall area and the total of cell lumen area + cell wall area of all species except *Trochodendron aralioides* increase significantly in the initial stages of [C2mim][Cl] treatment. Although cell wall area of tracheids of *Trochodendron aralioides* increases significantly, the total of cell lumen area + cell wall area increase to some extent. Thereafter, the cell wall area and total of cell lumen area + cell wall area of the *Quercus mongolica* in both latewood and earlywood increase gradually with prolonged treatment time like *Fagus crenata*. After 72 h of treatment, the cell wall areas in latewood and earlywood had increased by 5 and 3.5 times, respectively. The swelling behavior of the other two species differs from *Quercus mongolica* and *Fagus crenata*. After changes in the initial stages, the cell wall area and total cell lumen area + cell wall area of *Quercus glauca* in the latewood increase gradually with prolonged treatment time, but level off in earlywood. Meanwhile, those of *Trochodendron aralioides* level off in both latewood and earlywood. After 72 h of treatment, the cell wall areas of *Quercus glauca* in latewood and earlywood had increased

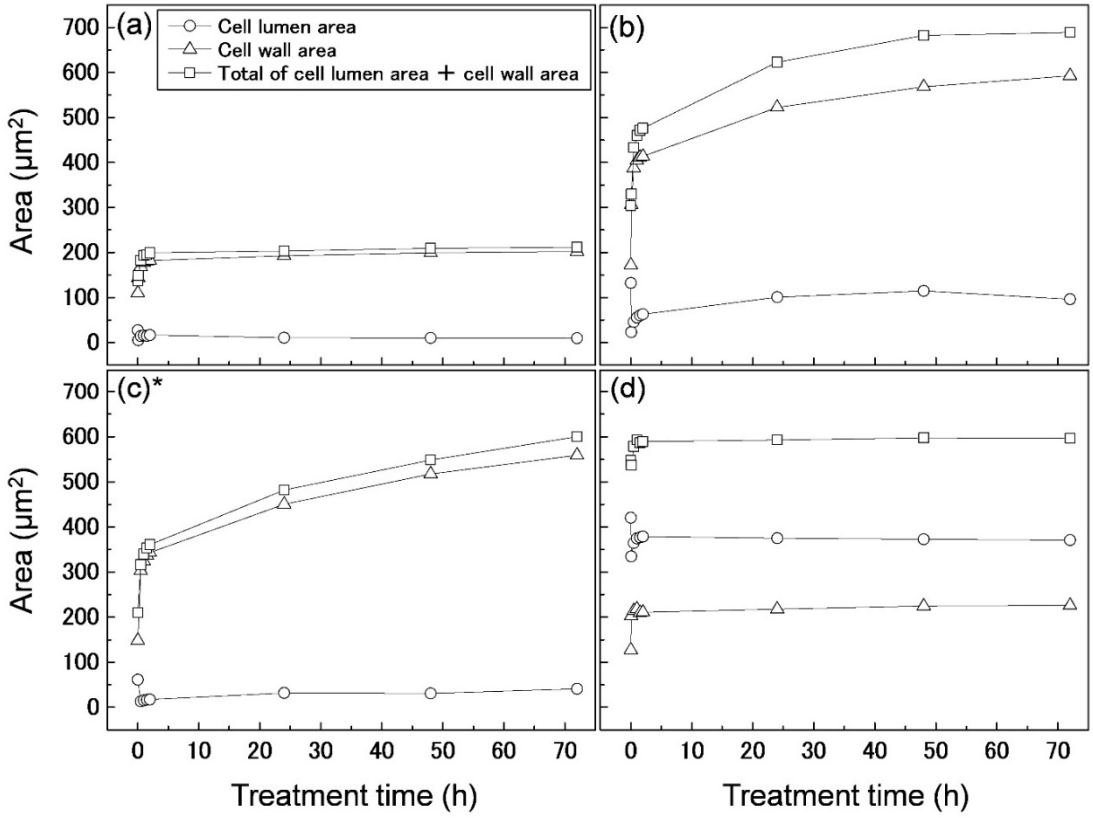

Fig. 2.10 Changes in cell wall area, cell lumen area, and total of cell lumen area + cell wall area for wood fiber of (a) *Quercus glauca*, (b) *Quercus mongolica*, (c) *Fagus crenata*, and tracheid of (d) *Trochodendron aralioides* in earlywood during [C2mim][Cl] treatment. *Refer to data in Fig. 2.3a.

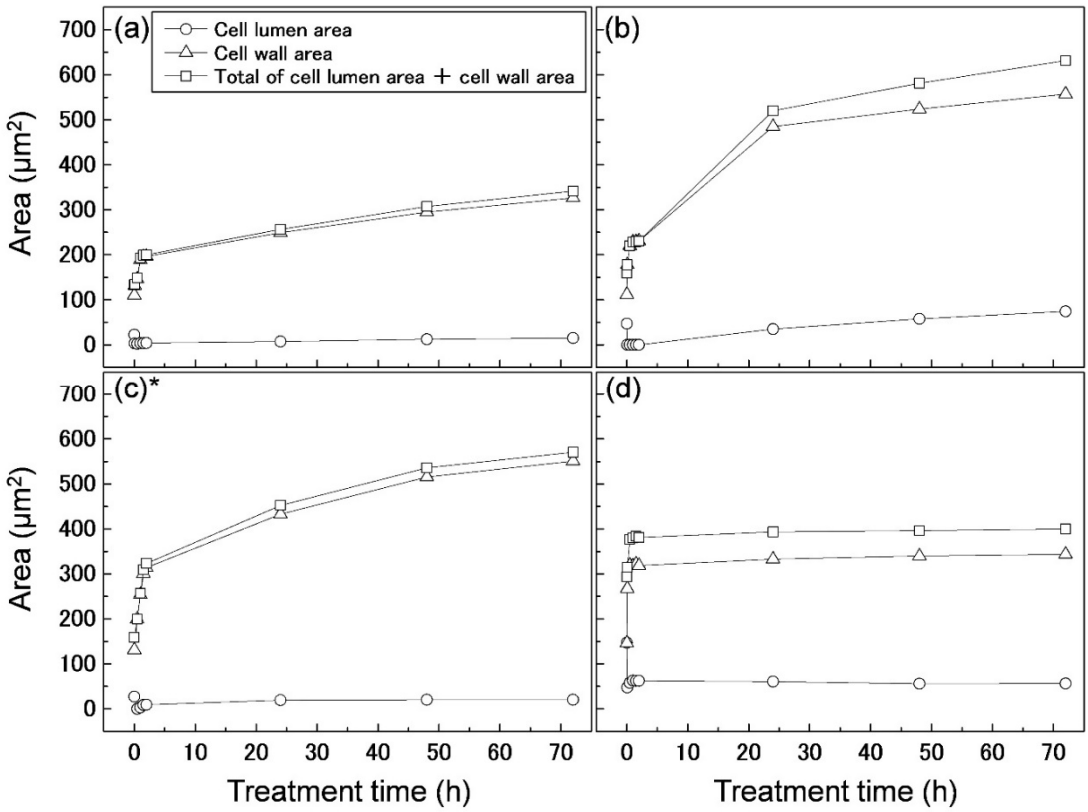

Fig. 2.11 Changes in cell wall area, cell lumen area, and total of cell lumen area + cell wall area for wood fiber of (a) *Quercus glauca*, (b) *Quercus mongolica*, (c) *Fagus crenata*, and tracheid of (d) *Trochodendron aralioides* in latewood during [C2mim][Cl] treatment. *Refer to data in Fig. 2.3a.

by 3 and 2 times, and that of *Trochodendron aralioides* in latewood and earlywood had increased by 2 and 1.5 times, respectively. The swelling behavior such as swelling ratio and time-dependent change of wood fibers during [C2mim][Cl] treatment therefore differs according to wood species and region such as latewood and earlywood.

Figure 2.12 shows SEM images of transverse sections before and after treatment for 72 h with [C2mim][Cl] at 120°C. The adjacent cell walls of wood fiber of *Quercus glauca* and *Trochodendron aralioides* are somewhat dissociated and the axial parenchyma cells of *Quercus glauca* are distorted (Fig. 2.12b, f). Axial parenchyma cells of *Trochodendron aralioides* could not be found after [C2mim][Cl] treatment, because they are present in small amounts only in latewood. Conversely, the cell walls of the wood fiber of *Quercus mongolica* were collapsed significantly, but the axial parenchyma cells (indicated by arrows) maintained their shape (Fig. 2.12d). These morphological changes could not be found in light microscopy images. It is necessary to dry the samples as pretreatment for SEM observation. The morphological changes such as dissociation and distortion in SEM images are due to shrinkage of the cell walls which swelled by [C2mim][Cl] during drying process. The swelling ratio of the wood fibers of *Quercus mongolica* was higher than the other two species as in Figs. 2.10 and 2.11. Therefore, the degree of cell wall shrinkage during drying increased and they showed remarkable deformation. The reasons for the difference in morphological changes between the wood fiber and axial parenchyma cells of *Quercus mongolica* are unclear but result from differences in chemical composition and tissue structure of the two kinds of cells. As the one reason, there is difference in chemical composition. The lignin concentration of the axial parenchyma cells is reported to be higher than that of the wood fibers (Fujii et al. 1987). In the previous studies on the liquefaction of wood (Miyafuji et al. 2009; Nakamura et al. 2010a), it was found that lignin has a higher resistance to [C2mim][Cl] than cellulose and hemicellulose. Thus, the reactivity of the axial parenchyma cells is thought to be lower than that of wood fibers. As another reason, there is difference in tissue structure. The axial parenchyma cells are separated into compartments by end walls. Because of the presence of the end walls, the cell walls of the axial parenchyma can resist the force perpendicular to the fiber axis. The morphological changes are therefore different from the wood fibers and the axial paren-

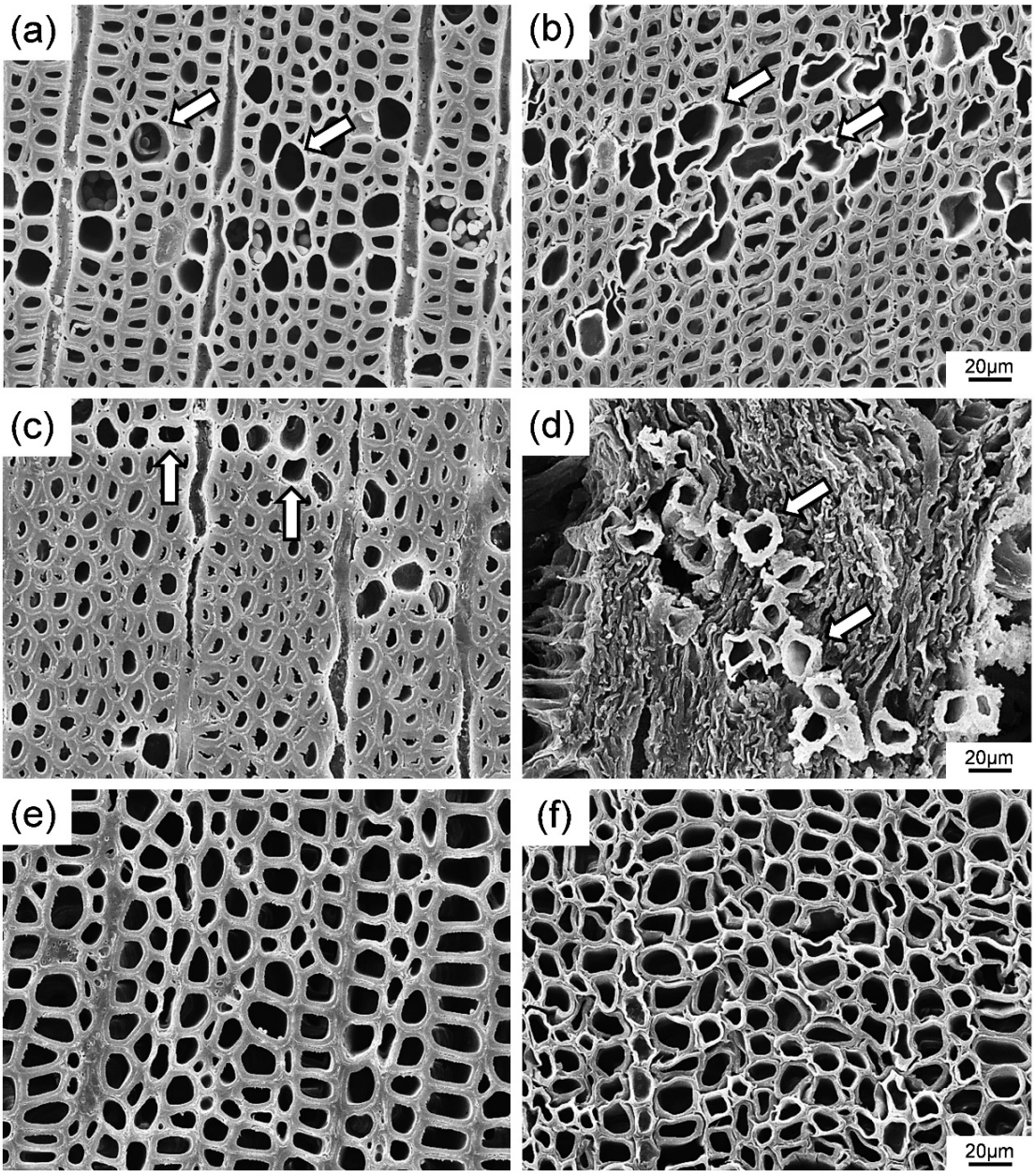

Fig. 2.12 SEM images of transverse section before and after treatment with [C2mim][Cl] at 120°C for (a, c, e) 0 h and (b, d, f) 72 h. (a, b) *Quercus glauca*. (c, d) *Quercus mongolica*. (e, f) *Trochodendron aralioides*. *open arrow*: axial parenchyma cell.

chyma cells.

Figure 2.13 shows light micrographs of ray parenchyma cells before and after treatment with [C2mim][Cl] at 120°C for 0 and 72 h. The lumen of ray parenchyma cells of *Quercus glauca* (Fig. 2.13b) and *Trochodendron aralioides* (data not shown) maintained their round shape after treatment for 72 h, whereas that of *Quercus mongolica* became elliptical (Fig. 2.13d) like that of *Fagus crenata*.

To study the swelling behavior of ray parenchyma cells during [C2mim][Cl] treatment in detail, the author used image analysis software for determining the cell wall area and thickness in the fiber and tangential direction. Results obtained as a swelling ratio calculated from Eq. 2.1 are shown in Table 2.1:

$$\text{Swelling ratio} = \frac{Cell\ wall\ area\ or\ cell\ wall\ thickness\ after\ treatment}{Cell\ wall\ area\ or\ cell\ wall\ thickness\ before\ treatment} \qquad (2.1)$$

After treatment for 72 h, the cell wall area of the ray parenchyma cells of all species increased by approximately 1.3–1.5. The cell wall area of the wood fibers increased significantly with the exception of the earlywood of *Trochodendron aralioides* as in Figs. 2.10 and 2.11. Therefore, in general, the degree of swelling for the ray parenchyma cells is lower than the wood fibers. The differential shrinkage and swelling by moisture is attributed mainly to the cell wall structure (Tsoumis 1991). Swelling of the cell walls is mainly caused by swelling of the amorphous region between microfibrils, and bundles of the microfibrils swell extensively in the perpendicular direction. The lower the microfibril angle for the longitudinal cell axis, the higher the swelling perpendicular to the longitudinal cell axis. In wood fibers, the S_2 that is usually oriented 5–20° to the fiber axis occupies a large area (Parham and Gray 1984). In ray parenchyma cells, S_1 and S_3 of the secondary wall that are oriented 30–60° to the longitudinal cell axis are thicker than the other layers (Wardrop and Dadswell 1952). Therefore, the occupancy rate and microfibril angle of their thickest layers affect their swelling behavior significantly and the wood fibers may swell more than the ray parenchyma cells during [C2mim][Cl] treatment. Other causes for the difference in swelling ratio may be the difference in chemical compo-

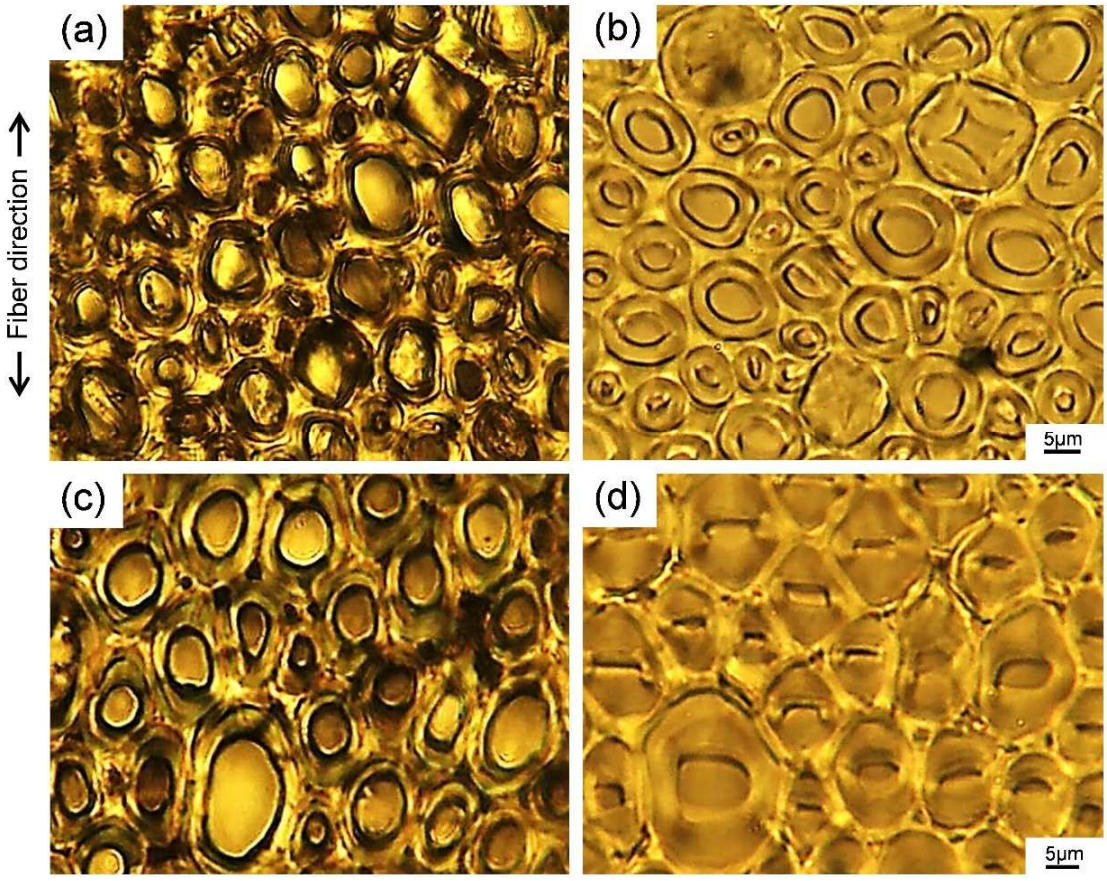

Fig. 2.13 Light microscopy images of ray parenchyma before and after treatment with [C2mim][Cl] at 120°C for (a, c, e) 0 h and (b, d, f) 72 h. (a, b) *Quercus glauca*. (c, d) *Quercus mongolica*.

Table 2.1 Swelling ratio of cell wall area and thickness of ray parenchyma cells after treatment for 72 h with [C2mim][Cl] at 120°C.

Wood samples	Cell wall area	Cell wall thickness	
		Fiber direction	Tangential direction
Quercus glauca	1.32	1.21	1.20
Quercus mongolica	1.41	1.66	1.33
Trochodendron aralioides	1.39	1.34	1.39
Fagus crenata	1.49	2.02	1.42

Swelling ratio = cell wall area or cell wall thickness after treatment/cell wall area or cell wall thickness before treatment.

sition. The lignin concentration of ray parenchyma cells is reported to be 1.5 times higher that of wood fibers (Eriksson et al. 1988). Ray parenchyma cells react with difficulty with [C2mim][Cl]. The cell wall thickness of *Quercus glauca* and *Trochodendron aralioides* increased in the fiber and tangential direction in almost the same ratio while that of *Quercus mongolica* and *Fagus crenata* increased significantly in the fiber direction in comparison with the tangential direction after [C2mim][Cl] treatment.

Figure 2.14 shows SEM images of various pits before and after treatment for 72 h with [C2mim][Cl] at 120°C. Ray-vessel pit membranes of *Quercus glauca* were broken after 72 h of treatment (Fig. 2.14b). This is similar to that of *Fagus crenata* (Fig. 2.8f). However, the ray-vessel pit membranes of *Quercus mongolica* protrude towards the lumen side of the vessel without being broken (indicated by arrows in Fig. 2.14d). This suggests that the ray-vessel pit membranes of *Quercus mongolica* are hardly liquefied by [C2mim][Cl]. No change in ray-ray pits was observed for all species studied in this paper (results for *Quercus glauca* only are shown here Fig. 2.14f). However, the ray-ray pits of *Fagus crenata* were occluded after 72 h of treatment (Fig. 2.8b).

2.3.3 Raman microscopic analysis of *Cryptomeria japonica* after treatment with [C2mim][Cl]

Figures 2.15–2.17 shows the Raman spectra for S_2, CML and CC of tracheids treated with [C2mim][Cl] at 120°C for 0, 24, or 72 h. In focus was the spectral range from 350 to 3150 cm^{-1}. No spectral features were found in the region from 1710 to 2750 cm^{-1} neither before nor after treatment with [C2mim][Cl], therefore this region is not presented. The spectral features for cellulose are very similar to those of hemicellulose because cellulose and hemicellulose have similar functional groups and chemical bonds (Gierlinger et al. 2013). In addition, the bands of hemicellulose are broader, and can be hidden under the cellulose bands because of their low concentration and amorphous nature (Agarwal and Ralph 1997). The bands from cellulose and hemicellulose could not be distinguished, thus they are referred to as polysaccharides in this study.

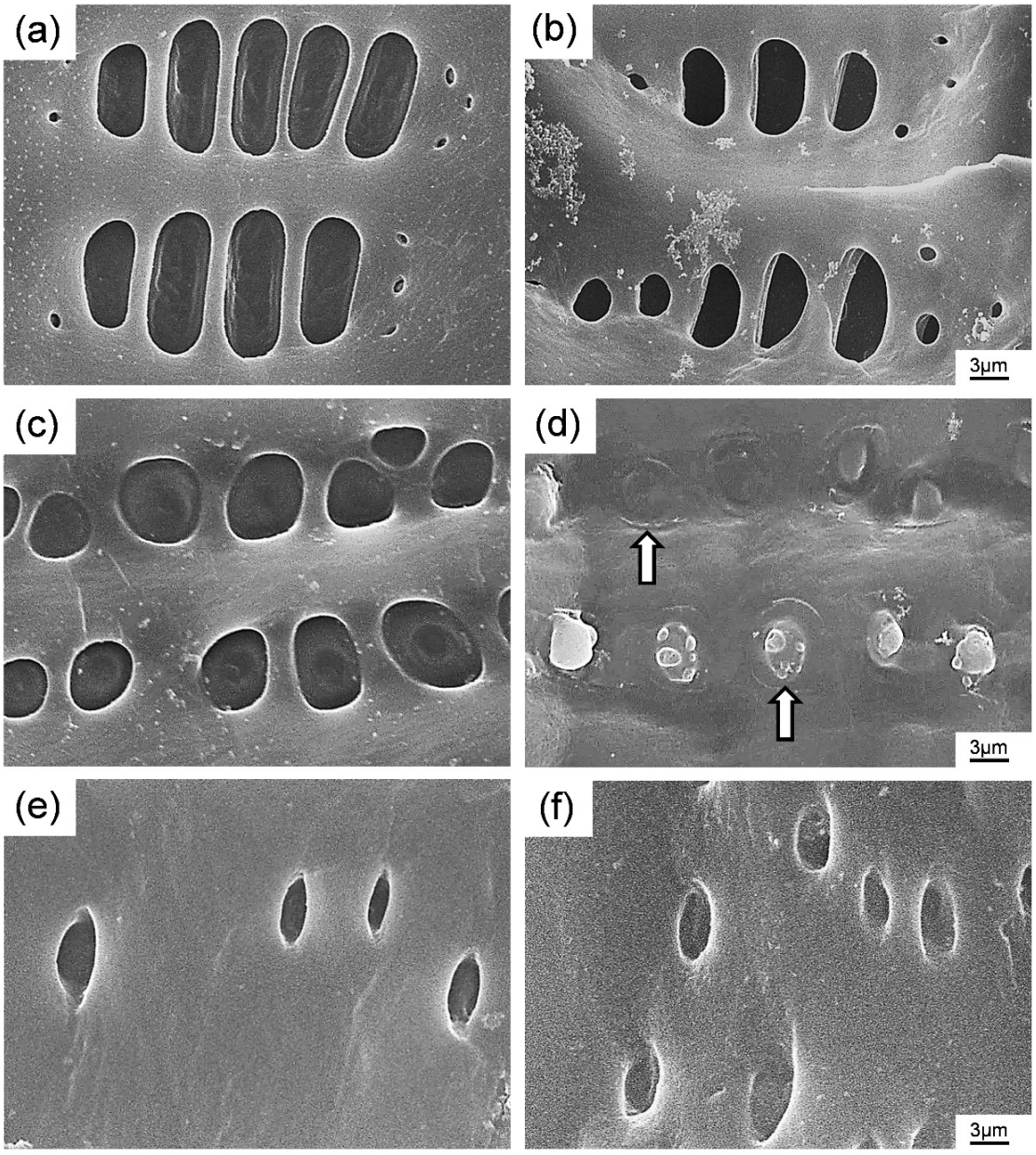

Fig. 2.14 SEM images of various pits before and after treatment with [C2mim][Cl] at 120°C for (a, c, e) 0 h and (b, d, f) 72 h. (a, b) Ray-vessel pits of *Quercus glauca*. (c, d) Ray-vessel pits of *Quercus mongolica*. (e, f) Ray-ray pits of *Quercus glauca*.

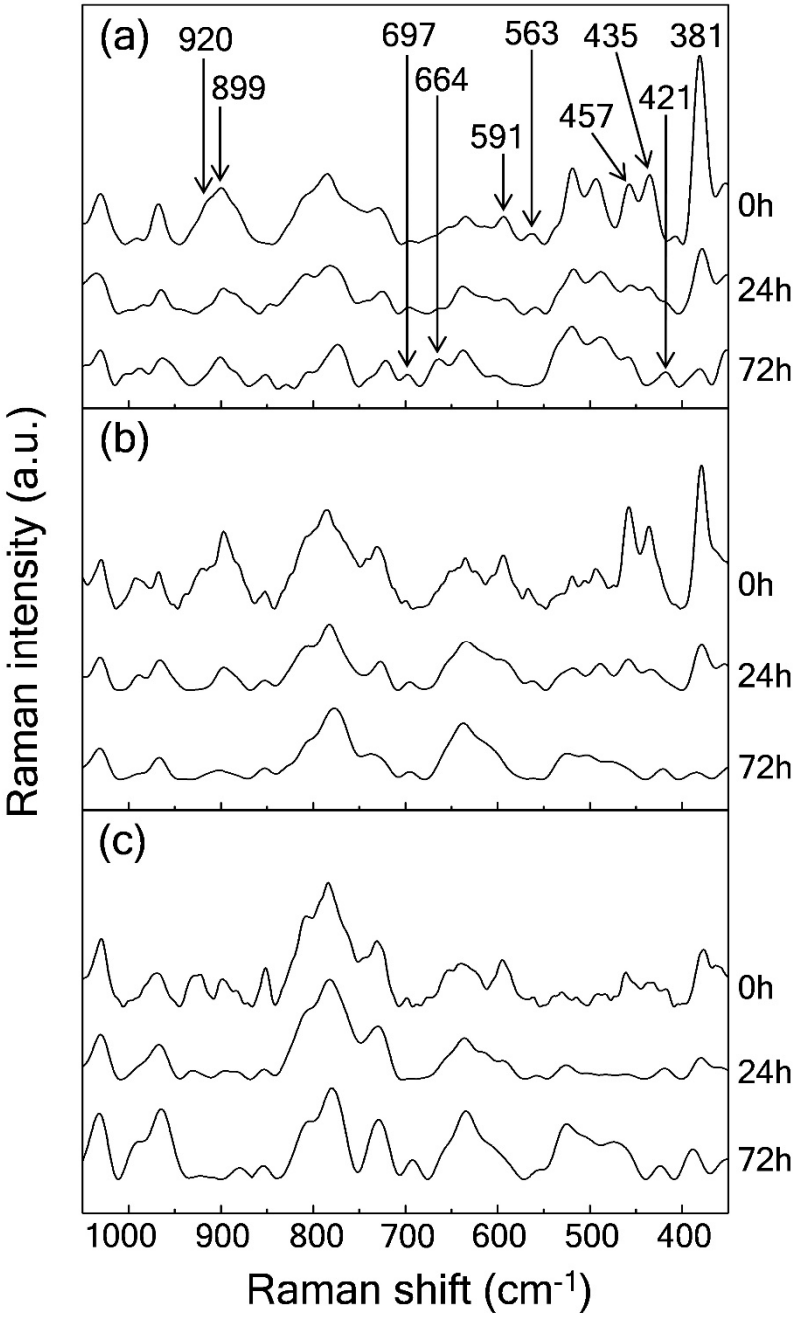

Fig. 2.15 Raman spectra for (a) S_2, (b) CML, and (c) CC of tracheids before and after treatment with [C2mim][Cl] at 120°C for 0 h, 24 h, and 72 h; enlargement of the region from 350 to 1050 cm^{-1}.

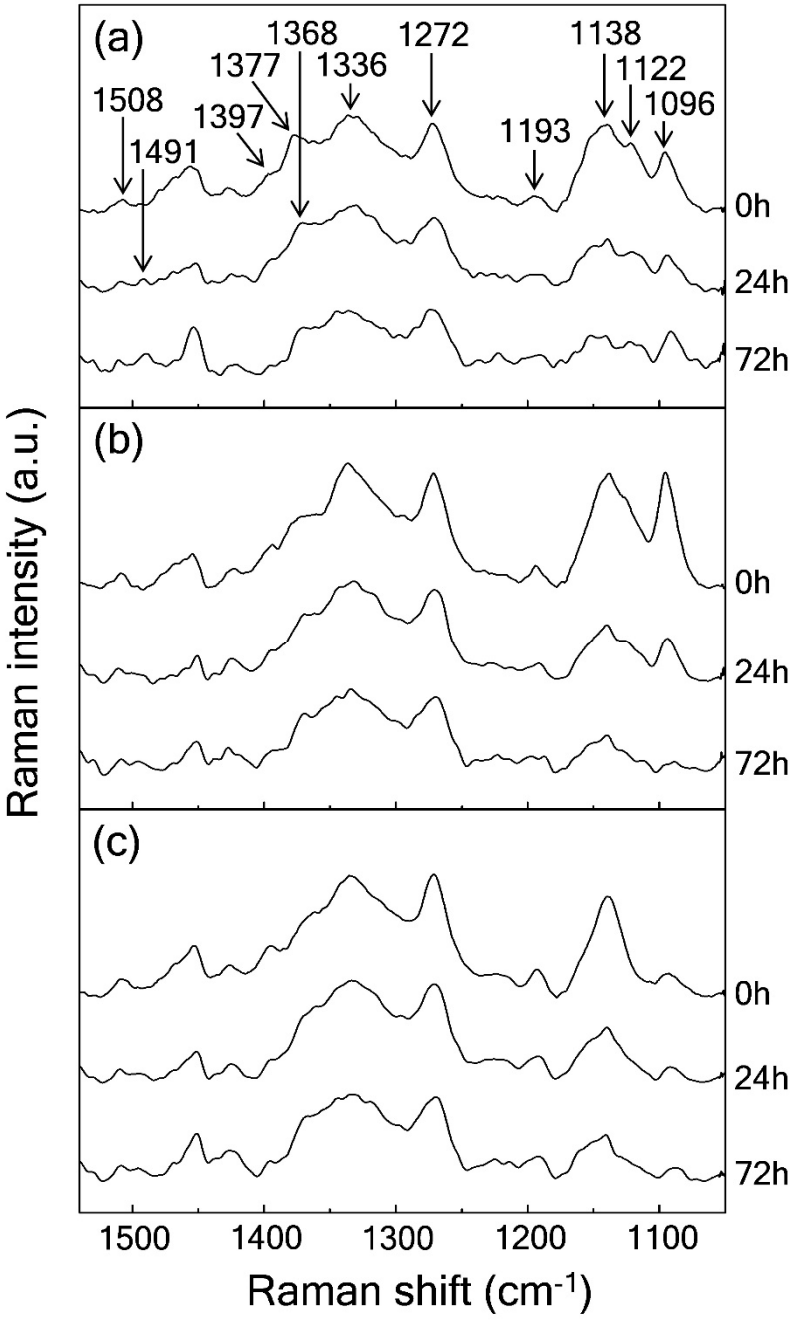

Fig. 2.16 Raman spectra for (a) S_2, (b) CML, and (c) CC of tracheids before and after treatment with [C2mim][Cl] at 120°C for 0 h, 24 h, and 72 h; enlargement of the region from 1050 to 1550 cm^{-1}.

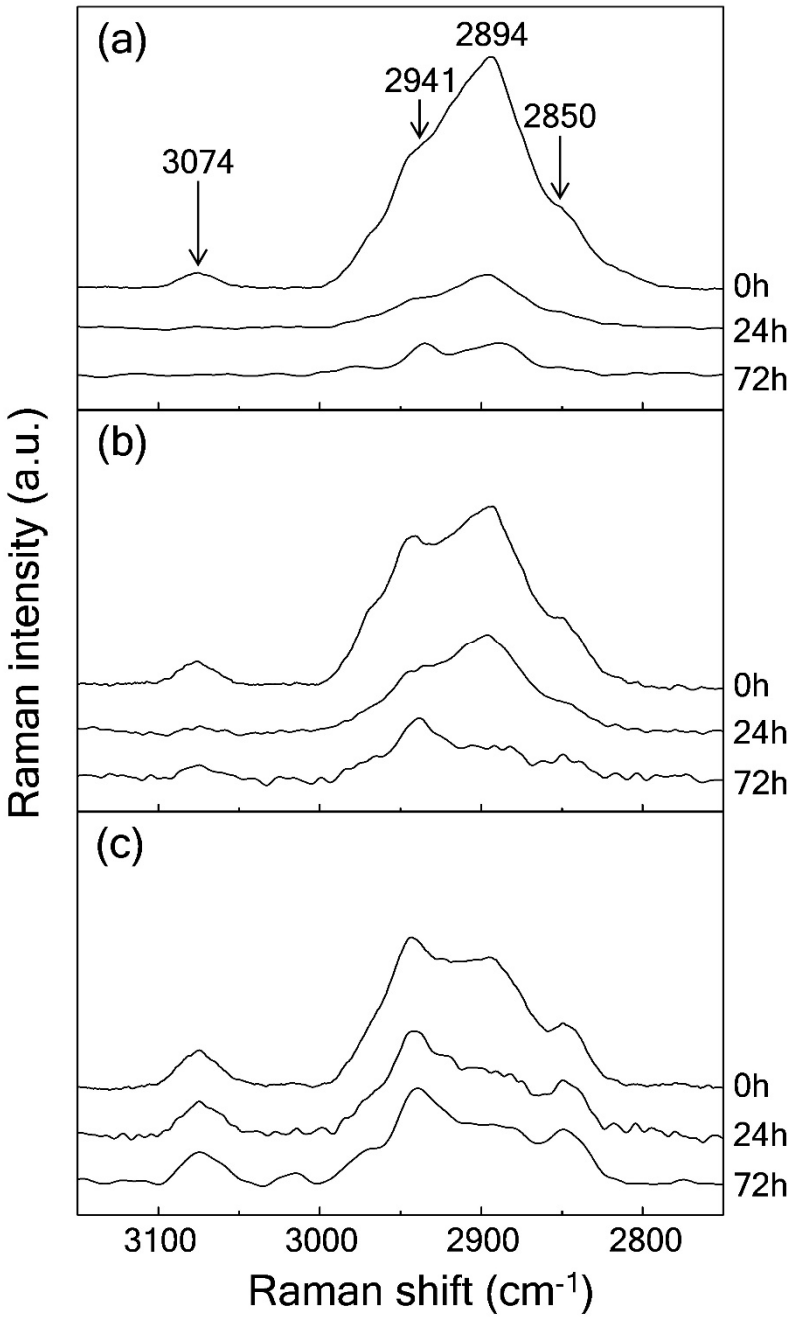

Fig. 2.17 Raman spectra for (a) S_2, (b) CML, and (c) CC of tracheids before and after treatment with [C2mim][Cl] at 120°C for 0 h, 24 h, and 72 h; enlargement of the region from 2750 to 3150 cm^{-1}.

2.3.3.1 Point analysis

Raman spectra of tracheids were divided into four regions, 350–1050 cm^{-1} (Fig. 2.15), 1050–1540 cm^{-1} (Fig. 2.16), 1540–1710 cm^{-1} (Fig. 2.18a), and 2750–3150 cm^{-1} (Fig. 2.17). Although Raman spectra of [C2mim][Cl]-treated ray parenchyma cells were also acquired, their quality were not high due to intense fluorescence. Therefore, only the clear spectral region 1540–1710 cm^{-1} is presented (Fig. 2.18b). The band assignments of polysaccharides and lignin that have been documented in the literature were summarized from previous reports (Agarwal 1999; Agarwal et al. 2011; Agarwal and Atalla 2010; Agarwal and Ralph 1997, 2008; Edwards et al. 1997; Schenzel and Fischer 2001; Wiley and Atalla 1987) and listed in Table 2.2. Each region will be discussed in detail below.

Region from 350 to 1050 cm^{-1}

Remarkable decrease in band intensity was observed at most of native cellulose bands, such as 381, 435, 457, 563, and 899 cm^{-1}. The intensities of some lignin bands, such as 591 and 920 cm^{-1}, decreased, but the intensities of many other lignin bands were unchanged. These results can be interpreted that most cellulose was dissolved and changed its nature after 72 h treatment with [C2mim][Cl], whereas the lignin structure is only partially altered.

An increase in band intensity at 421, 664, and 697 cm^{-1} was found after 72 h treatment. The band at 421 cm^{-1} was assigned to cellulose II, and the decreased bands at 381, 435, and 563 cm^{-1} to cellulose I (Schenzel and Fischer 2001). Ohno and Miyafuji (2013) reported that cellulose solubilized in [C2mim][Cl] can be regenerated as cellulose II. It could be observed by polarizing microscope that the crystalline structure appeared again after washing out the [C2mim][Cl] with distilled water (Fig. 2.19g, h), though the wood cells after treatment with [C2mim][Cl] did not show any crystalline structures (Fig. 2.19e, f), However, the brightness in Figure 2.19g, h is less than that in Fig. 2.19d. This implies that the solubilized cellulose I can be partially regenerated as cellulose II in wood cell walls. The bands at 664 and 697 cm^{-1} are not from native wood's components, and could not be assigned. The unassigned peak at 697 cm^{-1} was detected at all three cell wall

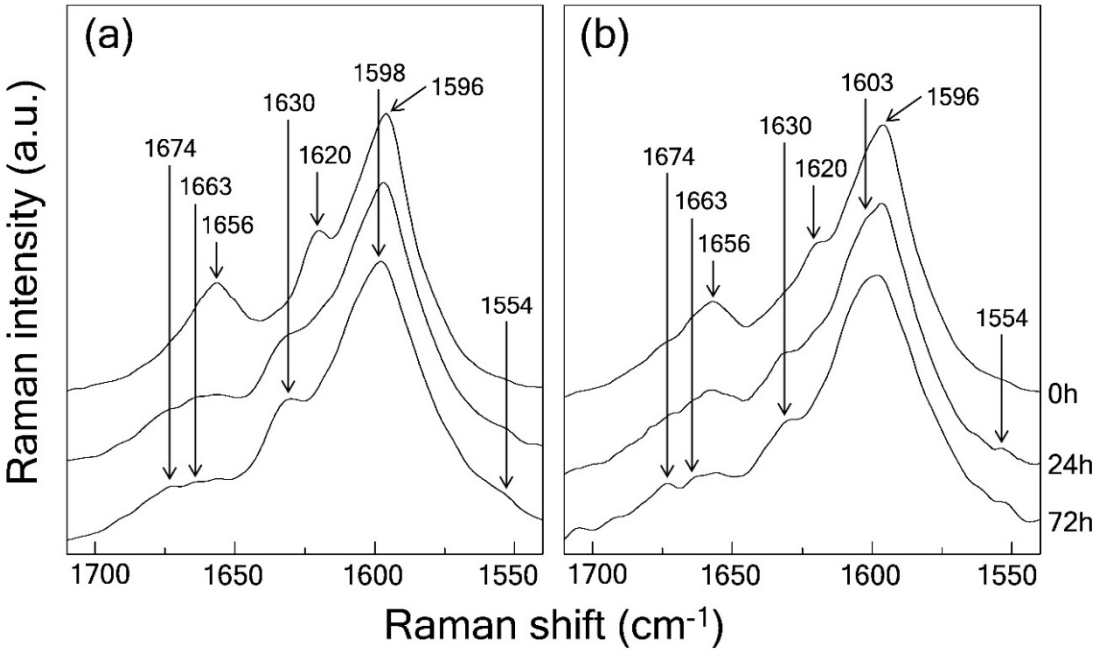

Fig. 2.18 Raman spectra for (a) CML of tracheids and (b) ray parenchyma cells before and after treatment with [C2mim][Cl] at 120°C for 0 h, 24 h, and 72 h; enlargement of the region from 1540 to 1710 cm^{-1}.

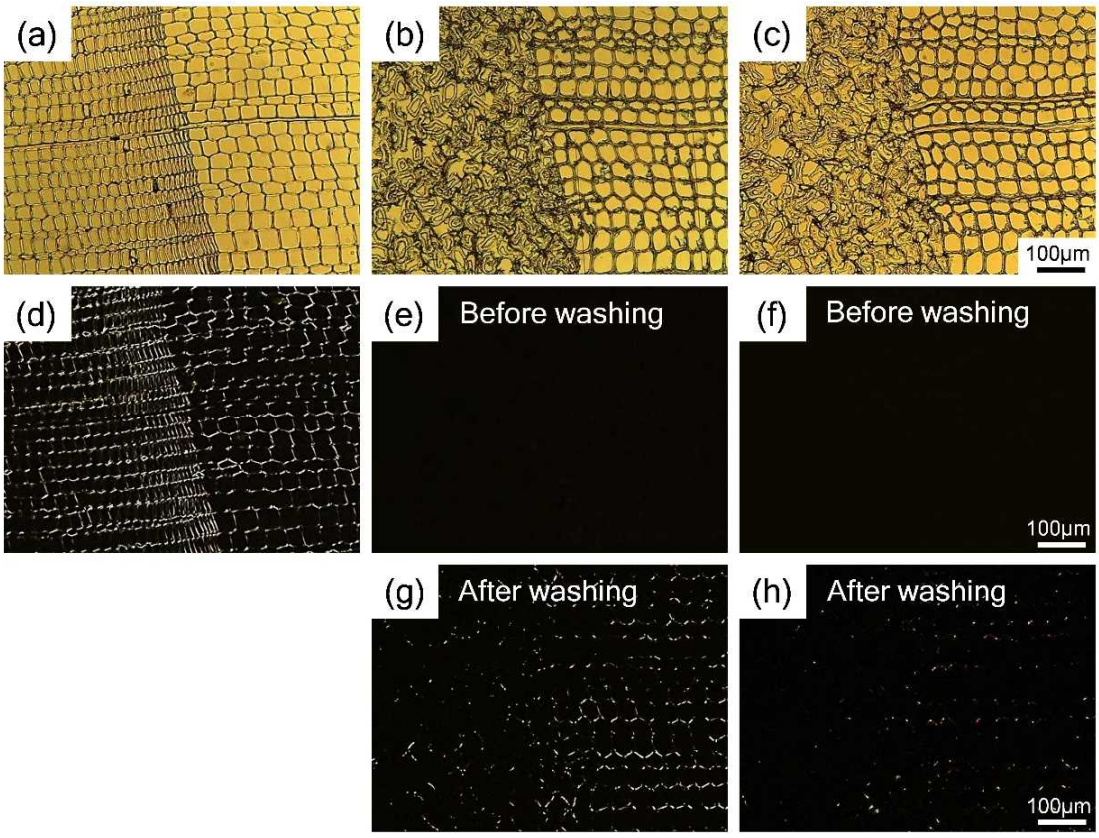

Fig. 2.19 Pictures of the wood samples before and after treatment with [C2mim][Cl] at 120°C for (a, d) 0 h, (b, e, g) 24 h, and (c, f, h) 72 h. (a−c) Light microscopy images and (d−f, g, h) polarized light microscopy images. (e, f) Before washing with water and (g, h) after washing with water.

Table 2.2 Raman bands used for the analysis, and their assignment to lignin and polysaccharides.

Raman band (cm^{-1})		Component	Band assignment
Cryptomeria japonica	*Fagus crenata*		
3074		Lignin	Aromatic C−H stretch
2941	2941	Lignin	C−H stretch in OCH_3, asymmetric
2894	2895	Polysaccharides	C−H and C−H_2 stretching
2850	2850	Lignin	C−H stretch in OCH3, symmetric
1656	1657	Lignin	C=C coniferyl/sinapyl alcohol + C=O coniferyl/sinapyl aldehyde
1620	1620	Lignin	C=C stretch of coniferyl/sinapyl aldehyde
1596	1600	Lignin	Aromatic ring stretch, symmetric
1508	1502	Lignin	Aromatic ring stretch, asymmetric
	1455	Polysaccharides	HCH and HOC bending
		lignin	CH_3 bending in OCH_3
	1427	Lignin	CH_3 bend + ring stretch
1397		Lignin	Phenolic O−H bend
1377	1378	Polysaccharides	HCC, HCO, and HOC bending
1368		Lignin	CH bend in R_3C−H
1336	1331	Polysaccharides	HCC and HCO bending
		Lignin	Aliphatic O−H bend
1272	1269	Lignin	Alyl−O of aryl−OH and aryl−O−CH_3; guaiasyl/syringyl ring (with C=O group) mode
	1224	Lignin	Alyl−O of aryl−OH and aryl−O−CH3; guaiasyl/syringyl ring (with C=O group) mode

1193	1191	Lignin	A phenol mode
	1152	Polysaccharides	Heavy atom (CC and CO) stretching, HCC and HCO bending
1138	1138	Lignin	A mode of coniferyl/sinapyl aldehyde
1122	1118	Polysaccharides	C−O−C stretch, symmetric
1096	1093	Polysaccharides	C−O−C stretch, asymmetric
	1038	Polysaccharides	Heavy atom (CC and CO) stretching
		Lignin	C−O of aryl−O−CH_3 and aryl−OH
	969	Polysaccharides	Heavy atom (CC and CO) stretching
920		Lignin	CCH wag
899	900	Polysaccharides	HCC and HCO bending at C6
		Lignin	Skeletal deformation
	729	Lignin	Skeletal deformation
591	597	Lignin	Skeletal deformation
563		Polysaccharides	COC ring
	526	Lignin	Skeletal deformation
	520	Polysaccharides	Some heavy atom stretching
	493	Polysaccharides	COC glycosidic
457	458	Polysaccharides	Some heavy atom stretching
435	436	Polysaccharides	Some heavy atom stretching
	411	Polysaccharides	Unassigned
381	380	Polysaccharides	Some heavy atom stretching
	370	Lignin	Skeletal deformation

Assignments are based on the literatures (Agarwal 1999; Agarwal et al. 2011; Agarwal and Atalla 2010; Agarwal and Ralph 1997, 2008; Edwards et al. 1997; Schenzel and Fischer 2001; Wiley and Atalla 1987).

areas, whereas the peak at 664 cm^{-1} was only detected at S_2.

Region from 1050 to 1540 cm^{-1}

The lignin band intensities at 1272, 1336, 1368, and 1508 cm^{-1} were unchanged after 72 h treatment. Conversely, those at 1138, 1193, and 1397 cm^{-1} decreased slightly. The band at 1138 cm^{-1} was assigned to coniferylaldehyde and the bands at 1193 and 1397 cm^{-1} to units with phenol structure (Agarwal 1999; Agarwal et al. 2011). The slight reductions in band intensity indicate a partial decomposition and deterioration of lignin functional groups such as cinnamaldehyde and phenol structures. With regard to polysaccharides, the band intensities at 1096, 1122, and 1377 cm^{-1} decreased significantly. Around 1491 cm^{-1}, a new band, which is not from native wood component, appeared and the intensity of this band increased with prolonged treatment time. The band increment in this region was strongest at S_2.

Region from 1540 to 1710 cm^{-1}

In this region, only the spectral changes in CML are presented (Fig. 2.18a) because the spectra of S_2, CML and CC show similar changes during treatment with [C2mim][Cl]. Peaks at 1620 and 1656 cm^{-1} decreased with prolonged treatment time. These bands are assigned to stretching vibrations of the ring-conjugated C=C bonds in coniferylaldehyde units and in coniferylalcohol units, respectively (Agarwal 1999; Agarwal et al. 2011; Kihara et al. 2002). Furthermore, several new bands were observed at 1554, 1630, 1663, and 1674 cm^{-1}. The Raman bands at 1554, 1674 cm^{-1} and 1630 cm^{-1} are reported to be due to the structures of *o*-quinone, *p*-quinone, and the C=C bond of the stilbene structures, respectively (Agarwal 1998; Agarwal and Atalla 2000). The appearance of peak at 1663 cm^{-1} (stretching vibration of the ring-conjugated C=O bond in coniferylaldehyde) correlates with the reduction of intensity in the adjacent band at 1656 cm^{-1}. The position of the band of aromatic rings at 1596 cm^{-1} shifted slightly towards the high frequency range as the treatment time increased. Agarwal et al. (2011) reported that the aromatic band shifts upon modification. Thus, it is possible that the slight shifting of this band is

due to the change in the substitution pattern after [C2mim][Cl] treatment. These results reflect the chemical changes of wood component during [C2mim][Cl] treatment.

The spectral changes of ray parenchyma cells after treatment were similar to that of tracheids. However, a new shoulder could be observed at 1603 cm^{-1} after 24 h treatment, which cannot be interpreted for the time being.

Region from 2750 to 3150 cm^{-1}

The intensity of the polysaccharide bands at 2894 cm^{-1} decreased significantly, while the lignin bands at 2850 and 2941 cm^{-1} show only minor intensity changes. Obviously, the polysaccharides are influenced more by [C2mim][Cl] than lignin. The decrement of the lignin band at 3074 cm^{-1} was only seen in S_2.

2.3.3.2 Raman mapping analysis

Raman maps give information on larger areas. Fig. 2.20a–c shows bright field microscopy images of tracheids in transverse sections before and after [C2mim][Cl] treatment. All photographs are of the same area, and mapping and line analysis were performed on the same cell walls. In the micrographs, the rectangles and lines indicate the selected areas for mapping and lines for line analysis, respectively.

Fig. 2.20d–f and g–i show Raman images of the distribution of lignin (1591–1613 cm^{-1}) and polysaccharides (2884–2905 cm^{-1}) before and after treatment with [C2mim][Cl], respectively. Bright areas indicate high concentrations of specific chemical compositions, whereas dark areas the low concentrations. The lignin concentration in S_2 decreased with prolonged treatment time, but that of CML and CC barely changed. Whiting and Goring (1982) found that the methoxy content of lignin is low in the CML and CC, and about 40% of lignin in this areas consists of *p*-hydroxyphenyl lignin. Additionally, the content of condensed lignin is higher in the CML and CC than in the S_2 (Terashima and Fukushima 1988). Condensed lignin formed be H-units are supposed to be less reactive, and this could explain the resistance of these regions towards [C2mim][Cl]. The concentration of the lignin in S_2 decreased inhomogeneously

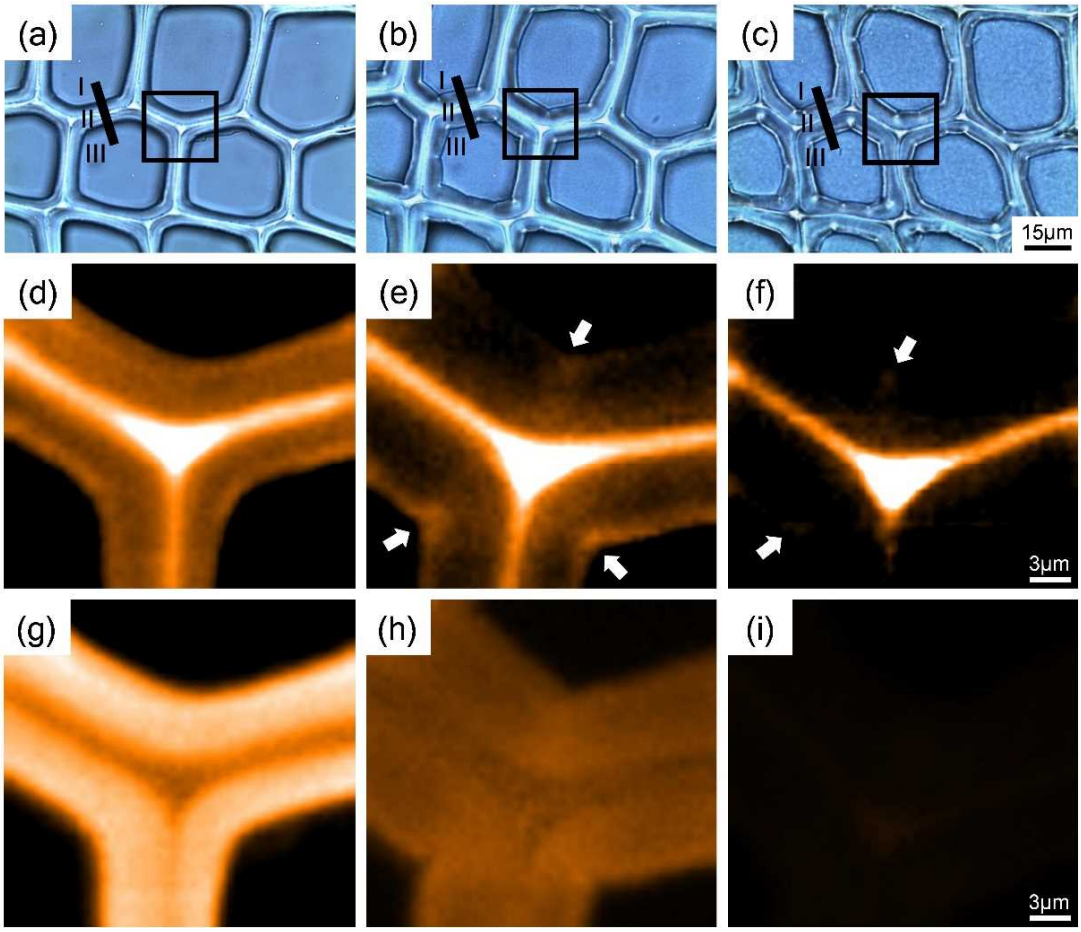

Fig. 2.20 Raman mapping on transverse sections of tracheids before and after treatment with [C2mim][Cl] at 120°C for (a, d, g) 0 h, (b, e, h) 24 h, and (c, f, i) 72 h. (a−c) Bright field images of the measured position. (d−f) Distribution of lignin (1591–1613 cm^{-1}). (g−i) Distribution of polysaccharides (2884–2905 cm^{-1}). Bright regions indicate high concentrations of specific chemical compositions, dark regions indicate low concentrations.

(indicated by arrows in Fig. 2.20e, f); the distribution of polysaccharides seems to be homogeneous during degradation.

2.3.3.3 Line analysis

Figure 2.21 illustrates the results of line analysis of the double cell wall of tracheids in transverse sections (shown by the lines in Fig. 2.20a−c) before and after [C2mim][Cl] treatment. The distributions of lignin and polysaccharides are presented in Fig. 2.21a, b, respectively. Remarkable concentration decrements can be observed in both polymer classes in S_2 after 24 h treatment. Obviously, all components are dissolved and eluted. Treatment with [C2mim][Cl] induces swelling of wood cells (Miyafuji and Suzuki 2012). Thus the observed changes may also be due to swelling of cell walls. The concentration of polysaccharides in S_2 continued to decrease with prolonged treatment time, whereas no significant change of lignin concentration is observable after 24 h and 72 h treatments. Accordingly, polysaccharides are dissolved in [C2mim][Cl] more readily.

2.3.4 Raman microscopic analysis of *Fagus crenata* after treatment with [C2mim][Cl]

Raman spectra were acquired from four morphological regions: secondary walls of wood fiber (WF_{SW}), vessel, and axial parenchyma cell, and the cell corner of wood fiber (WF_{CC}). The author obtained spectra ranging from 300 to 1750 cm^{-1} and from 2750 to 3150 cm^{-1}, as the Raman bands of the main chemical components of wood, including cellulose, hemicellulose, and lignin, primarily appeared in these regions, and no significant spectral changes were observed after [C2mim][Cl] treatment, except for these regions.

2.3.4.1 Point analysis

Raman spectra obtained from various morphological regions before and after treatment with [C2mim][Cl] at 120°C are shown in Figs. 2.22−2.25. To better visualize the spectral features, the spectra were divided into three different regions, 300–950 cm^{-1} (Fig. 2.22),

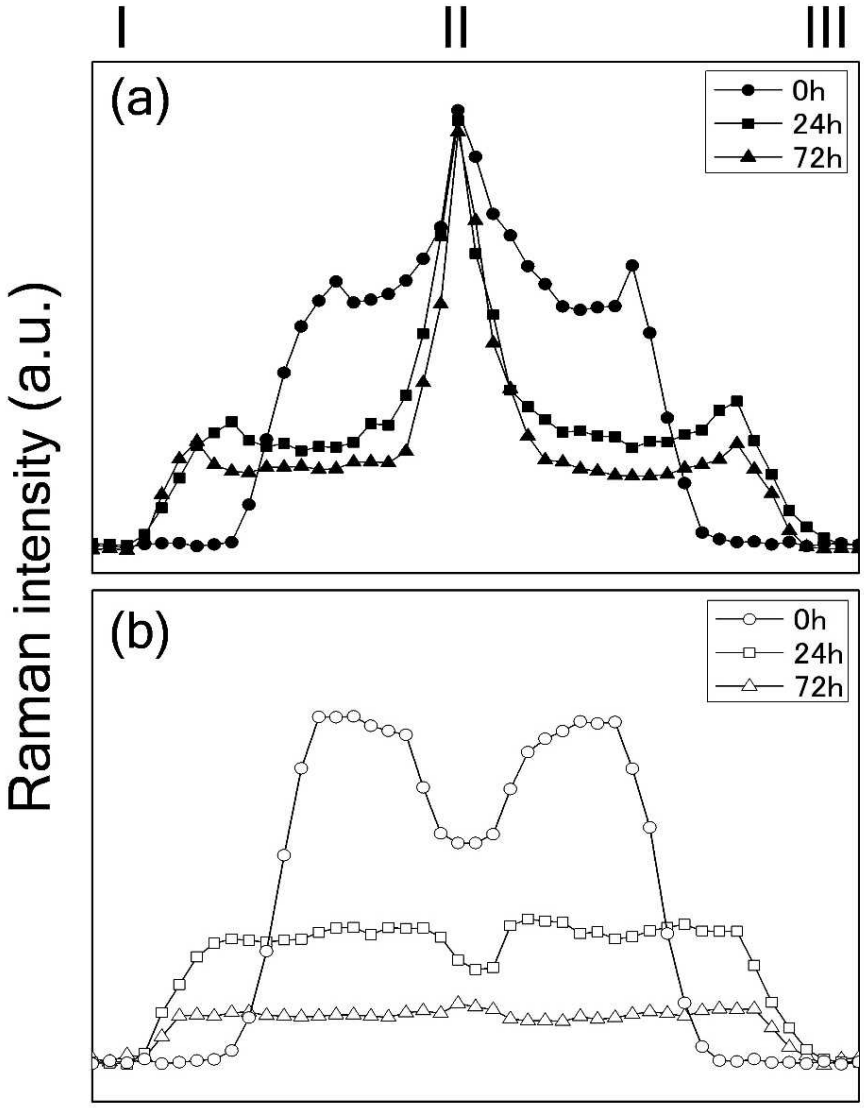

Fig. 2.21 Line analysis on the double cell wall of tracheids on transverse section (lines shown in Fig. 2.20) before and after treatment with [C2mim][Cl] at 120°C for various times: (a) distribution of lignin (1586−1607 cm^{-1}) and (b) distribution of polysaccharides (2884−2894 cm^{-1}).

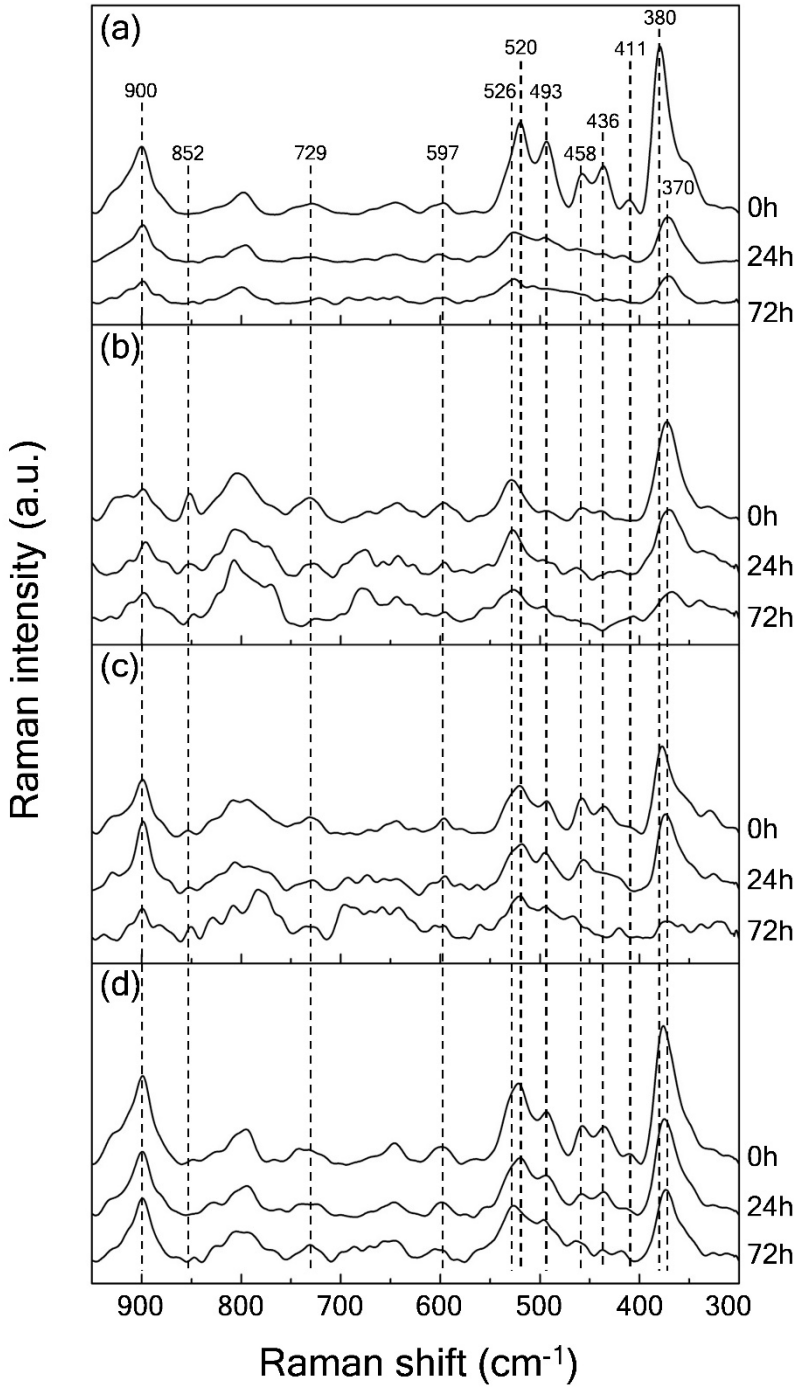

Fig. 2.22 Raman spectra for (a) WF_{SW}, (b) WF_{CC}, (c) vessel, and (d) axial parenchyma cell before and after treatment with [C2mim][Cl] at 120°C for 0 h, 24 h, and 72 h; enlargement of the region of 300–950 cm^{-1}.

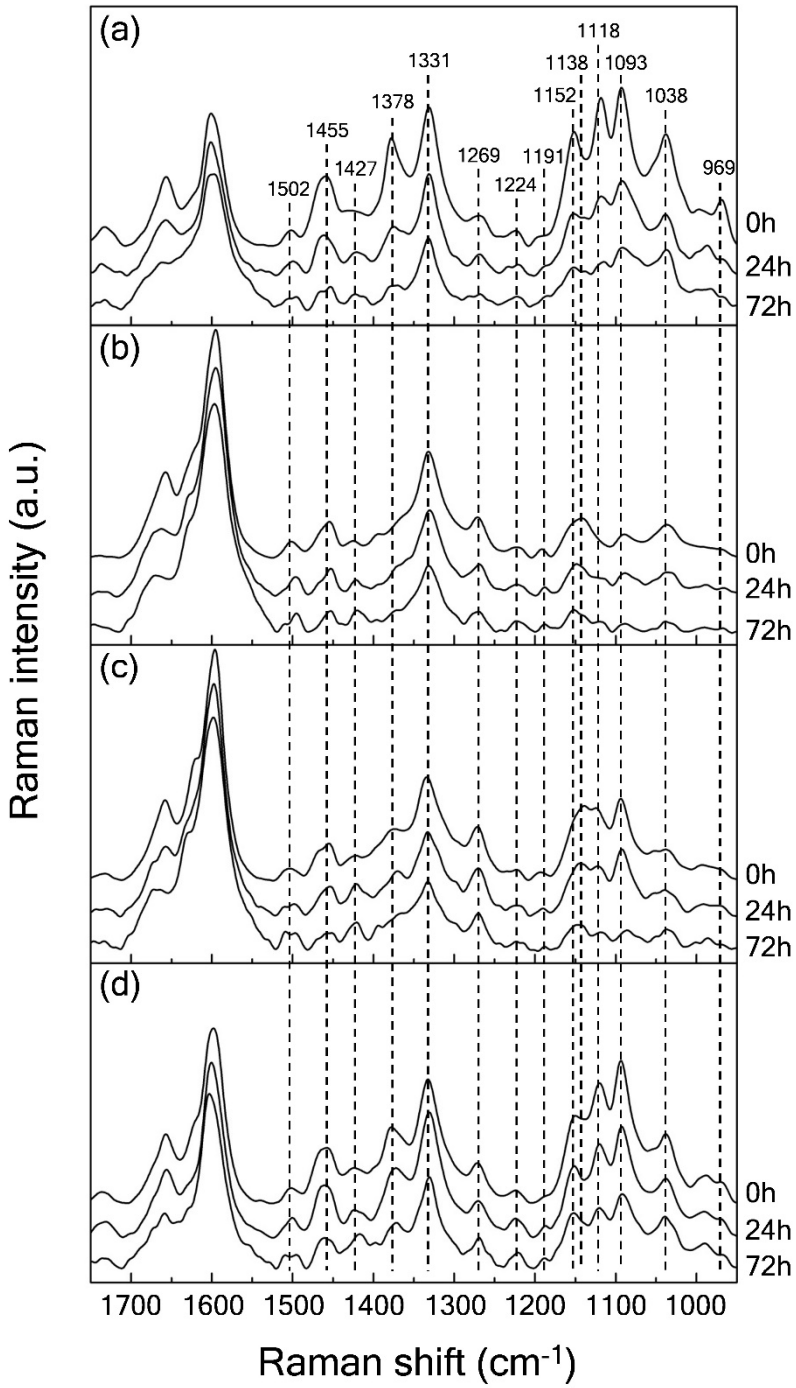

Fig. 2.23 Raman spectra for (a) WF_{SW}, (b) WF_{CC}, (c) vessel, and (d) axial parenchyma cell before and after treatment with [C2mim][Cl] at 120°C for 0 h, 24 h, and 72 h; enlargement of the region of 950–1750 cm^{-1}.

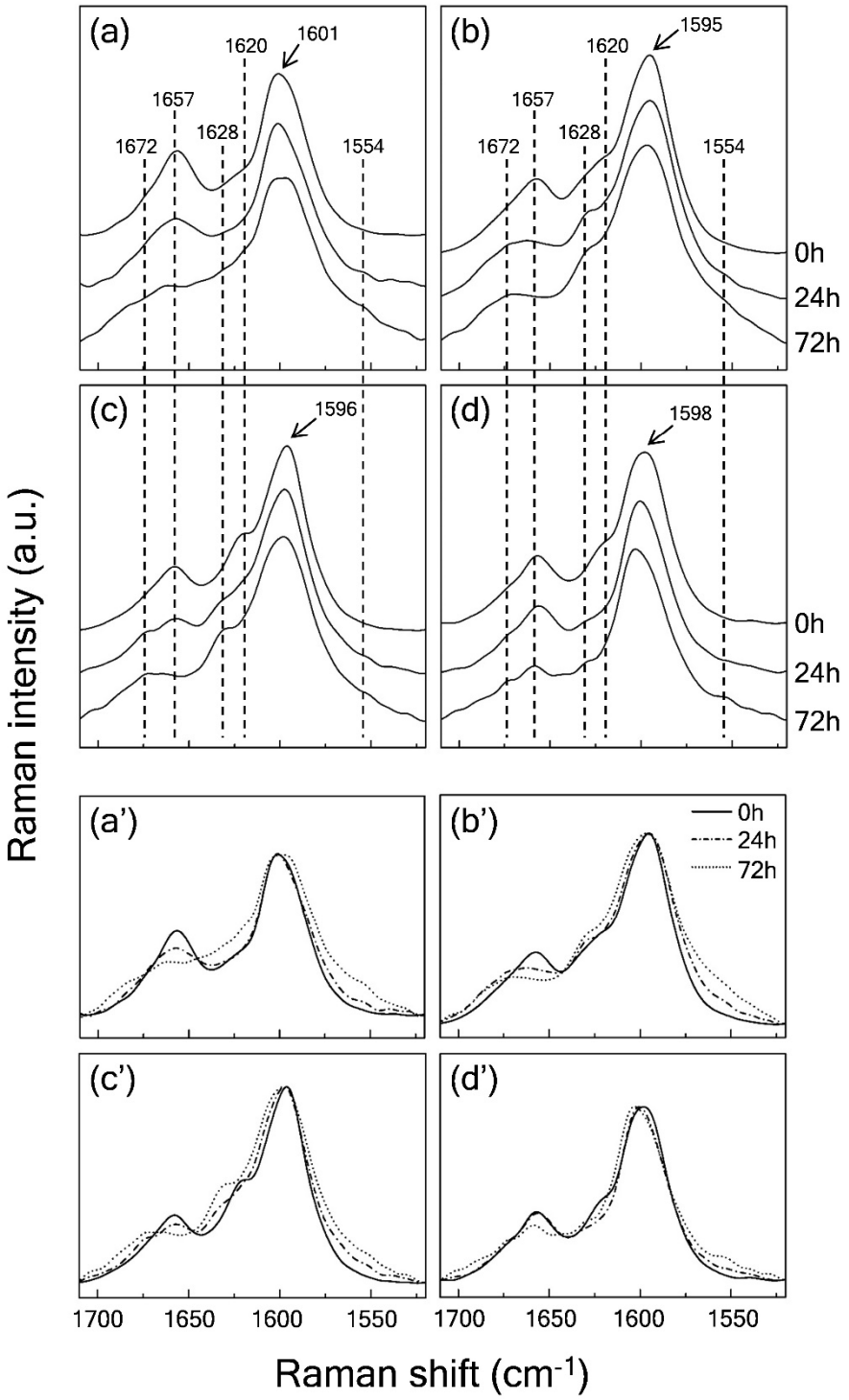

Fig. 2.24 Raman spectra for (a, a') WF_{SW}, (b, b') WF_{CC}, (c, c') vessel, and (d, d') axial parenchyma cell before and after treatment with [C2mim][Cl] at 120°C for 0 h, 24 h, and 72 h; enlargement of the region of 1520–1710 cm^{-1}. (a'−d') All spectra overlapped to clarify broadening of the peaks.

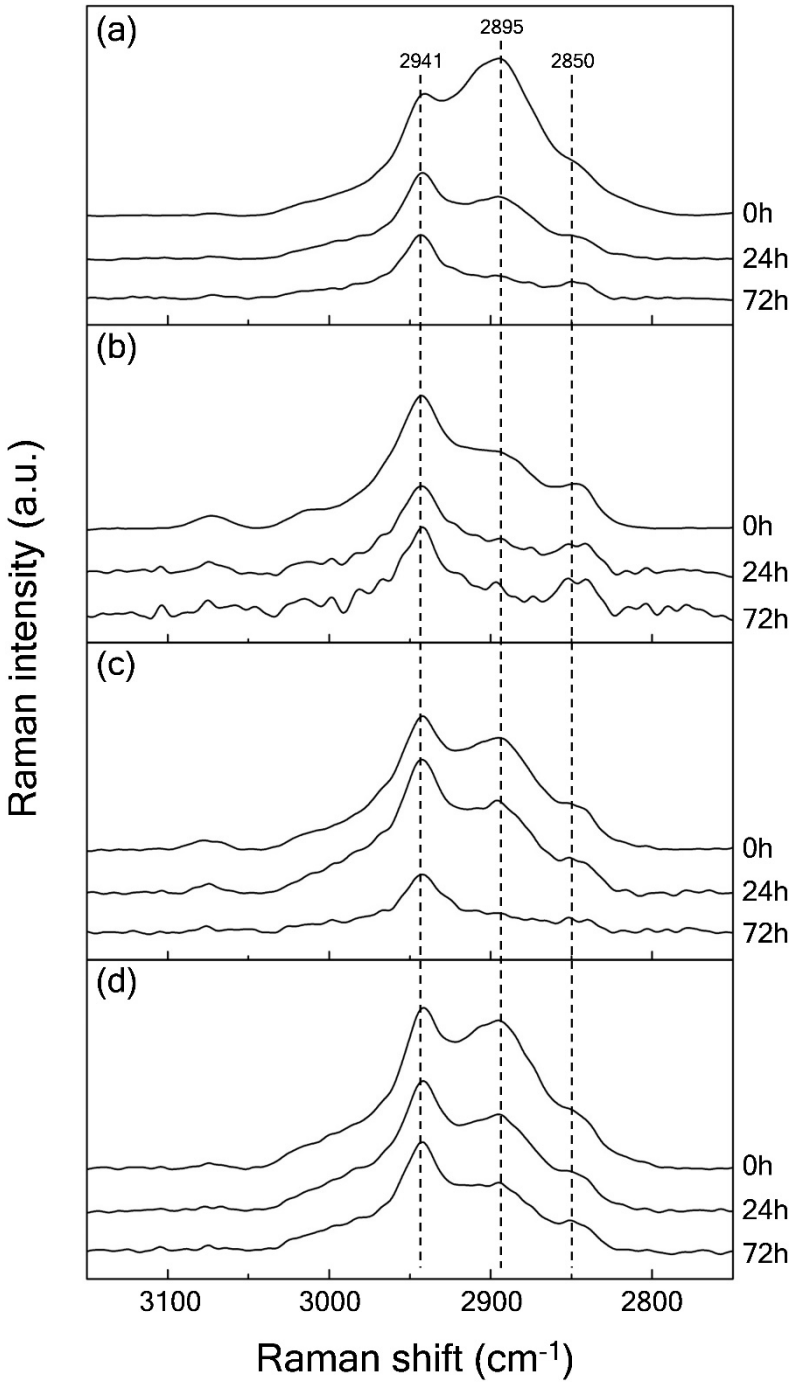

Fig. 2.25 Raman spectra for (a) WF_{SW}, (b) WF_{CC}, (c) vessel, and (d) axial parenchyma cell before and after treatment with [C2mim][Cl] at 120°C for 0 h, 24 h, and 72 h; enlargement of the region of 2750–3150 cm^{-1}.

950–1750 cm^{-1} (Figs 2.23, 2.24), and 2750–3150 cm^{-1} (Fig. 2.25). Each region will be discussed in detail below.

Region from 300 to 950 cm^{-1}

The low frequency region of the spectrum is difficult to assign in detail because of the many contributions from skeletal vibrations of wood components (Agarwal and Atalla 2010; Schenzel et al. 2009; Schenzel and Fischer 2001). However, a simple distinction between the features of polysaccharides and lignin can be made. Although the band intensities of polysaccharides, including those at 380, 411, 436, 458, 493, and 520 cm^{-1}, decreased for all measured areas during the treatment, the decrement differed in different morphological regions. The polysaccharide band intensities for WF_{SW} decreased significantly after 24 h of treatment, while those for axial parenchyma cell decreased gradually with an increase in treatment time and continued to exist after 72 h of treatment. This result indicates that polysaccharides in axial parenchyma cell are difficult to dissolve in [C2mim][Cl] compared with those in WF_{SW}; nevertheless [C2mim][Cl] preferentially dissolves polysaccharides.

The lignin-related bands were seen at 370, 526, 597, 729, and 900 cm^{-1}. The band at 370 cm^{-1} is associated with the structure of syringyl lignin (Agarwal and Atalla 2010; Agarwal et al. 2011). Although this band was hidden under the strong polysaccharide band before treatment for WF_{SW}, vessel, and axial parenchyma cell, it appeared after 24 h of treatment due to the reduction in polysaccharides. The syringyl lignin band intensities for WF_{CC} and vessel decreased rapidly from 24 h to 72 h of treatment (Fig. 2.22), whereas those for WF_{SW} and axial parenchyma cell decreased slightly. This result suggests that the syringyl structure of lignin was affected by [C2mim][Cl] in all morphological regions, although the interaction of syringyl lignin with [C2mim][Cl] varied in each region. At present, the reason for this result is not clear, but it is likely caused by differences in the chemical components of each region, as well as their distribution. For instance, hardwood lignin is based on both the guaiacylpropane and syringylpropane units, but their distributions are quite different in different morphological regions; WF_{CC} and vessel are

predominantly guaiacyl lignin, whereas WF_{SW} and axial parenchyma cell are syringyl lignin (Fergus and Goring 1970; Fujii et al. 1987; Musha and Goring 1975; Saka and Goring 1988) Lignin bands other than 370 cm^{-1} showed very low intensities, and most of them overlapped with the polysaccharide bands; thus, they were unsuitable for comparative study and are not discussed here.

In the spectral region between 650 and 800 cm^{-1}, many other small peaks appeared and increased as the treatment time increased, especially for WF_{CC} and vessel, which are regarded as lignin-rich regions (Eriksson et al. 1988; Saka and Goring 1988). In general, significant features of the C−Cl vibration appear around this spectral region (Smith and Dent 2005). Additionally, recent study showed that chlorine from [C2mim][Cl] is incorporated into milled wood lignin, which is the least modifiable chemical structure of lignin (Ogawa and Miyafuji 2015). Therefore, it is suggested that these spectral features are due to some C−Cl vibrations, and that chlorine from [C2mim][Cl] was heterogeneously incorporated into cell walls.

It is noted that a band that was neither assigned to polysaccharides nor lignin was detected at 852 cm^{-1}. This band is a marker for pectin due to C−O−C stretching of α-glycosidic bonds (Séné et al. 1994; Synsytsya et al. 2003). Although a distinctive pectin band was observed before treatment, especially for WF_{CC} (Fig. 2.22), its intensity decreased significantly after 24 h of treatment. However, this band intensity increased and shifted to a slightly lower frequency from 24 h to 72 h of treatment. This change is most likely due to the appearance of some new vibrational mode.

Region from 950 to 1750 cm^{-1}

In this region, the lignin bands that were distinguishable from polysaccharide features were detected at 1138, 1191, 1224, 1269, 1427, 1502, 1600, 1620, and 1657 cm^{-1}, whereas the polysaccharides bands that did not coincide with lignin features were detected at 969, 1093, 1118, 1152, and 1378 cm^{-1}. Additionally, several bands that overlapped lignin and polysaccharide features were observed at 1038, 1331, and 1455 cm^{-1}. All the polysaccharide band intensities showed marked reductions after 72 h of

treatment for WF_{SW} and vessel. The relatively significant reductions of the overlapping bands were observed specially for WF_{SW}, as polysaccharides contribute greatly to the decreasing range of these bands. Although most of the lignin band intensities showed no significant changes after treatment in any of the morphological regions, the peak at 1138 cm^{-1}, which was assigned to a mode of coniferylaldehyde and sinapylaldehyde (Agarwal et al. 2011), decreased. In addition, some peaks, such as those at 1191 and 1427 cm^{-1}, became sharper owing to the reduction of the intensities in adjacent polysaccharide bands.

The band region between 1520 and 1710 cm^{-1}, which mainly resulted from lignin features, showed several pronounced changes (Fig. 2.24). The strong intensity band at approximately 1600 cm^{-1}, which results from the aromatic ring vibration of lignin (Agarwal 1999; Agarwal et al. 2011), broadened for all regions, except for axial parenchyma cell, after 72 h of treatment (Fig. 2.24a'−d'). The gradual broadening implies a progression to deterioration in the lignin structure during [C2mim][Cl] treatment. The band intensity at 1657 cm^{-1}, which was assigned to the ethylenic C=C bond in coniferylalcohol and sinapylalcohol units and the γ−C=O bond in coniferylaldehyde and sinapylaldehyde units (Agarwal 1999; Agarwal et al. 2011), decreased gradually as the treatment time increased (Fig. 2.24a−d). In addition, the weak shoulder at 1620 cm^{-1}, which was assigned to the ethylenic C=C bond in coniferylaldehyde and sinapylaldehyde units, disappeared (Agarwal 1999; Agarwal 2011). However, new weak peaks at 1554, 1628, and 1672 cm^{-1}, which may be attributable to the structure of quinone and stilbene (Agarwal 1998; Agarwal and Atalla 2000), appeared after 72 h of treatment. These changes have also been observed for *Cryptomeria japonica* treated with [C2mim][Cl] (Fig. 2.18) and another ionic liquid, 1-ethylpyridinium bromide, which is described in chapter 3.

Taking a closer look at the aromatic ring vibration of lignin at approximately 1600 cm^{-1}, this peak position for the untreated sample was different in different morphological regions: the peak position of WF_{SW} and axial parenchyma cell were located in the slight high-frequency range, whereas those of WF_{CC} and vessel were in the slight low-frequency range. In the Raman spectrum obtained from *Cryptomeria japonica*, which is a softwood, the peak of the aromatic ring vibration was observed in a low-frequency range at 1596

cm^{-1} (Fig. 2.18). The band position of the aromatic ring vibration shifts upon modification or removable of its units (Agarwal et al. 2011); thus, the different positions of this band in different morphological regions possibly represent the lignin structure and the ratio of guaiacyl to syringyl units. A previous study, which used the near-infrared Fourier transform Raman spectroscopic technique, showed that guaiacyl and syringyl lignin marker bands exist at 1599 and 1594 cm^{-1}, respectively (Takayama et al. 1997). In addition, Agarwal and Atalla reported these bands at 1597 and 1595 cm^{-1}, respectively, for mostly guaiacyl lignin and syringyl-enriched lignin (Agarwal and Atalla 2010). However, the reason for these small changes in peak position for the same lignin is not clear. Therefore, further studies will be necessary in the future to address this issue.

Overall, the Raman spectra for axial parenchyma cell were not altered significantly during [C2mim][Cl] treatment compared to those of the other morphological regions. This result implies that both polysaccharides and lignin of axial parenchyma cell are difficult to react with [C2mim][Cl]. In addition, this result is in good agreement with the SEM study that showed that axial parenchyma cell have a high resistance to [C2mim][Cl] in morphology (Fig. 2.5).

Region from 2750 to 3150 cm^{-1}

In all morphological regions, the polysaccharide band intensities at 2895 cm^{-1} decreased with prolonged treatment (Fig. 2.25), while those of lignin at 2850 and 2941 cm^{-1} showed no significant changes except for vessle. The tendency observed in polysaccharide band was similar to that in low-frequency regions. With respect to C−H stretch in methoxyl group at 2941 cm^{-1}, its tendency was similar to syringyl lignin band at 370 cm^{-1} for WF_{SW}, vessel and axial parenchyma cell but not for WF_{CC} (Figs. 2.22, 2.25). Unfortunately, the detailed relationship between 370 and 2941 cm^{-1} is not known at the moment. From 24 h of treatment onward, a large number of new weak peaks appeared and increased in intensity, particularly for WF_{CC} (Fig. 2.25). This development likely reflected the partial deterioration such as changes in the functional group and chemical bonding of lignin.

2.3.4.2 Raman mapping analysis

Changes in the distribution of lignin and polysaccharides in the cell walls over a larger area during [C2mim][Cl] treatment at 120°C were visualized by a time-sequential Raman mapping technique. Raman mapping analysis was performed on wood fibers because they constitute the main tissue mass of hardwoods. All experiments were conducted on the same cell walls in transverse sections. As shown in the bright field images, a part of the compound middle lamella of wood fiber (WF_{CML}) severed under the strain caused by the swelling of WF_{SW} from 24 h of treatment onward (Fig. 2.26b, c).

The distribution of lignin before and after treatment with [C2mim][Cl] was specified by the band region of an aromatic ring vibration between 1581 and 1613 cm^{-1} (Fig. 2.26d−f respectively, for 0, 24, and 72 h). Within the untreated sample, lignin concentrations were higher in WF_{CML} and WF_{CC} than in WF_{SW}. Although this tendency did not change after [C2mim][Cl] treatment, the lignin concentration in WF_{SW} decreased slightly, whereas those in WF_{CML} and WF_{CC} did not change after 72 h of treatment. This result was very similar to the result of a study that used *Cryptomeria japonica*. We suggest that lignin in specific areas, such as WF_{CML} and WF_{CC}, is highly resistant to [C2mim][Cl] attack. These characteristics in each morphological region are attributed to many factors, including lignin structure, lignin concentration, and the penetrability of [C2mim][Cl].

The distribution of polysaccharides before and after treatment was specified by the band region of C−H and $C-H_2$ stretching of polysaccharides between 2884 and 2905 cm^{-1} (Fig. 2.26g−i respectively, for 0, 24, and 72 h). Although a large amount of polysaccharides existed in WF_{SW} before treatment, their concentration decreased significantly after treatment for 24 h, and the reduction continued as the treatment time increased. However, a relatively high-concentration area was observed for WF_{SW} after 24 h of treatment (indicated by the arrow). More detailed work is necessary to resolve this inhomogeneity.

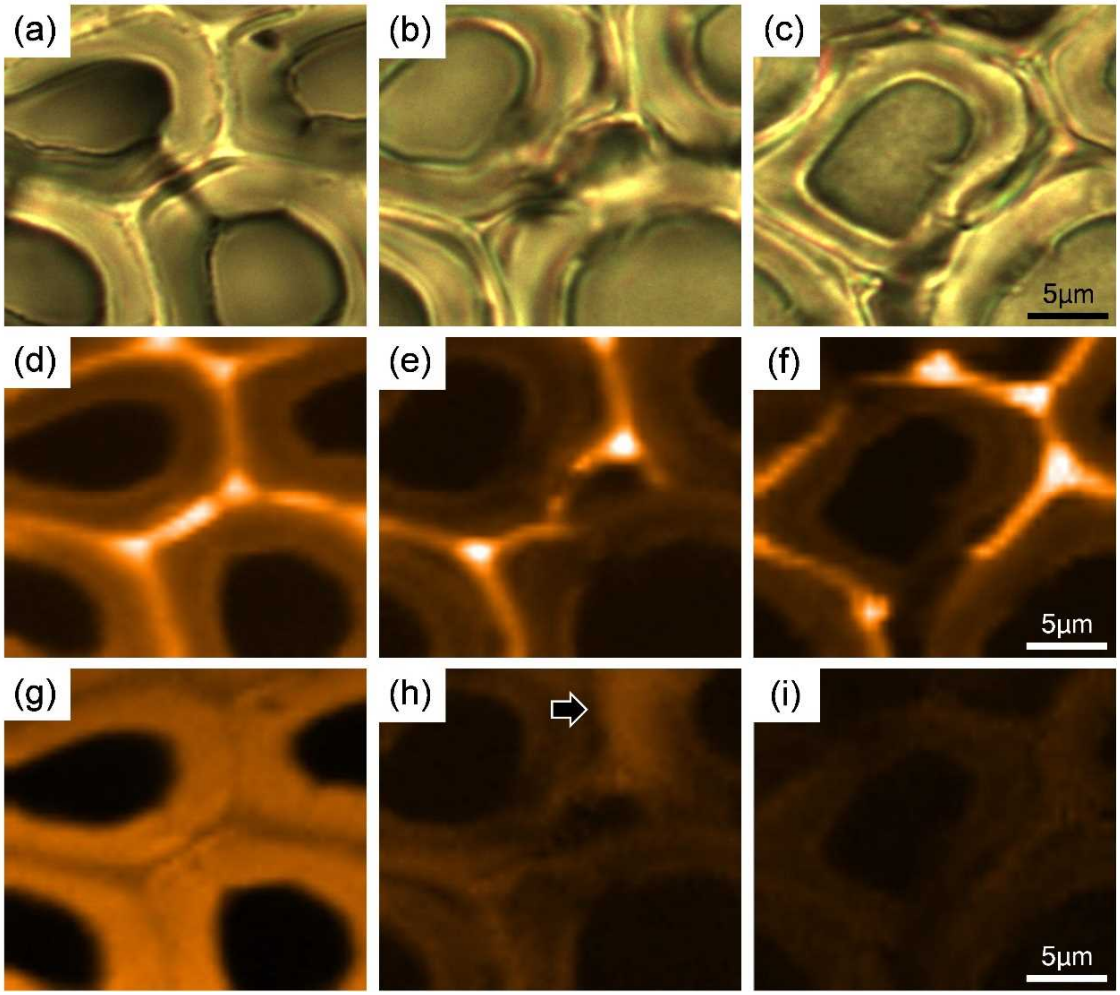

Fig. 2.26 Raman mapping on transverse sections of wood fibers before and after treatment with [C2mim][Cl] at 120°C for (a, d, g) 0 h, (b, e, h) 24 h, and (c, f, i) 72 h. (a−c) Bright field images of the measured position. (d−f) Distribution of lignin (1581–1613 cm^{-1}). (g−i) Distribution of polysaccharides (2884–2905 cm^{-1}). Bright regions indicate high concentrations of specific chemical compositions, dark regions indicate low concentrations.

2.4 Conclusions

Changes in the ultrastructure and chemical components, and their distribution in softwood and hardwood upon treatment with the ionic liquid [C2mim][Cl], which preferentially dissolves cellulose, were examined at the cellular level by various microscopy techniques. Morphological study on various hardwoods after [C2mim][Cl] treatment revealed that the swelling behavior of wood fibers varied among wood species of hardwoods and according to location such as earlywood and latewood. The ray parenchyma cells did not swell and deform easily by [C2mim][Cl] treatment compared with wood fibers and two kinds of swelling behavior exist. Furthermore, the pit reaction behavior revealed various differences in wood species and pit type. Raman microscopic study has clearly shown chemical changes in various morphological regions of wood cell walls. Polysaccharides reacted with [C2mim][Cl] more readily than lignin, so the cell wall structure is maintained during the advanced dissolution of the polysaccharides. Lignin in CML and CC was especially resistant to reactions with [C2mim][Cl], but coniferylaldehyde and sinapylaldehyde structures were partly degraded and other chemical structures related to lignin were generated during [C2mim][Cl] treatment. In addition, polysaccharides are generally highly soluble in [C2mim][Cl], but [C2mim][Cl] could hardly dissolve the polysaccharides in specific tissues, such as axial parenchyma cells.

CHAPTER 3

Microscopic Study on Woody Biomass after Treatment with the Ionic Liquid, 1-Ethylpyridinium Bromide ([EtPy][Br])

3.1 Introduction

The interaction of wood with ionic liquids has gradually been clarified from chemical point of view (Fort et al. 2007; Kilpeläinen et al. 2007; Miyafuji et al. 2009; Nakamura et al. 2010a, b; Sun et al. 2009; Yokoo and Miyafuji 2014). In addition, the cellular scale investigations of the effects of ionic liquid treatment on wood have also been performed using various microscopic techniques (Kanbayashi and Miyafuji 2013, 2014, 2015a, 2016a; Lucas et al. 2011; Miyafuji and Suzuki 2011, 2012; Viell and Marquardt 2011; Zhang et al. 2014).

As in the references given above, imidazolium-based ionic liquids are mainly used in this research field and few studies exist on the use of other types of ionic liquids. Earlier research on liquefaction of wood by ionic liquids revealed that both [C2mim][Cl] and [EtPy][Br] can liquefy all components of wood although the reaction rate of the wood components with these ionic liquids is different for the types of the ionic liquids (Miyafuji et al. 2009; Nakamura et al. 2010a; Yokoo and Miyafuji 2014). The yield of residue of *Thuja plicata* after treatment with [C2mim][Cl] at 120°C for 8 h can be reduced to 30%, and the decrease in yield of residue was caused mainly by decrease in the amount of cellulose (Nakamura et al. 2010a). On the other hand, the yield of residue of *Cryptomeria japonica* after treatment with [EtPy][Br] at 120°C for 24 h can be reduced to 43%, and the decrease in yield of residue was caused mainly by decrease in the amount of lignin (Yokoo and Miyafuji 2014).

However, little is known about the interaction of wood with ionic liquids with respect

to the pyridinium-based ionic liquid. For a better understanding of the effects of the pyridinium-based ionic liquid [EtPy][Br], the author investigated the morphological and chemical changes in wood cell walls after treatment with [EtPy][Br] at the cellular level. Light microscopy and SEM were used to observe morphological changes. Confocal Raman microscopy was employed to investigate spectral changes in the different types of layers and to visualize chemical changes in the cell walls during [EtPy][Br] treatment.

3.2 Materials and Methods

3.2.1 Samples and chemicals

The woods used were: Japanese cedar (*Cryptomeria japonica*) and Japanese beech (*Fagus crenata*). They were cut into block samples [approximately 5(R) × 5(T) × 5(L) mm] that were extracted with ethanol/benzene (1:2, v/v) for 8 h in a Soxhlet apparatus. The extracted wood was oven dried at 105°C for 24 h prior to further treatment. The ionic liquid, [EtPy][Br] (>98% purity) was purchased from Tokyo Chemical Industry Co., Ltd..

3.2.2 Treatment with [EtPy][Br] for light microscopy analysis

The extracted wood samples were cut with a sliding microtome into 15-μm-thick sections and mounted in a 20-μm-deep hemocytometer. Each mounted section was dried for 2 h at 105°C, then 100 μL of [EtPy][Br], heated to 120°C, was dropped onto the mounted section. The hemocytometer was immediately closed with a glass cover; this was designated as the beginning of the treatment. The hemocytometer was placed in an oven at 120°C for various time periods, and then removed from the oven to examine the anatomical changes in the wood section using light microscopy. Three areas (cell lumen area, cell wall area, and total of cell lumen area + cell wall area; defined as shown in Fig. 2.1) were measured for five neighboring cells in both latewood and earlywood, using image analysis software and the average was calculated for each area.

3.2.3 Treatment with [EtPy][Br] for SEM observation

Extracted wood samples were surfaced with a sliding microtome. The surfaced samples were dried for 24 h at 105°C and the surfaced area was then treated by dipping into [EtPy][Br] and heating to 120°C for various periods of time. During the dipping treatment, the [EtPy][Br] was stirred gently with a magnetic stirrer. The treated specimens were dipped into DMSO to remove [EtPy][Br] and then washed with distilled water to remove DMSO. After drying for 24 h at 105°C, each specimen was mounted on a specimen holder using carbon tape and sputter-coated with Au using an auto fine coater. The exposed surface was examined by SEM at beam accelerating voltages from 10 to 25 kV.

3.2.4 Treatment with [EtPy][Br] for confocal Raman microscopy analysis

For Raman microscopy the [EtPy][Br] treatment was the same as that for light microscopy. To perform analysis on the same cell wall area with respect to Raman mapping and line analysis, 15-μm-thick serial sections were prepared. After a specific treatment time, a large amount of distilled water was poured into the hemocytometer from its lateral direction, and then the hemocytometer was placed in a Petri dish filled with distilled water for 24 h at room temperature to completely remove [EtPy][Br].

Raman analyses were performed with a confocal microRaman system equipped with a confocal microscope and a motorized x, y stage. To ensure high spatial resolution, the measurements were conducted with a high numerical aperture (NA=1.40) oil immersion microscope objective, and a 532 nm diode-pumped solid state laser. Immersion oil was used as the medium between the objective and the glass cover. The theoretical lateral resolution on the sample was about 0.23 μm (0.61λ/NA), where λ is the wavelength of the laser and NA is the numerical aperture of the microscope objective. The incident laser power on the sample was approximately 10 mW. Scattered Raman light was detected by a CCD detector behind either a 300 or 1800 lines/mm grating. A confocal pinhole diameter of 300 μm was used for all experiments.

To obtain high-quality spectra and avoid damaging the wood samples with the heat from the laser during the point analysis, the Raman spectra were measured in 10 cycles,

with each cycle consisting of a 1-s integration time for one spot. 10 spectra were obtained and averaged, and the averaged spectra from 10 different locations were again averaged. The grating used in the point analysis was 1800 lines/mm. For mapping analysis, measurements were conducted every 0.4 μm steps and the spectra were obtained by averaging 4 cycles, each with a 0.2 s integration time. The grating used for line analysis and mapping was 300 lines/mm.

The data acquisition and analysis was done by means of LabSpec5 software. To remove the background from fluorescence, the raw spectral data were baseline-corrected. The smoothing to reduce spectral noise was performed with the Savitzky-Golay algorithm. In the point analysis, to clarify differences in the spectra after [EtPy][Br] treatment, the spectra were normalized using an internal reference band. In this study, the strong band of an aromatic ring around 1600 cm^{-1}, which has superior chemical stability under the present ionic liquid treatment conditions, was selected.

3.3 Results and discussion

3.3.1 Morphological and topochemical study on *Cryptomeria japonica* cell walls treated with [EtPy][Br]

3.3.1.1 Morphological observation using light microscopy and SEM

The light micrographs revealed the morphology of the cell walls in [EtPy][Br]. Fig. 3.1 shows light microscopy and polarized light microscopy images of a transverse section before and after treatment for 72 h with [EtPy][Br] at 120°C. The cell walls of the tracheids were swollen and the structure was slightly disordered. However, they were hardly dissociated in both the latewood and earlywood after [EtPy][Br] treatment (Fig. 3.1e, g, h). In the earlier research into morphological changes during [C2mim][Cl] treatment, the cell walls of *Cryptomeria japonica* tracheids were found to be dissociated in the latewood but not in the earlywood (Miyafuji and Suzuki 2012). For the other tissues the ray parenchyma cells were partly destroyed in the latewood but not in the earlywood (indicated by filled arrows), and the axial parenchyma cells collapsed on the cell lumen

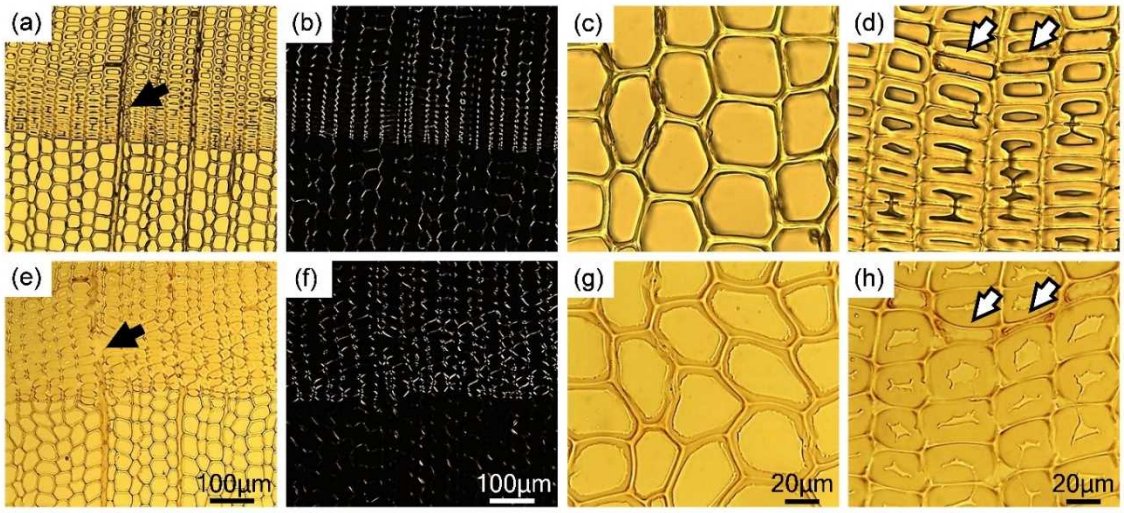

Fig. 3.1 Light microscopy and polarized light microscopy images of transverse sections before and after treatment with [EtPy][Br] at 120°C for (a–d) 0 h and (e–h) 72 h. (a, e) Around annual ring boundary. (b, f) Polarized light micrographs of (a) and (e). (c, g) Magnified view of earlywood. (d, h) Magnified view of latewood. *Filled arrow*: ray parenchyma cell, *open arrow*: axial parenchyma cell.

side (indicated by open arrows). These morphological changes in the parenchyma cells were triggered by pressure from neighboring swollen tracheids. From polarized light microscopy observation the brightness from the birefringence of cellulose did not change after [EtPy][Br] treatment (Fig. 3.1f). This result indicates that the crystalline structure of cellulose in the wood cell walls was preserved after treatment for 72 h with [EtPy][Br] at 120°C.

To analyze the swelling behavior of the tracheids during [EtPy][Br] treatment in detail, time sequential measurements of the cell wall area, the cell lumen area, and the total cell lumen area + cell wall area (defined in Fig. 2.1) were obtained using image analysis software. The results are shown in Fig. 3.2. During the initial stages of [EtPy][Br] treatment, all the measured areas in the earlywood only changed slightly. The cell wall area and the total of the cell lumen area + the cell wall area in the latewood increased significantly. Thereafter, the changes varied. In the latewood, although the cell wall area and the total of the cell lumen area + the cell wall area increased gradually with an increase in treatment time, the cell lumen area hardly changed. In the earlywood the cell wall area increased slightly but the total cell lumen area + the cell wall area and the cell lumen area decreased. This decrease is caused by the deformation of the cell walls because of pressure from the swelling of the cell walls in the latewood. After 72 h of treatment, the cell wall areas in the earlywood and the latewood increased 1.3 and 2 times, respectively. In the previous paper, it is reported that the cell wall areas in the latewood of the tracheids of *Cryptomeria japonica* increased 5 times after treatment for 48 h with [C2mim][Cl] (Miyafuji and Suzuki 2012). These results indicate that the swelling efficiency of [EtPy][Br] in the cell walls is lower than that of [C2mim][Cl], and morphological changes in the cell walls are different for each type of ionic liquid.

The SEM images in Fig. 3.3 show ultrastructural changes in the various cell wall structures before and after treatment for 72 h with [EtPy][Br] at 120°C. After the 72 h treatment cracks were observed around the annual ring boundary (Fig. 3.3b). Additionally, large parts of the CML and the CC disappeared in both the earlywood and the latewood (Fig. 3.3d, f). The surface of S_2 was full of large pores in the latewood (Fig. 3.3f). The observed cracks and the disappearance of the CML and the CC was not evident by light

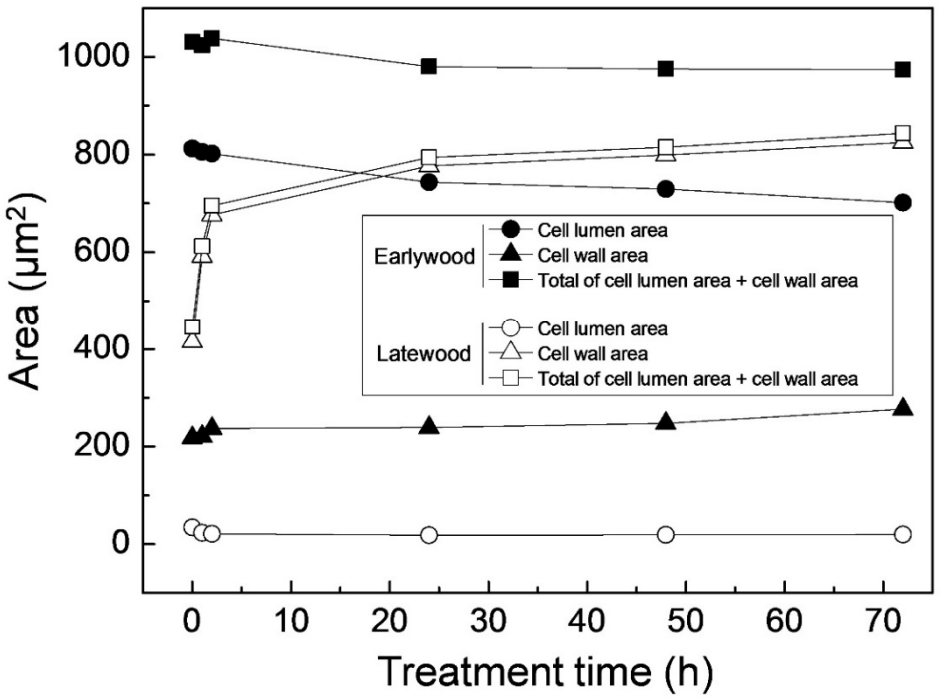

Fig. 3.2 Changes in cell wall area, cell lumen area and total of cell lumen area + cell wall area for tracheids of *Cryptomeria japonica* during [EtPy][Br] treatment.

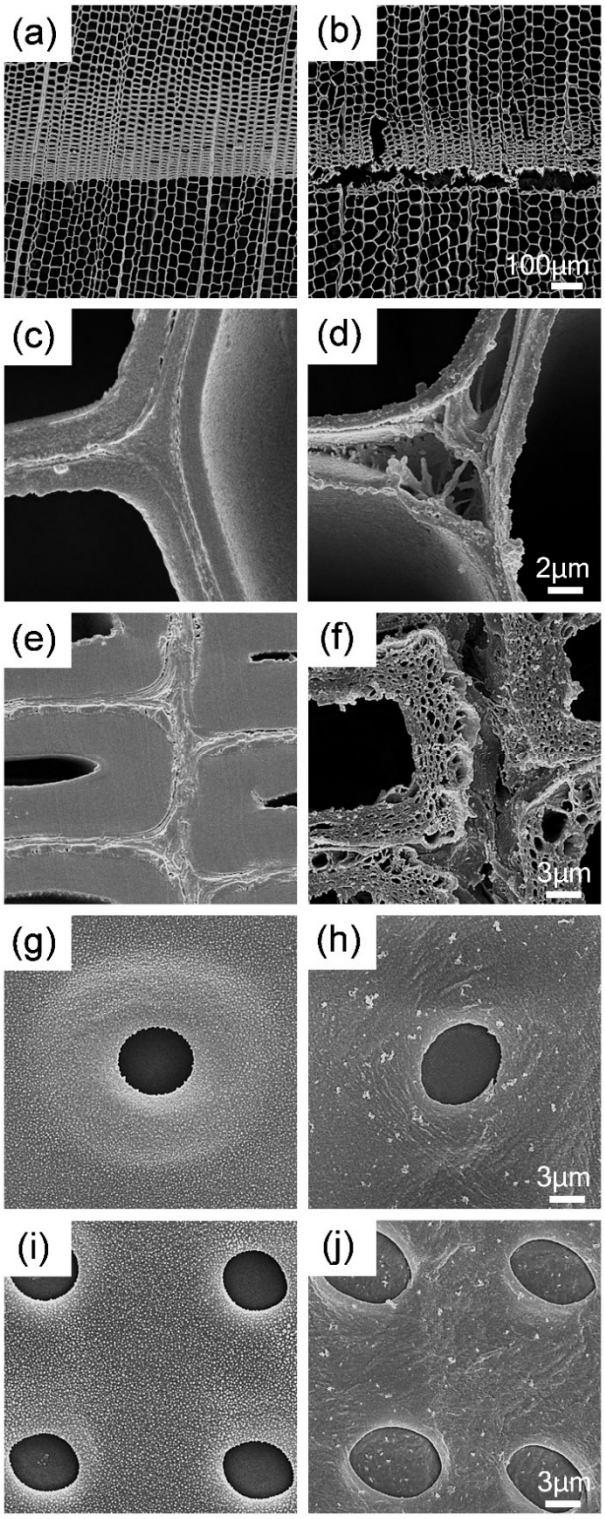

Fig. 3.3 SEM images of various tissues before and after treatment with [EtPy][Br] at 120°C for (a, c, e, g, i) 0 h and (b, d, f, h, j) 72 h. (a, b) Around annual ring boundary. (c, d) Magnified view of earlywood. (e, f) Magnified view of latewood. (g, h) Bordered pits. (i, j) Taxodioid pits.

microscopy and these changes may thus be attributed to a shrinkage of the cell wall structure during SEM pretreatment, likely in the drying process. The disappearance of the CML and the CC may also be related to lignin distribution in the wood cells. The CML and the CC regions contain more than 50% and 70% lignin, respectively, whereas the S_2 region contains about 20% lignin (Donaldson 2001). Recent study revealed that lignin can be liquefied more rapidly than cellulose by [EtPy][Br] (Yokoo and Miyafuji 2014). Therefore, a significant liquefaction and elution of chemical components occurred in the CML and the CC regions, and these regions, in which the volume decreased, shrunk significantly upon subsequent drying. The formation of pores in the transverse section's surface of the secondary wall has also been observed during chemical and physicochemical treatments such as an alkaline treatment (Ji et al. 2014a), steam explosion (Corrales et al. 2012), and ammonia fiber expansion (Chundawat et al. 2011). The formation of large pores may be associated with the partial liquefaction and elution of chemical components, particularly lignin; however, the details still require further investigation.

As shown in Fig. 3.3h, j, the pit membranes in the bordered pits and in the taxodioid pits hardly changed. Most of the warts on the surface of the tracheids (Fig. 3.3g, i) disappeared after [EtPy][Br] treatment. The pit membranes are mainly composed of cellulose microfibrils (Harada and Côté 1985) whereas the warts are chemically composed of lignin and hemicellulose (Jansen et al. 1998; Watanabe et al. 2006). The difference in the reactivity of [EtPy][Br] with these tissues comes from their different chemical components.

3.3.1.2 Topochemical analysis using confocal Raman microscopy

Raman spectra of the tracheids treated with [EtPy][Br] at 120°C for 0, 24, and 72 h were obtained for the S_2, the CML, and the CC regions. Spectra from 350 to 3150 cm^{-1} were studied because this spectral range includes bands from the components of wood including cellulose, hemicellulose, and lignin. However, no spectral features were found between 1710 and 2750 cm^{-1} before or after treatment with [EtPy][Br]. Therefore, this

region is not shown here.

3.3.1.2.1 Point analysis

The Raman spectra were divided into four regions: from 350 to 1050 cm^{-1} (Fig. 3.4), from 1050 to 1540 cm^{-1} (Fig. 3.5), from 1540 to 1710 cm^{-1} (Fig. 3.6) and from 2750 to 3150 cm^{-1} (Fig. 3.7). Each region is discussed in detail below.

Region from 350 to 1050 cm^{-1}

The bands in this spectral region have not all been assigned but the bands of components such as the polysaccharides and lignin are known. A decrease in band intensity was observed at 591, 731, and 920 cm^{-1} for the whole cell wall area. All these peaks, with decreased intensity, are assigned to lignin. Other lignin bands were observed at 457, 785, and 899 cm^{-1}. However, these bands partially overlap with the polysaccharides bands. Changes in the intensity of these bands differed among the respective cell wall areas. For example, the band intensity at 457 cm^{-1} only changed slightly for the S_2 during the treatment whereas it decreased for the CML and the CC with an increase in the treatment time. Additionally, the band at 381 cm^{-1}, which is only assigned to cellulose (Agarwal 1999; Agarwal and Ralph 1997; Wiley and Atalla 1987), decreased significantly for the CML and the CC after the 72 h treatment. These differences in spectral changes among the S_2, the CML, and the CC indicate that the reactivity of [EtPy][Br] in wood cell walls is inhomogeneous.

Several new peaks were observed at 687, 774, 828, and 950 cm^{-1}. The band intensity at 687 and 774 cm^{-1} increased for the CML and the CC after the 24 h treatment and decreased after the 72 h treatment whereas the intensity of these bands continued to increase after 72 h for the S_2. The band intensity at 698 cm^{-1}, which has not been assigned, increased significantly for all the cell wall areas. A peak at 852 cm^{-1} was observed in both before and after treatment with [EtPy][Br]. This band has not been detected in other wood species (Agarwal and Ralph 1997) and, therefore, this band may be characteristic of *Cryptomeria japonica*.

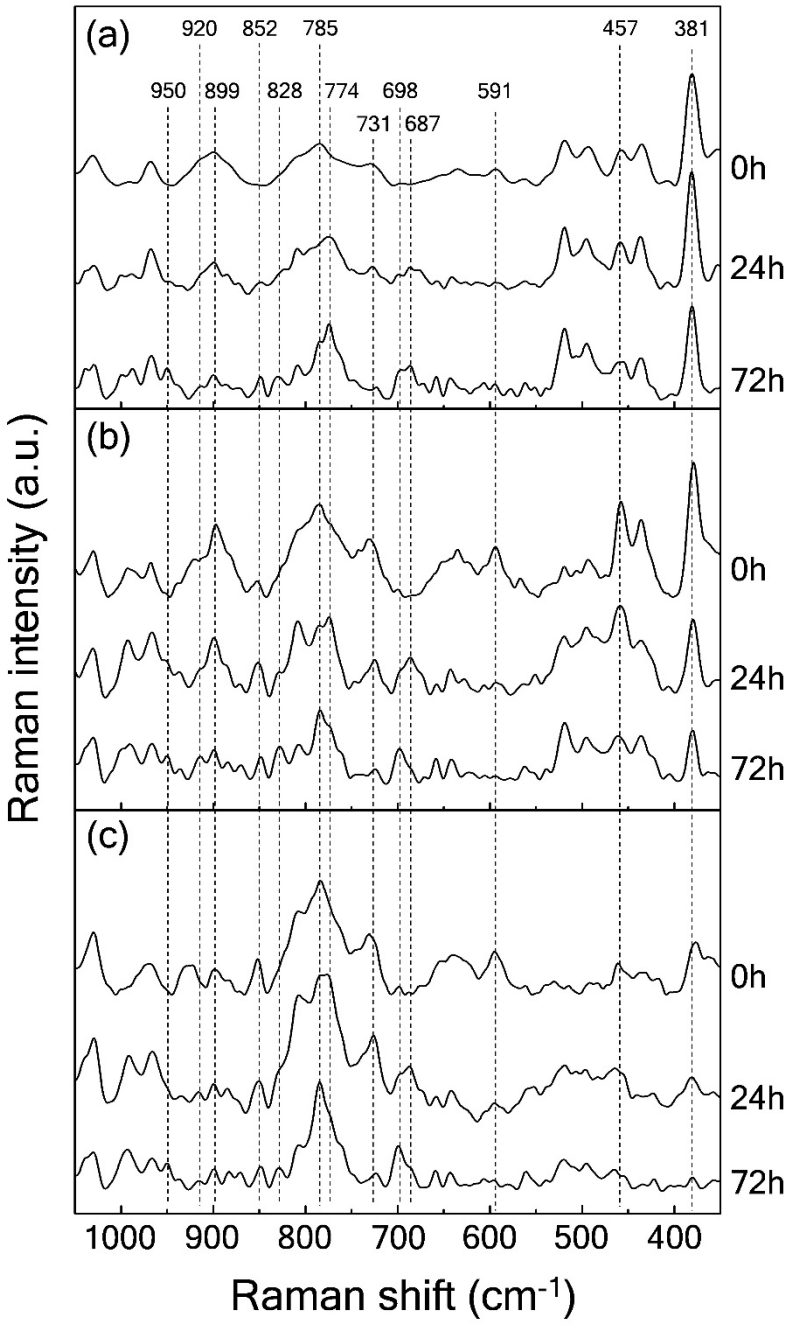

Fig. 3.4 Raman spectra for (a) S_2, (b) CML, and (c) CC of tracheids before and after treatment with [EtPy][Br] at 120°C for 0 h, 24 h, and 72 h; enlargement of the region from 350 to 1050 cm^{-1}.

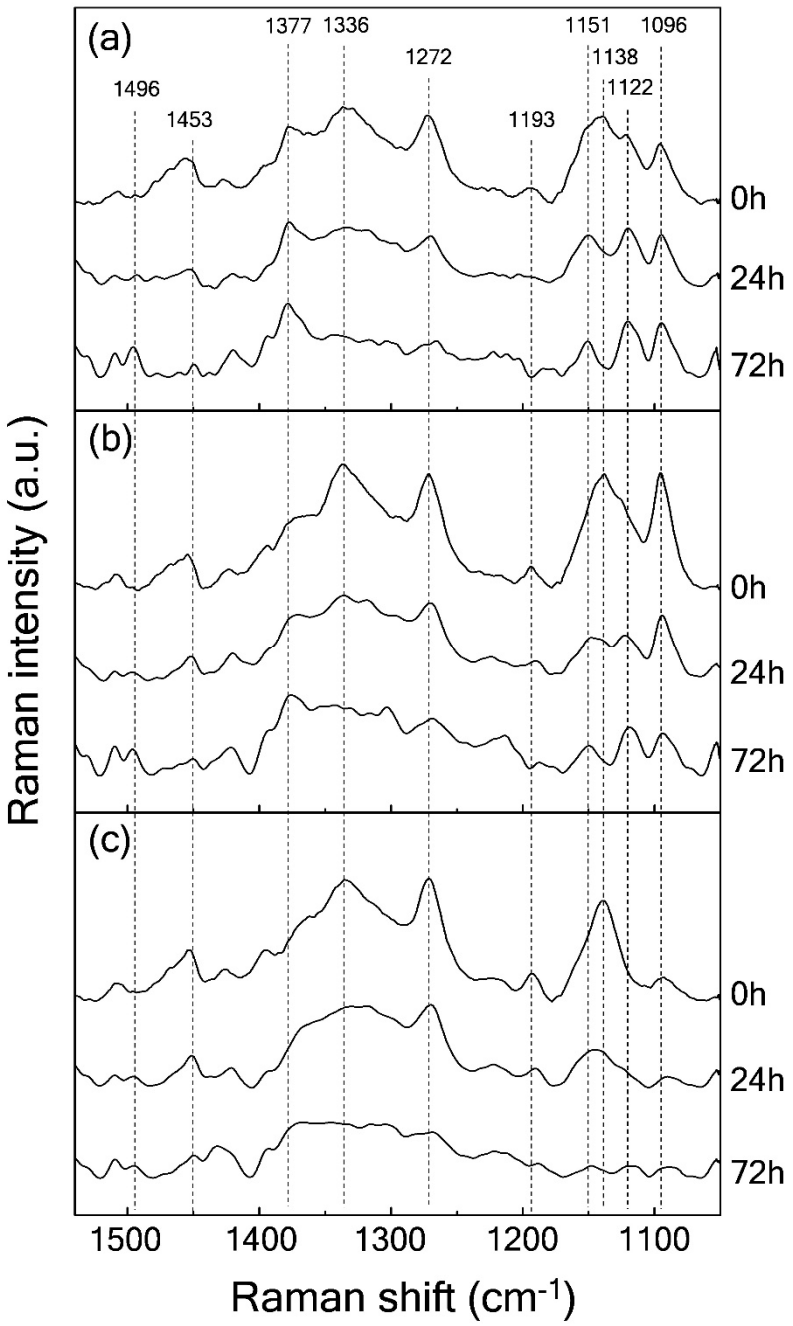

Fig. 3.5 Raman spectra for (a) S_2, (b) CML, and (c) CC of tracheids before and after treatment with [EtPy][Br] at 120°C for 0 h, 24 h, and 72 h; enlargement of the region from 1050 to 1540 cm^{-1}.

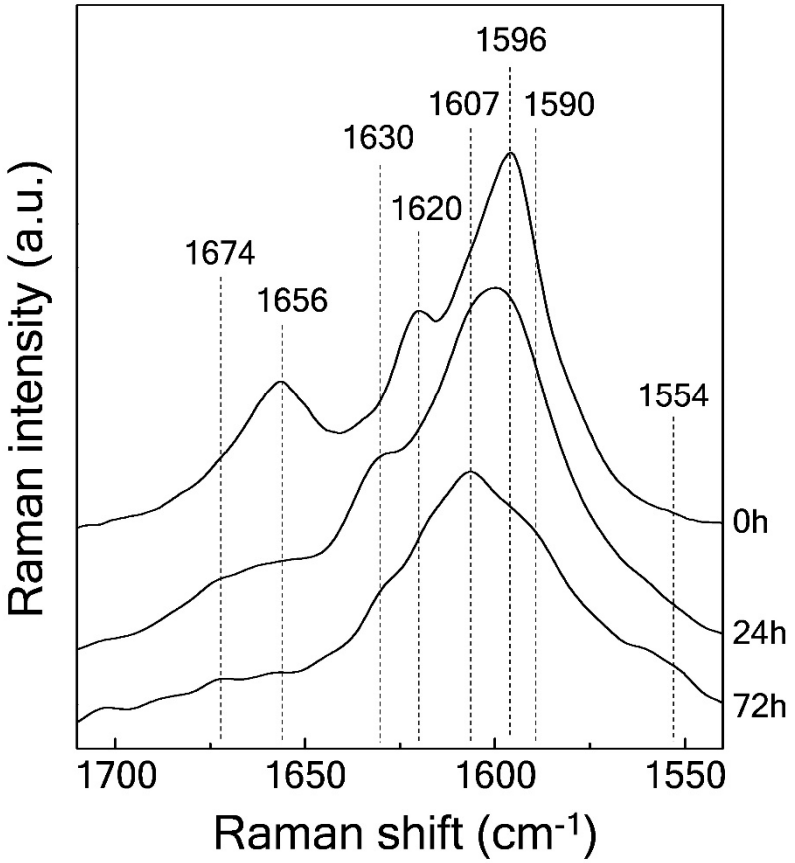

Fig. 3.6 Raman spectra for CML of tracheids before and after treatment with [EtPy][Br] at 120°C for 0 h, 24 h, and 72 h; enlargement of the region from 1540 to 1710 cm^{-1}.

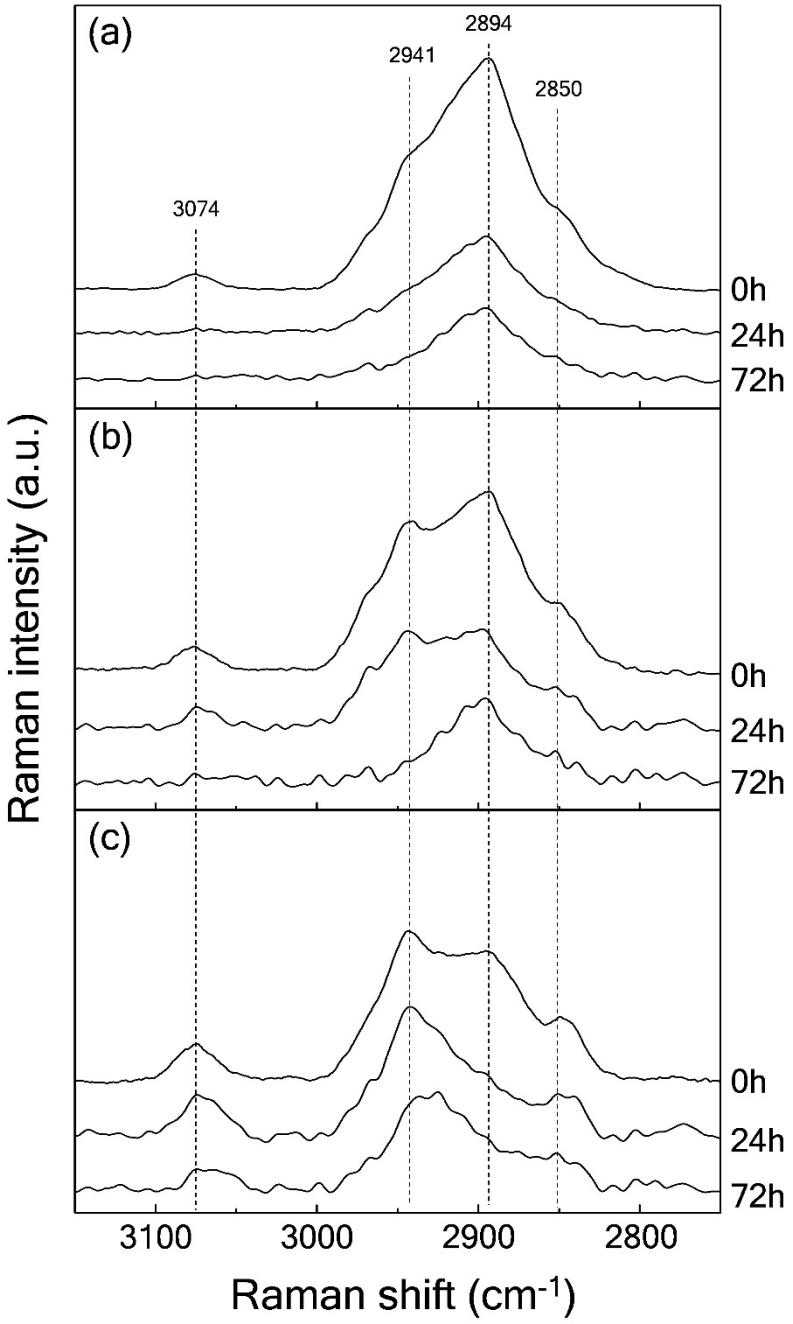

Fig. 3.7 Raman spectra for (a) S_2, (b) CML, and (c) CC of tracheids before and after treatment with [EtPy][Br] at 120°C for 0 h, 24 h, and 72 h; enlargement of the region from 2750 to 3150 cm^{-1}.

Region from 1050 to 1540 cm^{-1}

In all the cell wall areas the band intensities at 1138, 1193, 1272, 1336, and 1453 cm^{-1} decreased with an increase in treatment time. Most of these bands can be assigned to lignin. The most significant decrease was at the positions where coniferylaldehyde (1138 cm^{-1}) was present. On the other hand, the peaks at 1122, 1151, and 1377 cm^{-1} became sharper after the treatment. All these bands come from the polysaccharides. However, the band intensity at 1096 cm^{-1} in the CML and the CC decreased gradually with an increase in the treatment time, and this band can be assigned to the polysaccharides. These changes come from a decrease in the peripheral lignin bands. From these results, lignin preferentially reacts with [EtPy][Br] compared with the polysaccharides in wood cell walls. This result is similar to the previous paper on liquefaction of the wood flour of *Cryptomeria japonica* by [EtPy][Br] which reported that lignin can be easily liquefied in [EtPy][Br] than cellulose (Yokoo and Miyafuji 2014).

A new band appeared at 1496 cm^{-1}, and this band's intensity increased as the treatment time increased. This change is similar to the result of the treatment of *Cryptomeria japonica* with the ionic liquid [C2mim][Cl] (Fig. 2.16).

Region from 1540 to 1710 cm^{-1}

As shown in Fig. 3.6, several marked changes are observed in the spectral region from 1540 to 1710 cm^{-1}. These mainly originate from lignin. In this region, only spectral changes for the CML were observed because the Raman spectra of the S_2, the CML and the CC show similar changes upon [EtPy][Br] treatment. The band intensity decreased at 1596, 1620, and 1656 cm^{-1} whereas several new peaks and shoulders appeared at 1554, 1590, 1607, 1630, and 1674 cm^{-1}. The new peaks at 1554, 1674, and 1630 cm^{-1} are assigned to *o*-quinone, *p*-quinone, and the C=C bond of stilbene, respectively (Agarwal 1998; Agarwal and Atalla 2000). Therefore, it is possible that the C=C bonds in the coniferylaldehyde units and in the coniferylalcohol units decreased and thus quinone and stilbene derivatives were produced upon [EtPy][Br] treatment. Although most of these changes also occurred upon [C2mim][Cl] treatment (Fig. 2.18), the peak shift at 1596

cm^{-1} because of an aromatic ring vibration after treatment with [EtPy][Br] was more significant than that after treatment with [C2mim][Cl]. The band at 1596 cm^{-1} in the spectrum of untreated wood was found to shift to 1607 cm^{-1}. Additionally, a weak shoulder appeared at 1590 cm^{-1}. These changes are thought to come from the modification or removal of functional groups related to the aromatic ring. The difference in band shifts after treatment with [EtPy][Br] or [C2mim][Cl] indicates that the interaction of wood with ionic liquids is different. Furthermore, it is suggested that the specific structure of lignin is altered whereas most of the aromatic rings remain, without change, after treatment with [EtPy][Br] for 72 h.

Region from 2750 to 3150 cm^{-1}

All the lignin bands at 2850, 2941, and 3074 cm^{-1} decreased with prolonged treatment for all the cell wall areas. The decrease in the band intensity of the CC was lower than that of the S_2 and the CML. The polysaccharides band intensity at 2894 cm^{-1} decreased after 24 h but no change was observed from 24 h to 72 h for all the cell wall areas. In this spectral region, many small peaks were detected particularly for the CML and the CC after [EtPy][Br] treatment. The appearance of small peaks may be attributed to C−H stretching in the modified woody components.

3.3.1.2.2 Raman mapping analysis

To investigate chemical changes in the cell walls over a larger area during [EtPy][Br] treatment, a time sequential Raman map of lignin and the polysaccharides was obtained. Fig. 3.8a−c shows bright field images of the tracheids in the transverse sections before and after [EtPy][Br] treatment. All the micrographs are images of the same area, and Raman mapping was performed on these cell walls. In the micrographs, the rectangles show the areas selected for mapping. The cell walls gradually became discolored upon prolonged treatment. This discoloration of the cell walls supports the point analysis results where the components of the cell walls change their nature upon treatment with [EtPy][Br].

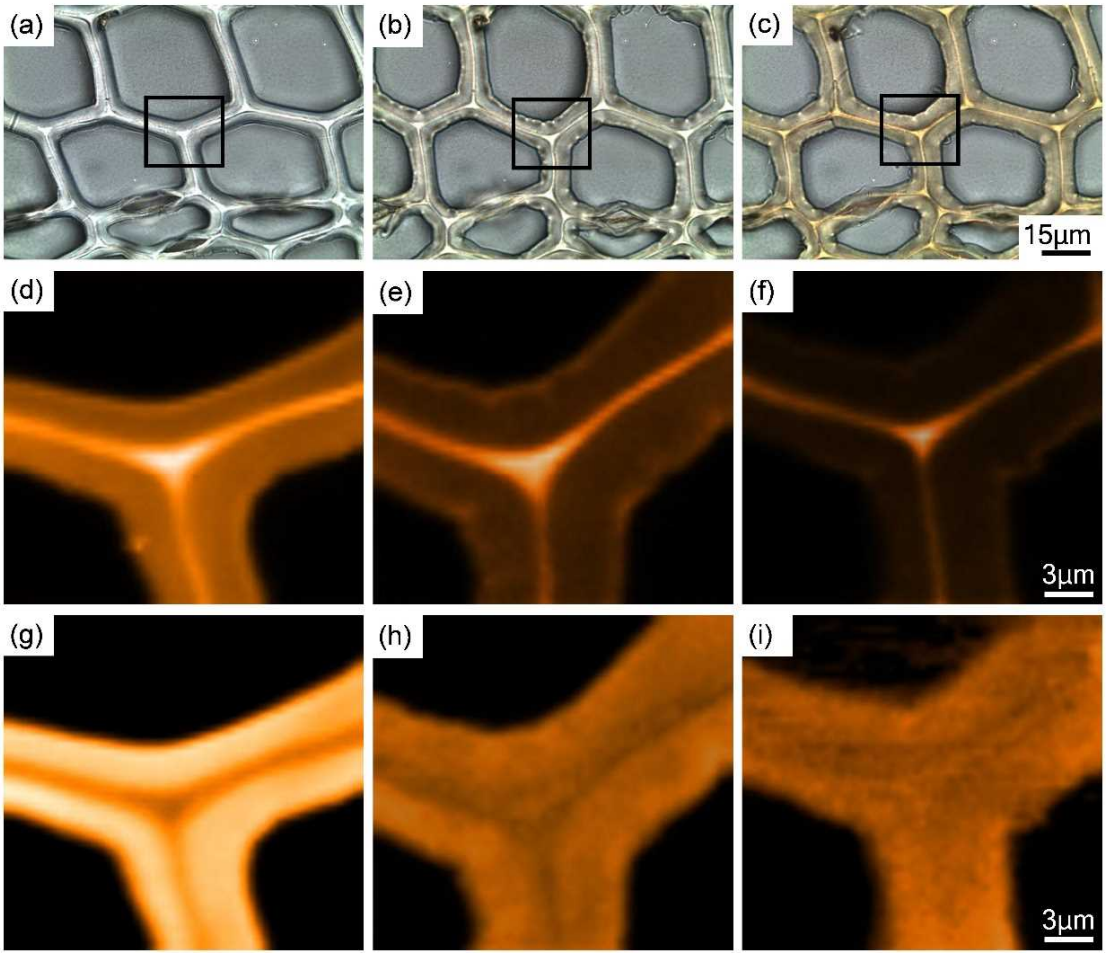

Fig. 3.8 Raman mapping on transverse sections of tracheids before and after treatment with [C2mim][Cl] at 120°C for (a, d, g) 0 h, (b, e, h) 24 h, and (c, f, i) 72 h. (a−c) Bright field images of the measured position. (d−f) Distribution of lignin (1591–1613 cm^{-1}). (g−i) Distribution of polysaccharides (2884–2905 cm^{-1}). Bright regions indicate high concentrations of specific chemical compositions, dark regions indicate low concentrations.

Fig. 3.8d−f and g−i shows Raman images of the distribution of lignin and the polysaccharides before and after treatment with [EtPy][Br], respectively. The band regions from 1591 to 1613 cm^{-1} and from 2884 to 2905 cm^{-1} in the Raman spectra were selected for the Raman images of lignin and Polysaccharides distribution, respectively. Although the lignin concentration in S_2 decreased significantly with treatment time the lignin concentration in the CML and the CC only changed slightly. The lignin in the CML and the CC contains many *p*-hydroxyphenyl propane units and it forms a highly condensed structure (Terashima and Fukushima 1988; Whiting and Goring 1982). This lignin structure is highly stable against delignification (Akim et al. 2001; Whiting and Goring 1982). Therefore, the CML and the CC retain high concentrations of lignin after the 72 h treatment. However, the reduction in the amount of lignin in the CML and the CC upon treatment with [EtPy][Br] was greater than that upon treatment with [C2mim][Cl]. Additionally, the concentration of lignin in the S_2 decreased homogeneously unlike the case of [C2mim][Cl] treatment. In the Raman image of the 24 h treatment product it was found that the lignin concentration of the nearby S_3 is higher than that of the S_2. This difference is probably due to differences in the original lignin concentration of the cell wall layers. It has been reported that certain wood species have lignin concentrations in the S_3 of the tracheid that are higher than that of the S_2 (Donaldson 1987; Scott and Goring 1970; Wood and Goring 1971), and *Cryptomeria japonica* may be one of these species. However, these results were not obtained from the S_3 of the non-treated tracheids. This is because the spatial resolution was not sufficient for the observation of the S_3, which is approximately 0.1-μm-thick (Harada and Côté 1985). After the 24 h treatment, the thin S_3 swelled because of [EtPy][Br] and it could be distinguished from the S_2. With respect to the polysaccharides, their concentrations decreased significantly after 24 h (Fig. 3.8h) but no significant changes were observed after 72 h (Fig. 3.8i). The first decrease in the polysaccharides is likely caused by a reduction in cell wall density because of cell wall swelling.

3.3.2 Morphological and topochemical study on *Fagus crenata* cell walls treated with [EtPy][Br]

3.3.2.1 Morphological observation using light microscopy and SEM

Morphological characterization of the main elements of wood tissues treated with [EtPy][Br] was performed by light microscopy. Figure 3.9 shows the light and polarized light micrographs of the transverse sections treated with [EtPy][Br] at 120°C for 72 h. The cell walls of wood fibers (as indicated by arrows in Fig. 3.9) were swollen and vessels (as indicated by "V" in Fig. 3.9) were slightly distorted after [EtPy][Br] treatment (Fig. 3.9b). These morphological changes were nearly the same as the result using the ionic liquid, [C2mim][Cl] (Fig. 2.2). From the polarized light microscopic observations, the brightness from the birefringence of cellulose was slightly reduced after [EtPy][Br] treatment (Fig. 3.9d). This result indicates that most of the crystalline structure of cellulose in the cell walls was preserved but was partially amorphized by [EtPy][Br] treatment.

In order to determine detailed swelling behavior of wood cell walls during [EtPy][Br] treatment, time sequential area measurements were performed on wood fibers and vessels in latewood and earlywood. Although the cell wall areas of wood fibers in both latewood and earlywood increased with progressing treatment within 24 h, they showed no change from that time onward (Fig. 3.10a). This tendency to be leveled off was also observed on vessel cell walls in both latewood and earlywood (Fig. 3.10b). Eventually, after 72 h of treatment, the cell wall areas of wood fibers and vessels in both latewood and earlywood increased by a factor of 1.8 and 1.5 times, respectively. The cell walls of vessels were hard to be swelled by [EtPy][Br] than that of wood fibers. Treatment with [EtPy][Br] for 72 h can result in swelling of *Cryptomeria japonica* tracheids in latewood up to 2 times (Fig. 3.2). In addition, treatment with another type of the ionic liquid [C2mim][Cl] can result in swelling of *Fagus crenata* wood fibers in both latewood and earlywood up to 4 times (Fig. 2.3a). These discrepancies in swelling behavior imply that the interaction of wood cell walls with ionic liquids is different for wood species and types of ionic liquids.

Figure 3.11 shows the light micrographs of the tangential sections of ray parenchyma

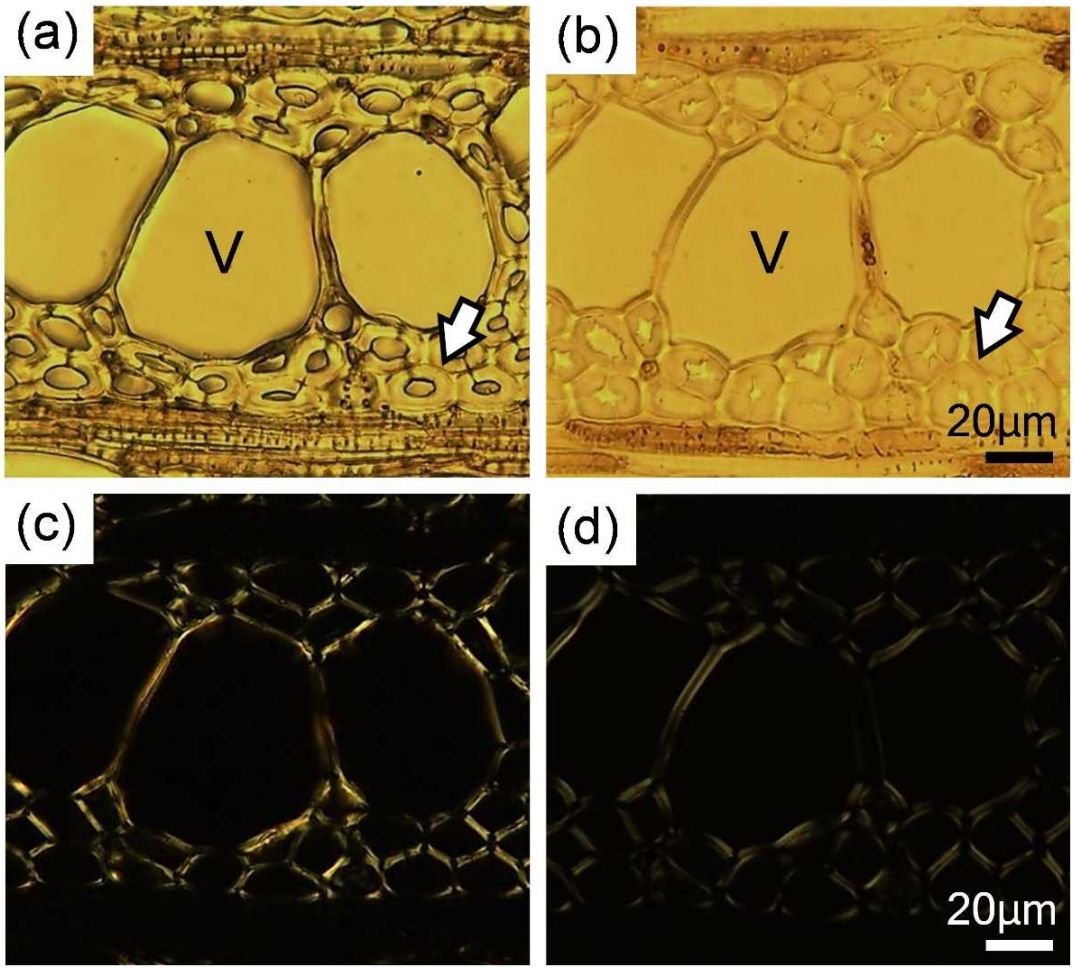

Fig. 3.9 Light microscopy and polarized light microscopy images of transverse sections before and after treatment with [EtPy][Br] at 120°C for (a, c) 0 h and (b, d) 72 h. (c, d) Polarized light micrographs of (a) and (b). *V*: vessel, *arrow* wood fiber.

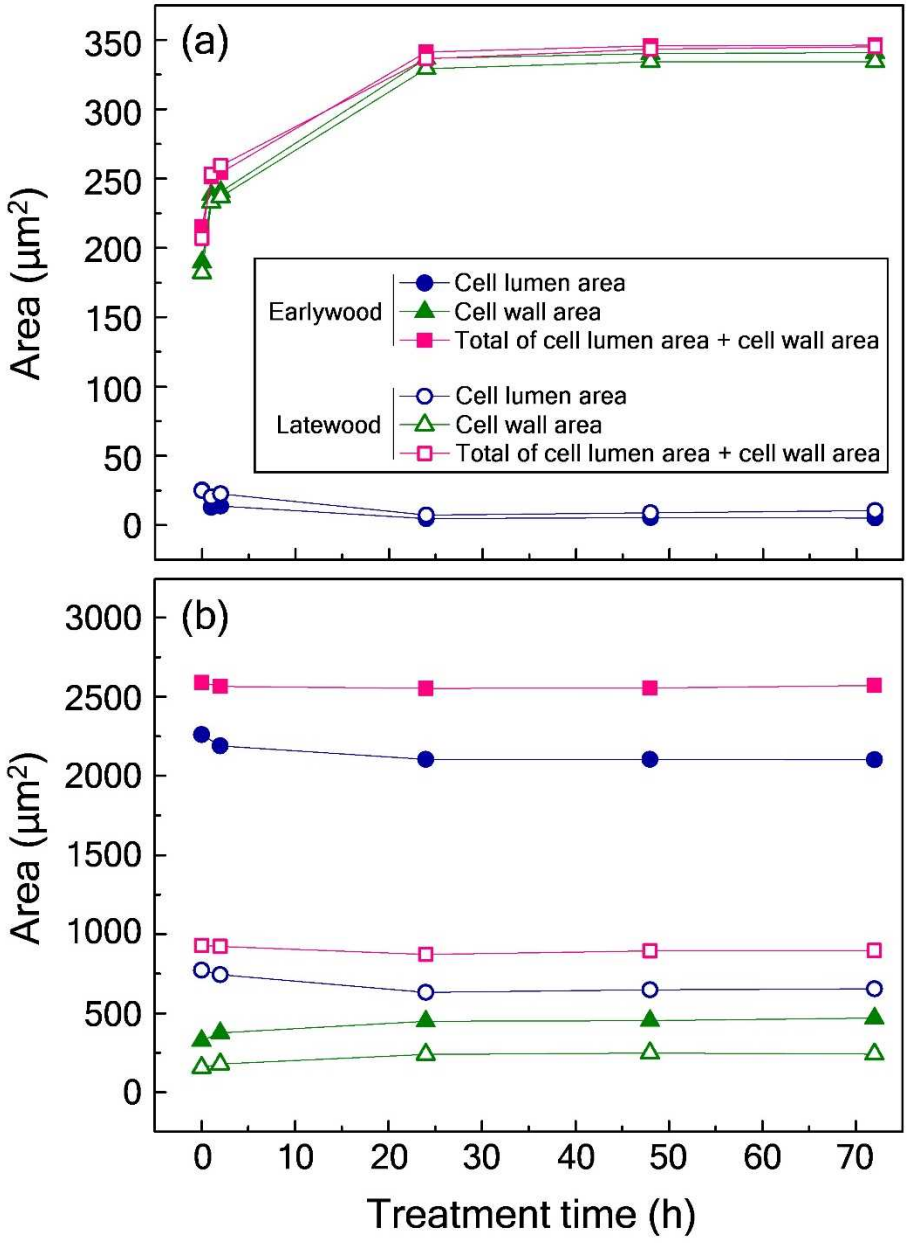

Fig. 3.10 Changes in cell wall area, cell lumen area and total of cell lumen area + cell wall area for (a) wood fiber and (b) vessel of *Fagus crenata* during [EtPy][Br] treatment.

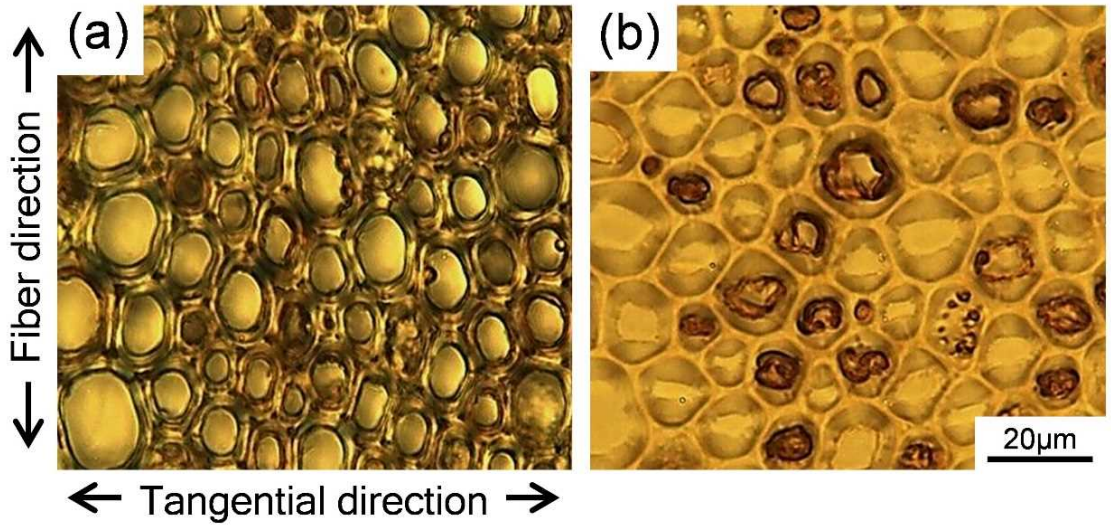

Fig. 3.11 Light microscopy images of tangential sections of ray parenchyma before and after treatment with [EtPy][Br] at 120°C for (a) 0 h and (b) 72 h.

treated with [EtPy][Br] at 120°C for 72 h. The swelling ratio of ray parenchyma cells as with the value of vessels was lower than that of wood fibers. The cell walls areas of ray parenchyma cells increased by a factor of 1.6 times after 72 h of treatment. In addition, changes of their cell walls thickness were different for swelling direction; increment of the cell wall thickness was greater in the fiber direction than in the tangential direction. After 72 h of treatment, the cell walls thickness along the fiber and the tangential direction increased by 1.8 and 1.5 times, respectively. As shown in Fig. 2.4, ray parenchyma cells of *Fagus crenata* swell significantly in the fiber direction in comparison with the tangential direction after [C2mim][Cl] treatment. Therefore, it is concluded that the ray parenchyma cell walls of *Fagus crenata* show anisotropic swelling within ionic liquids and are easy to swell along the fiber direction.

Ultrastructural changes in various tissues due to [EtPy][Br] treatment were observed by SEM. We analyzed transverse sections of wood samples before and after treatment with [EtPy][Br] at 120°C for 72 h. The native tissues had a well-ordered structure and each of cell including wood fibers, vessels and parenchyma cells was tightly combined with each other (Fig. 3.12a). However, the solid cell walls were low-densified and dissociated after [EtPy][Br] treatment, while outlines of the original cell walls were still preserved (Fig. 3.12b). Higher magnified images described in Fig. 3.12c, d showed that [EtPy][Br] treatment transformed the smooth and highly densified surface of secondary wall of untreated wood fibers into coarse and porous surface. In addition, the greater part of CML and CC which are generally highly lignified (Agarwal 2006; Bailey 1936; Boutelje 1972; Donaldson 1985, 1987, 2001; Fergus et al. 1969; Fergus and Goring 1970; Gierlinger and Schwanninger 2006; Hänninen et al. 2011; Lehringer et al. 2008; Ma et al. 2011, 2013; Pohling et al. 2014; Ritter 1925; Röder et al. 2004; Saka and Thomas 1982a, b; Schmidt et al. 2009; Scott et al. 1969; Sun et al. 2011; Tirumalai et al. 1996; Westermark et al. 1988; Wood and Goring 1971; Xu et al. 2006; Zhang et al. 2012) disappeared. It is known that [EtPy][Br] has a feature of predominantly dissolving lignin rather than cellulose (Yokoo and Miyafuji 2014). Thus, these significant morphological changes are mainly the result of the progress of delignification.

To observe the detailed morphological changes in ray and axial parenchyma cells due

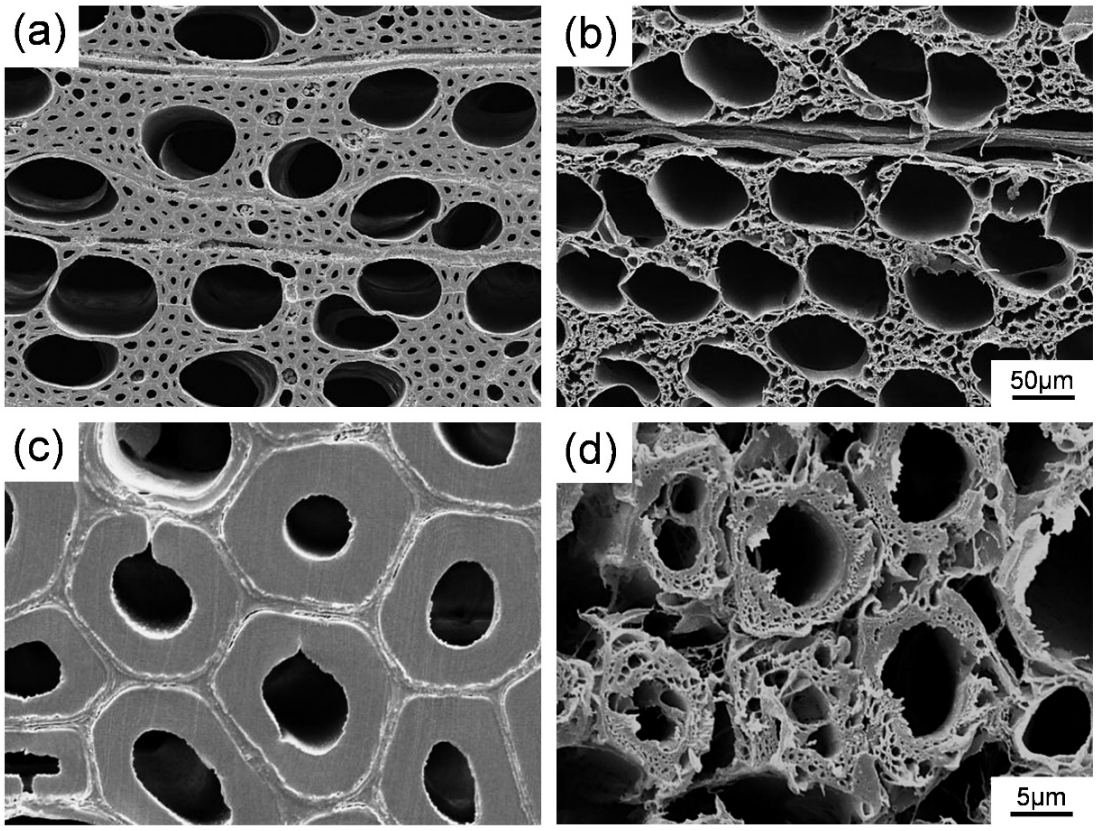

Fig. 3.12 SEM images of transverse sections before and after treatment with [EtPy][Br] at 120°C for (a, c) 0 h and (b, d) 72 h. (c, d) Magnified view of wood fibers.

to [EtPy][Br] treatment, the author analyzed tangential and radial sections of wood samples before and after treatment with [EtPy][Br] (Fig. 3.13). Although the cell wall thickness decreased significantly in both ray and axial parenchyma cells as with wood fibers, pores were not observed on the sections of parenchyma cells. Wood fibers and parenchyma cells have the primary wall (P), the outer (S_1), the S_2, and the S_3 layers of secondary wall, whereas their proportion, in thickness, and their microfibril angle are different for cell types (Harada 1965; Tsoumis 1991). In addition, the lignin distribution is also different for cell types (Fergus and Goring 1970; Saka and Goring 1988). The variety of cell wall structure and chemical composition maybe induced the differences in morphological changes among cell types. Compare ray and axial parenchyma cells from the view of radial direction, axial parenchyma cells dissociated at the border between end walls (as indicated by arrow in Fig. 3.13f) while ray parenchyma cells did not come to look like it. The dissociation is presumably due to the facts that the swelling ratio of the axial parenchyma cells was lower than that of the other cells adjacent to them and the binding power between axial parenchyma cells was weaken by the delignification of CML and CC.

The author also observed the morphological changes in vessel elements before and after treatment with [EtPy][Br]. Figure 3.14 shows two types of vessel perforations: simple perforation and scalariform perforation. As seen in the axial parenchyma cells (Fig. 3.13f), dissociation was also observed at the boundary of the two adjacent vessel elements particularly in simple perforation (as indicated by arrows in Fig. 3.14b). On the other hand, the scalariform perforation plate was slightly distorted, and the warts which exist on the inner surface of small vessel lumen and scalariform perforation plate disappeared (Fig. 3.14d). The warts are chemically composed of lignin and hemicellulose (Jansen et al. 1998; Watanabe et al. 2006), thus these elements dissolved in [EtPy][Br]. Various vessel pits are shown in Fig. 3.15. The pit membranes in ray-vessel pits still have remained after 72 h of treatment, while their smooth surface was partially transformed into porous and net-like morphology (as indicated by arrow in Fig. 3.15b). This morphological change is likely to be attributed to the liquefaction of lignin and hemicellulose which are slightly contained in pit membranes; however, the details still

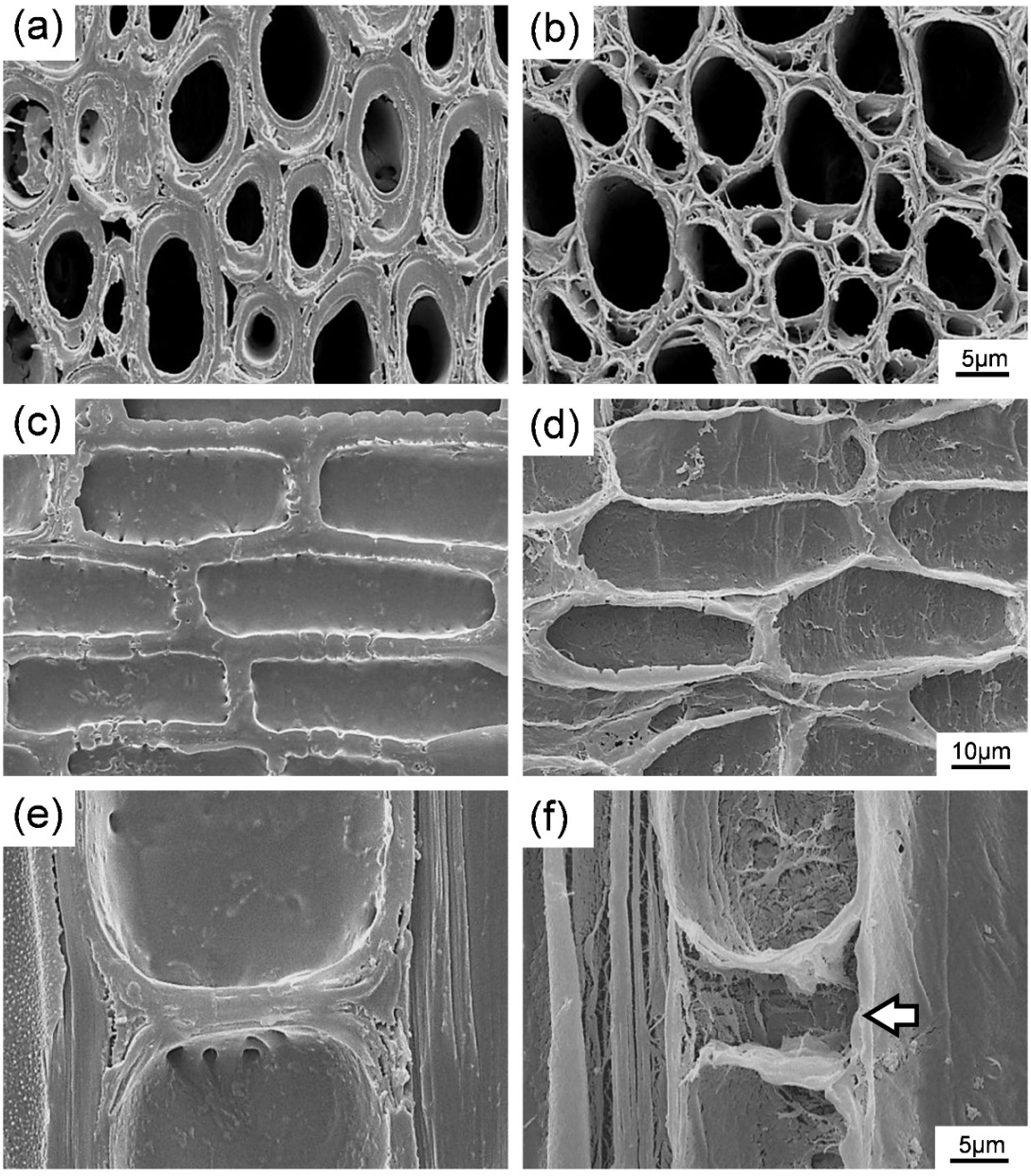

Fig. 3.13 SEM images of parenchyma before and after treatment with [EtPy][Br] at 120°C for (a, c, e) 0 h and (b, d, f) 72 h. (a, b) Ray parenchyma in tangential sections. (c, d) Ray parenchyma in radial sections. (e, f) Axial parenchyma cells.

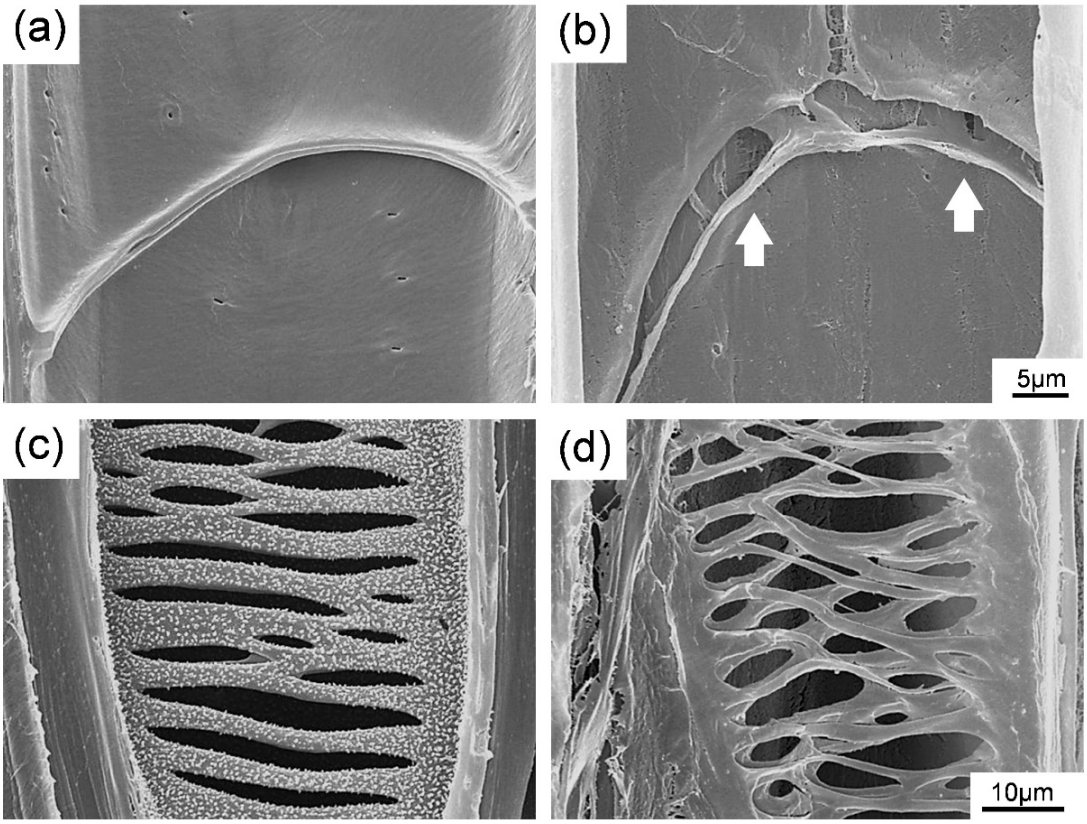

Fig. 3.14 SEM images of parenchyma before and after treatment with [EtPy][Br] at 120°C for (a, c) 0 h and (b, d) 72 h. (a, b) Perforation rim. (c, d) Scalariform perforation plate.

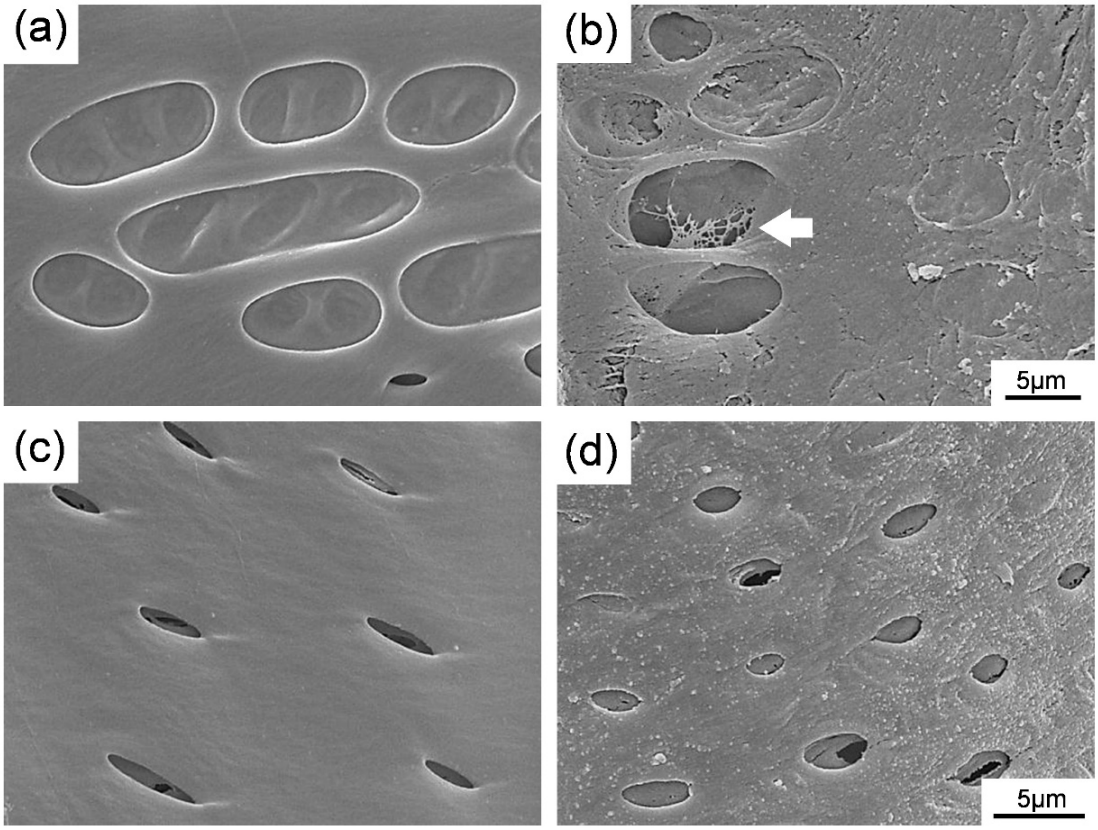

Fig. 3.15 SEM images of vessel pits before and after treatment with [EtPy][Br] at 120°C for (a, c) 0 h and (b, d) 72 h. (a, b) Ray-vessel pits. (c, d) Intervascular pits.

require further investigation. With regard to intervascular pits, they showed no significant change (Fig. 3.15d).

3.3.2.2 Topochemical analysis using confocal Raman microscopy

Characterization of the chemical changes in cell walls treated with [EtPy][Br] at a cellular level was carried out by confocal Raman microscopic method which has a potential to determine the molecular information with a high spatial resolution. Wood fibers contain the great amounts of mass in *Fagus crenata* and are of the great importance to the conversion process, thus we performed Raman analysis on the wood fibers.

3.3.2.2.1 Point analysis

Raman spectra obtained from S_2 and CC of the wood fibers as treated with [EtPy][Br] are presented in Fig. 3.16. In *Fagus crenata*, the main Raman bands of lignin appeared such as at 370, 1138, 1331, 1459, 1600, 1657, 2848, and 2943 cm^{-1} (solid lines), whereas those of polysaccharides appeared such as at 380, 436, 520, 1093, 1118, 1152, 1378, and 2895 cm^{-1} (dashed lines). These bands assignment was based on the previous reports (Agarwal and Ralph 1997; Agarwal 1999; Agarwal et al. 2011; Wiley and Atalla 1987). As shown in the spectra of untreated samples (0 h, Fig. 3.16a, b), S_2 contained both lignin and polysaccharides bands, while CC had almost only lignin features. During the treatment, although almost of all the band intensities of lignin rapidly decreased with the elapse of the treatment time in both two morphological regions, most of the band intensities of polysaccharides decreased only a little. These spectral changes were in accord with the previous report on liquefaction of wood flour; lignin is liquefied more readily than cellulose in [EtPy][Br] (Yokoo and Miyafuji 2014). Slight reduction of the band intensities of polysaccharides was probably attributed to swelling of the cell walls and partial liquefaction of polysaccharides particularly at amorphous regions, and significant reduction of certain of the polysaccharides band intensities arose from the reduction of the lignin features overlapped with polysaccharides bands regions.

Some new peaks appeared at 676, 770, and 808 cm^{-1} and increased with progress of

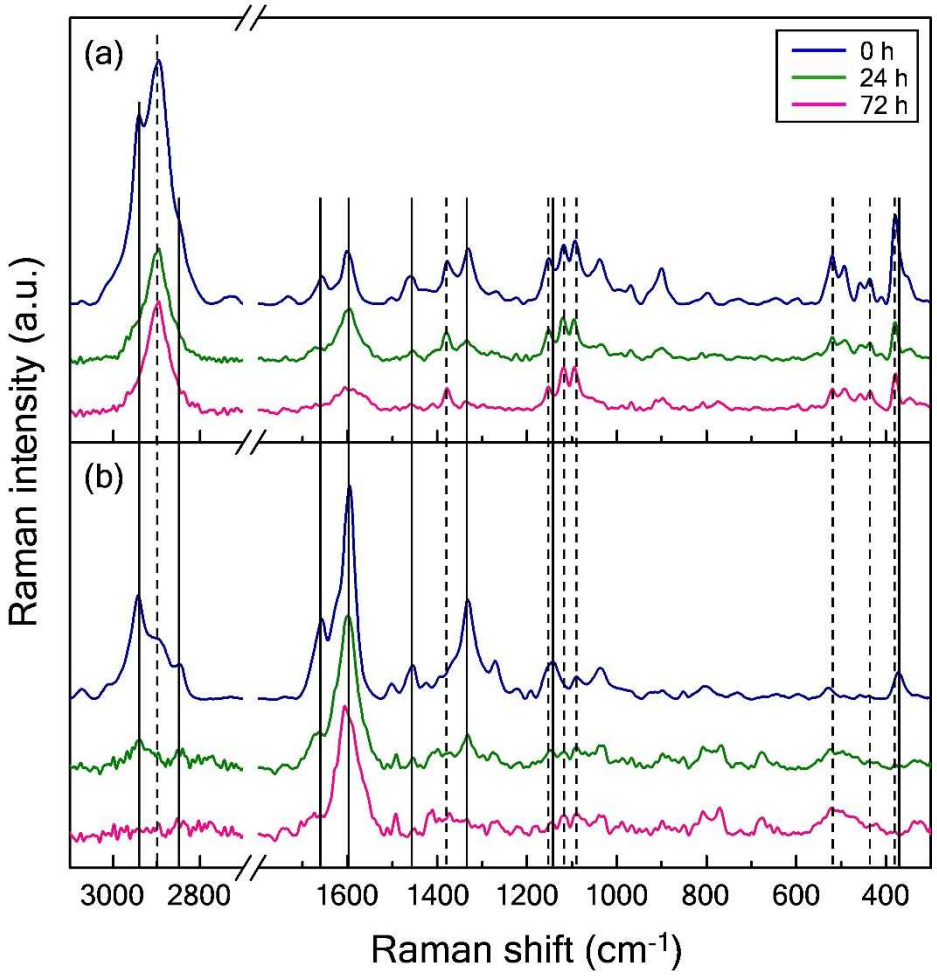

Fig. 3.16 Raman spectra for (a) S_2 and (b) CC of wood fibers before and after treatment with [EtPy][Br] at 120°C for 0 h, 24 h, and 72 h. *solid lines*: lignin, *dashed lines*: polysaccharides.

the treatment, especially for the morphological region of CC. These spectral changes were also observed at the wood sample *Cryptomeria japonica* treated with [EtPy][Br] (Fig. 3.4). In addition, the stretching modes for Carbon−Halogen atoms vibration generally present the spectral region at 500−800 cm^{-1} (Smith and Dent 2005). Thus, the author suggested that bromine atoms derived from [EtPy][Br] were incorporated into the cell walls and C−Br stretching vibration increased, especially for CC.

3.3.2.2.2 Raman mapping analysis

In order to get insights into the compositional changes in the cell walls over a wide range during [EtPy][Br] treatment, Raman mapping technique was applied on the transverse sections and visualized the distribution of lignin and polysaccharides. All the experiments were performed on the same cell walls by using serial thin sections. In the bright field images, the rectangles indicate the selected positions for mapping analysis (Fig. 3.17a−c). The Raman images were constructed by integrating over the specific band regions (Fig. 3.17d−i).

The band regions from 1580 to 1622 cm^{-1} assigned to symmetric stretching of aromatic ring and from 2871 to 2897 cm^{-1} assigned to C−H and C−H_2 stretching vibration in polysaccharides were selected for the Raman images of the distribution of lignin and polysaccharides, respectively.

On the untreated wood fibers, CML and CC were more highly lignified than S_2 and lignin was uniformly distributed throughout the region of S_2 (Fig. 3.17d). The lignin concentration in S_2 significantly decreased with increasing treatment time, but the morphological regions including CML, CC, the lumen side of S_2, and pits showed high lignin concentration after 72 h of treatment (Fig. 3.17f). The difference in the decrement of lignin concentration for S_2 from CML and CC was mainly attributed to the difference in their lignin structure; in hardwood, lignin in S_2 is mainly composed of syringyl units, whereas that in CML and CC are of guaiacyl units (Fergus and Goring 1970; Musha and Goring 1975; Saka and Goring 1988). Because the components of lignin in CML and CC is strongly connected by covalent binding, it has high recalcitrance to degradation and

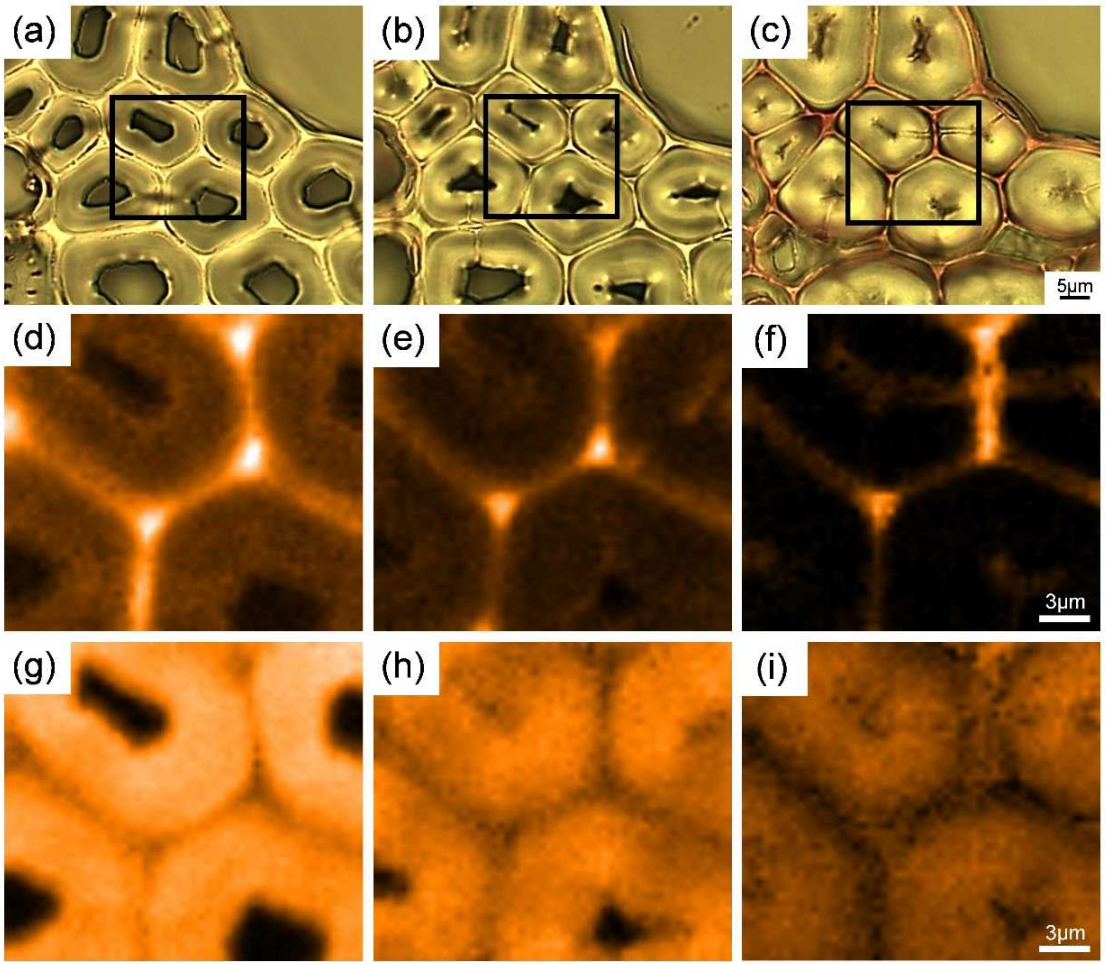

Fig. 3.17 Raman mapping on transverse sections of wood fibers before and after treatment with [EtPy][Br] at 120°C for (a, d, g) 0 h, (b, e, h) 24 h, and (c, f, i) 72 h. (a−c) Bright field images of the measured position. (d−f) Distribution of lignin (1580–1622 cm^{-1}). (g−i) Distribution of polysaccharides (2871–2897 cm^{-1}). Bright regions indicate high concentrations of specific chemical compositions, dark regions indicate low concentrations.

was greatly remained even after 72 h of treatment. Selig et al. (2007) and Donohoe et al. (2008) observed that lignin in cell walls was dissolved and then it was re-deposited on the cell lumen surface, middle lamella, and pits during dilute acid treatment. Our experimental result may also imply the deposition of liquefied lignin during [EtPy][Br] treatment, but further detailed work is necessary to resolve this phenomenon.

As shown in Fig. 3.17g, the distribution of polysaccharides on the untreated wood fibers was opposite to that of lignin; S_2 contains much polysaccharides rather than CML and CC. During [EtPy][Br] treatment, their concentrations slightly decreased with prolonged treatment time (Fig. 3.17h, i). The decreasing is because of the cell wall swelling and partial liquefaction of hemicellulose and amorphous part of cellulose.

3.4 Conclusions

The effects of the ionic liquid [EtPy][Br], which prefers to react with lignin rather than cellulose on the wood cell walls of *Cryptomeria japonica* and *Fagus crenata*, were investigated from a morphology and topochemistry point of view. The treatment of both two wood species with [EtPy][Br] induced a swelling of the wood cell walls without a significant deconstruction of the original cell wall outlines and the cellulose crystalline structure. In addition, the swelling behaviors and ultrastructural changes of the cell walls were different for the types of tissues and ionic liquids. Although prolonged treatment time increased delignification particularly in S_2, it also induced a slight loss of polysaccharides. In *Cryptomeria japonica*, changes in the Raman spectra of S_2, CML and CC varied partially during the treatment. In *Fagus crenata*, the lignin distribution changed significantly after treatment with [EtPy][Br]; much lignin still remained at the edge of cell walls including the lumen side of the secondary wall and pits.

Consequently, it was revealed that the interaction of wood with [EtPy][Br] is extremely inhomogeneous from a morphological and a topochemical point of view. These new insights into the interaction of wood with ionic liquid at the microscopic cellular level provides further comprehension of liquefaction mechanism of woody biomass in ionic liquids. Furthermore, these findings will lead to efficient utilization of wood and

bio-refinery processes.

CHAPTER 4

Microscopic Study on Reaction Wood Treated with Ionic Liquid

4.1 Introduction

The utilization of renewable woody biomass for alternative to fossil resources has attracted great interest to solve the world-wide problems of global warming and future shortage of energy-generating resources. With increasing in global wood demands, short-rotation afforestation and complete-tree utilization has been emphasized, to date.

In general, when the trees grow under the stress such as wind and gravitational force, abnormal wood parts which are comprehensively called reaction wood occur on the stems and branches. Gymnosperms form compression wood on the lower side of learning stems and branches (Timell 1986a), whereas angiosperms form tension wood on the upper side (Henriksson et al. 2009; Pilate et al. 2004). In addition, opposite wood locates on the opposite side of the reaction wood (Timell 1986b). The anatomical structure and chemical composition of reaction wood are distinctively different from those of normal wood. Compression wood forms thick circular outlined tracheids, intercellular spaces at CC, helical cavity on the inner surface of secondary wall, and is absent from S_3 layer (Ruelle 2014). From the chemical point of view, compression wood has higher lignin and galactan content but lower cellulose and galactoglucomannan content than normal wood (Timell 1982). In addition, lignin in compression wood has large proportion of *p*-hydroxyphenyl propane units (Nanayakkara et al. 2009). On the other hand, a thick additional layer named gelatinous layer appears at the inner side of the wood fibers of tension wood. Gelatinous layer has some characteristic features such as high cellulose content whereas low lignin content. In addition, the cellulose microfibrils are highly crystallized and oriented nearly parallel to the fiber axis (Côté et al. 1969; Jourez et al. 2001; Müller et al.

2006; Norberg and Meier 1966). With regard to opposite wood, in gymnosperms, opposite wood and normal wood are nearly the same chemically but are different in anatomy (Timell 1986b). From these properties, compression wood and tension wood are generally difficult to use for industrial processing (Wimmer and Johansson 2014). However, softwood and hardwood especially juvenile wood are estimated to contain non-negligible amount of compression wood and tension wood, respectively (Harris 1977; Zobel 1981). In addition, compression wood and tension wood appear even in perfectly straight and vertical stems (Barnett et al. 2014; Henriksson et al. 2009; Timell 1969). Therefore, the development of their effective chemical conversion process and their complete utilization are of extreme importance to non-wasteful woody biomass utilization.

Although a number of studies on ionic liquid treatment of wood have already been performed, the knowledge of the impact of ionic liquid treatment on reaction wood is very little (Torr et al. 2012). Thus, in this chapter, for a better understanding of the interaction of reaction wood with ionic liquids, ultrastructural and topochemical characterization of reaction wood cell walls treated with ionic liquid was conducted.

4.2 Materials and Methods

4.2.1 Samples and chemicals

Compression wood and opposite wood were collected from the branch of *Cryptomeria japonica*. Tension wood samples were cut from the branch of *Fagus crenata*. They were cut into small blocks [approximately 5(R) × 5(T) × 5(L) mm] that were extracted with ethanol/benzene (1:2, v/v) for 24 h in a Soxhlet apparatus. The extracted wood was oven dried for 8 h in an oven at 105°C prior to further treatment. The ionic liquids, [C2mim][Cl] (>97% purity) and [EtPy][Br] (>98% purity), were purchased from Tokyo Chemical Industry Co., Ltd..

4.2.2 Ionic liquid treatment for light microscopy analysis

The extracted samples were sectioned to 15-μm-thick with a sliding microtome and

mounted in a 20-μm-deep hemocytometer. The mounted sections were dried for 2 h at 105°C before adding 100 μL of ionic liquid that was heated to 120°C by dropping the ionic liquid onto the mounted section. The hemocytometer was closed with a glass cover after adding the ionic liquid. Then it was placed in an oven at 120°C for various time periods. After a specified treatment time, the hemocytometer was analyzed using light microscopy. Three areas (cell lumen area, cell wall area, and total of cell lumen area + cell wall area; defined as illustrated in Fig. 2.1) were measured for five cells, using image analysis software and the average was calculated.

4.2.3 Ionic liquid treatment for SEM observation

The extracted samples were surfaced with a sliding microtome. The surfaced samples were dried for 24 h at 105°C and the surfaced area was treated by dipping into ionic liquid and heating to 120°C for various periods of time. During dipping treatment, the ionic liquid was stirred gently with a magnetic stirrer. The treated specimens were dipped in DMSO for 24 h to remove ionic liquid and then washed with distilled water to remove DMSO. After drying for 24 h at 105°C, each specimen was mounted on a specimen holder using carbon tape and sputter-coated with Au at 40 mA for 120 s using an auto fine coater. The exposed surface was examined by SEM at an accelerating voltage of 10 kV.

4.2.4 Ionic liquid treatment for confocal Raman microscopy analysis

For Raman microscopy, the ionic liquid treatment was the same as that for light microscopy. To perform analysis on the same cell wall area, 15-μm-thick serial sections were prepared. After a specific treatment time, 100 mL of distilled water was poured into the hemocytometer from the lateral direction, and then the hemocytometer was placed in a Petri dish filled with distilled water for 24 h at room temperature to remove ionic liquid completely.

The samples were analyzed by a confocal microRaman system equipped with a confocal microscope and a motorized x, y stage. To obtain high spatial resolution, the measurements were performed with an oil immersion objective having a high NA

(NA=1.40). The instrument was equipped with a diode-pumped solid state laser (λ=532 nm). Immersion oil was used as the medium between the objective and the glass cover. The incident laser power on the sample was approximately 10 mW. Scattered Raman light was detected by a CCD detector behind either a 300 or 1800 lines/mm grating. A confocal pinhole diameter of 300 μm was used for all experiments.

To obtain high-quality spectra and avoid damaging the wood samples with the heat from the laser during the point analysis, the Raman spectra were measured in 10 cycles, with each cycle consisting of a 1-s integration time for one spot. 10 spectra were obtained and averaged, and the averaged spectra from 10 different locations were again averaged. The grating used in the point analysis was 1800 lines/mm. For mapping analysis, measurements were conducted every 0.4 μm steps and the spectra were obtained by averaging 4 cycles, each with a 0.1 s integration time. The grating used in mapping analysis was 300 lines/mm.

The data acquisition and analysis was done by means of LabSpec5 software. To remove the background from fluorescence, the raw spectral data were baseline-corrected. The smoothing to reduce spectral noise was performed with the Savitzky-Golay algorithm.

4.3 Results and discussion

4.3.1 Effect of ionic liquid treatment on morphological and topochemical features of compression wood in *Cryptomeria japonica*

4.3.1.1 Compression wood

Light microscopy analysis

The morphological changes in compression wood tissues during ionic liquid treatment were observed by bright-field microscopy (Fig. 4.1). Compression wood tracheids were collapsed after [C2mim][Cl] treatment in earlywood, but not in latewood (Fig. 4.1c). This result was contrary to the changes in normal wood. It is reported that treatment with [C2mim][Cl] led to distortion and dissociation of normal wood tracheids in latewood, but not in earlywood (Miyafuji and Suzuki, 2012). With regard to the compression wood

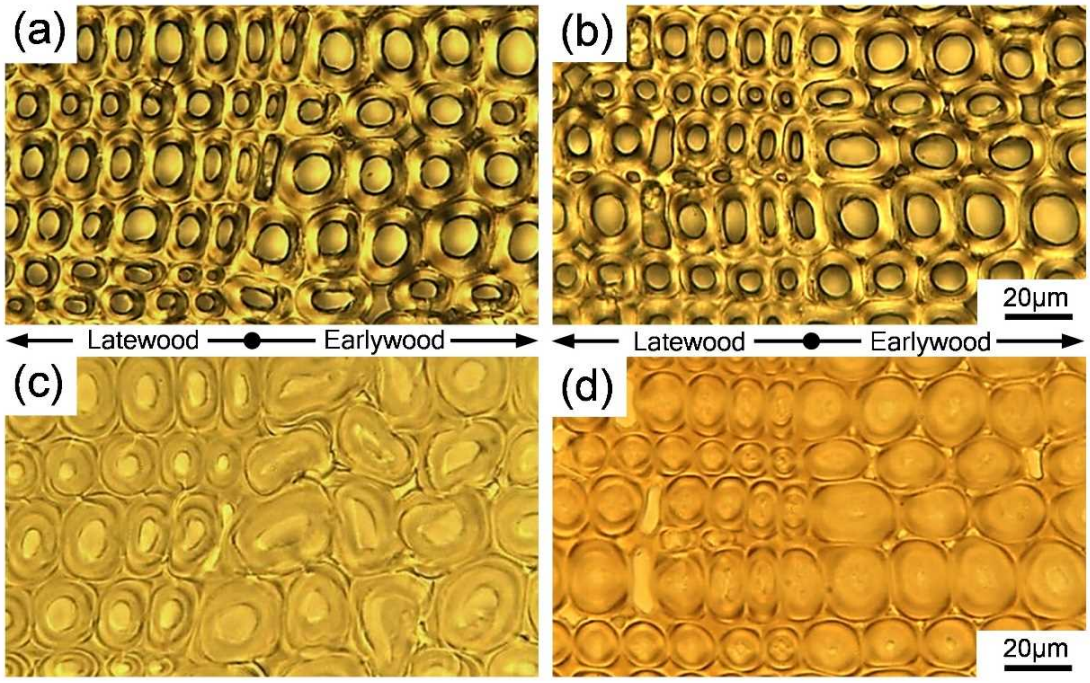

Fig. 4.1 Light microscopy images of transverse sections in compression wood (a, b) before and after treatment with (c) [C2mim][Cl] and (d) [EtPy][Br] at 120°C for 72 h.

tracheids treated with [EtPy][Br], no significant morphological changes were observed in both earlywood and latewood (Fig. 4.1d) as with the result of normal wood (Fig. 3.1).

The author performed polarized light microscopy observation at the same positions which were observed by bright-field microscopy (Fig. 4.2). The brightness from the birefringence of crystalline cellulose could be clearly seen in untreated samples (Fig. 4.2a, b). After 72 h of [C2mim][Cl] treatment, the brightness disappeared completely (Fig. 4.2c); nevertheless the cell walls preserved their forms as seen in bright-field images (Fig. 4.1c). Meanwhile, after 72 h of [EtPy][Br] treatment, the brightness has been still visible even though the brightness decreased slightly (Fig. 4.2d). These results imply that the crystalline structure of cellulose in compression wood is broken by [C2mim][Cl] treatment before complete liquefaction of the cell walls, but is barely affected by [EtPy][Br] treatment.

Swelling process of compression wood tracheids during ionic liquid treatment was determined by means of measuring three areas: cell lumen area, cell wall area, and total of cell lumen and cell wall area (defined in Fig. 2.1); the results are described in Fig. 4.3. All the cell walls showed inward swelling in an early stage of both ionic liquids treatment. In the case of [C2mim][Cl] treatment, the total of cell lumen and cell wall area of earlywood increased significantly after 24 h (Fig. 4.3a), while that of latewood increased just a little (Fig. 4.3c). In addition, at 72 h of treatment, the cell wall areas of earlywood and latewood had increased by 1.8 and 1.6 times, respectively. On the other hand, after 72 h of [EtPy][Br] treatment, the cell wall areas of both earlywood and latewood had increased by only 1.3 times without outward swelling (Fig. 4.3b, d). From the above results, the collapse of earlywood tracheids during [C2mim][Cl] treatment as shown in Fig. 4.1c can be considered to arise from the significant outward swelling of cell walls.

It is reported that the cell wall areas in latewood of normal wood tracheids increased by 5 times after 48 h of [C2mim][Cl] treatment (Miyafuji and Suzuki 2012). In addition, in the case of [EtPy][Br] treatment, the cell wall areas in earlywood and latewood of normal wood tracheids increased by 1.3 and 2 times after 72 h, respectively (Kanbayashi and Miyafuji 2015b). Thus, the degree of swelling for compression wood tracheids was gentler than normal wood tracheids. These differences were mainly caused by the

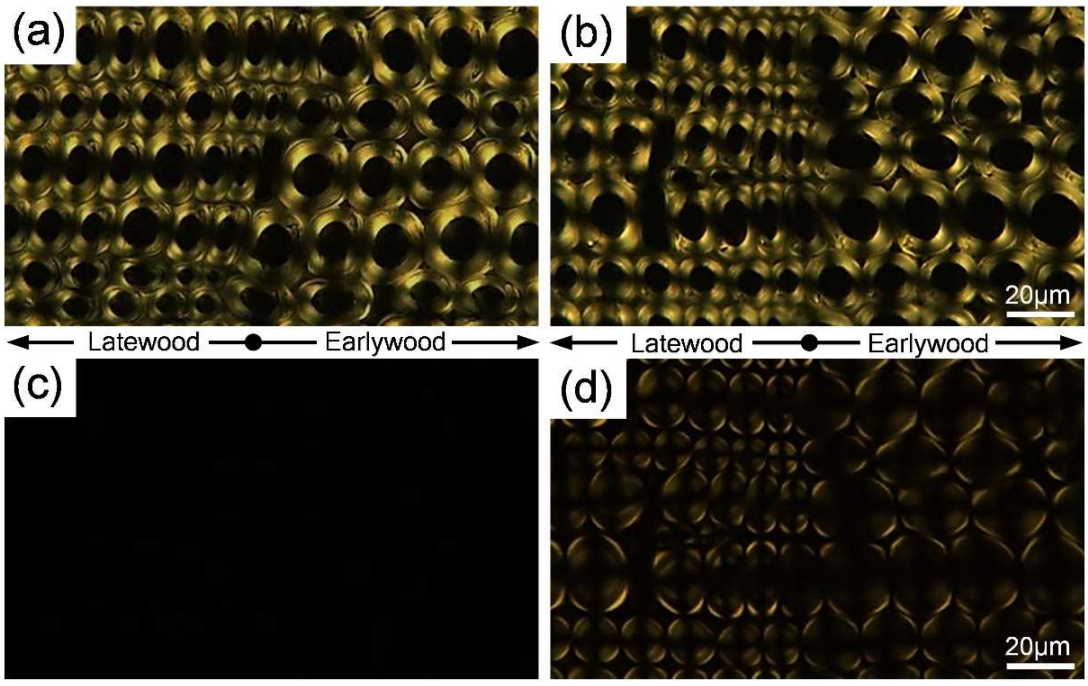

Fig. 4.2 Polarized light microscopy images of transverse sections in compression wood (a, b) before and after treatment with (c) [C2mim][Cl] and (d) [EtPy][Br] at 120°C for 72 h.

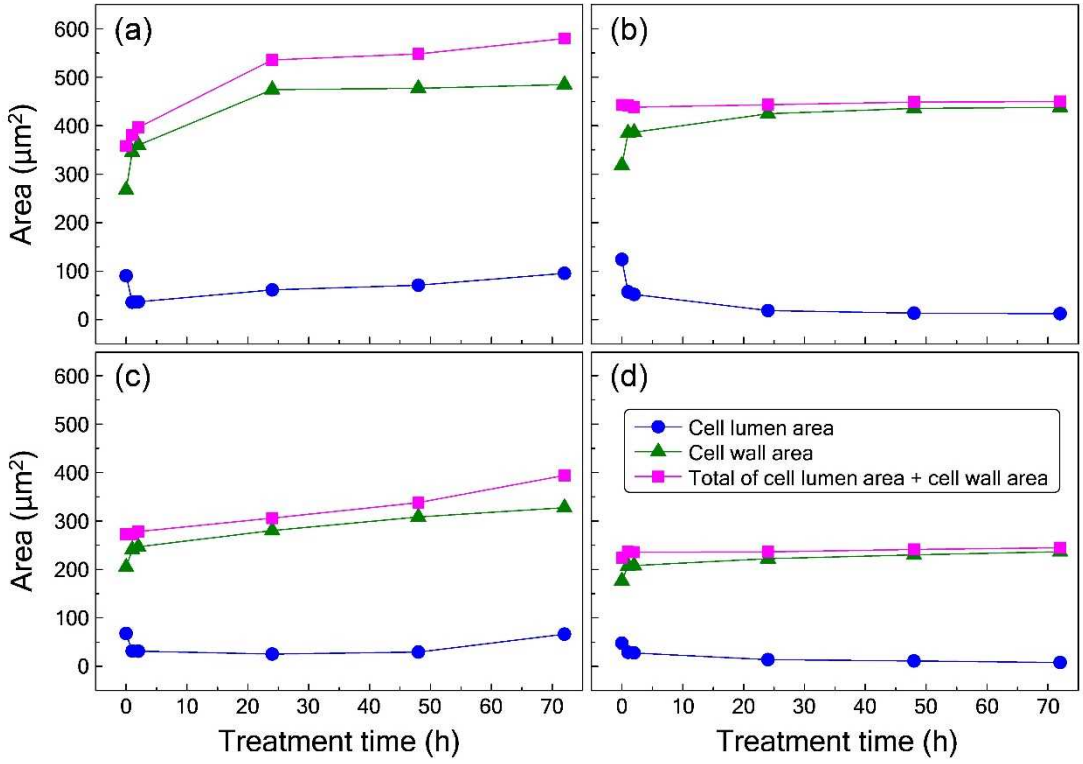

Fig. 4.3 Changes in cell wall area, cell lumen area and total of cell lumen area + cell wall area for compression wood tracheids of *Fagus crenata* in (a, b) earlywood and (c, d) latewood during (a, c) [C2mim][Cl] and (b, d) [EtPy][Br] treatment.

ultrastructure and chemical composition of tracheids. As the one reason, there is difference in microfibril angle. In general, swelling of the cell walls is mainly attributed to swelling of the bundles of cellulose microfibrils for perpendicular direction to the fibril axis (Tsoumis 1991). The more the angle between microfibrils and longitudinal cell axis decreases, the more the swelling ratio toward perpendicular to longitudinal cell axis increases. The microfibril angle in S_2 which composes large part of the cell wall in compression wood tracheids are higher than in normal wood; their microfibril angles are considered to be approximately 5−20° (Parham and Gray 1984) and 45° (Wardrop and Dadswell 1950), respectively. In addition, the S_1 which has very high microfibril angle (approx. 70−90°) in compression wood tracheids is considerably thicker than in normal wood (Timell 1986a). Thus, compression wood tracheids are difficult to swell outwards rather than normal wood. As another reason, there is difference in chemical composition. It is reported that compression wood tracheids contain more lignin and less cellulose than normal wood (Timell 1982). Previous study revealed that lignin has high recalcitrance to [C2mim][Cl] attack compared with cellulose and hemicellulose (Miyafuji et al. 2009; Nakamura et al. 2010a). Thus, the reactivity of [C2mim][Cl] with compression wood tracheids are lower than with normal wood. From the above factors, the high microfibril angle of S_2 layer, high proportion of S_1 layer and high lignin concentration, caused gentle swelling of compression wood tracheids during ionic liquid treatment.

SEM observation

The author analyzed transverse and radial surface of intact and ionic liquid treated samples by SEM (Fig. 4.4). As can be seen from the transverse sections of tracheids treated with [C2mim][Cl], S_2 layers were dissociated from S_1 layers (indicated by arrows) and S_1 layers and CML were partially torn (indicated by arrowheads) in earlywood (Fig. 4.4d). These breakage and dissociation were caused by the significant swelling of S_2 layer (as seen in Fig. 4.1c) and decreasing in adhesion between S_1 and S_2 layers during the treatment. With respect to latewood, no significant destruction occurred but the thickness of the cell walls was decreased due to the liquefaction of chemical components of the cell

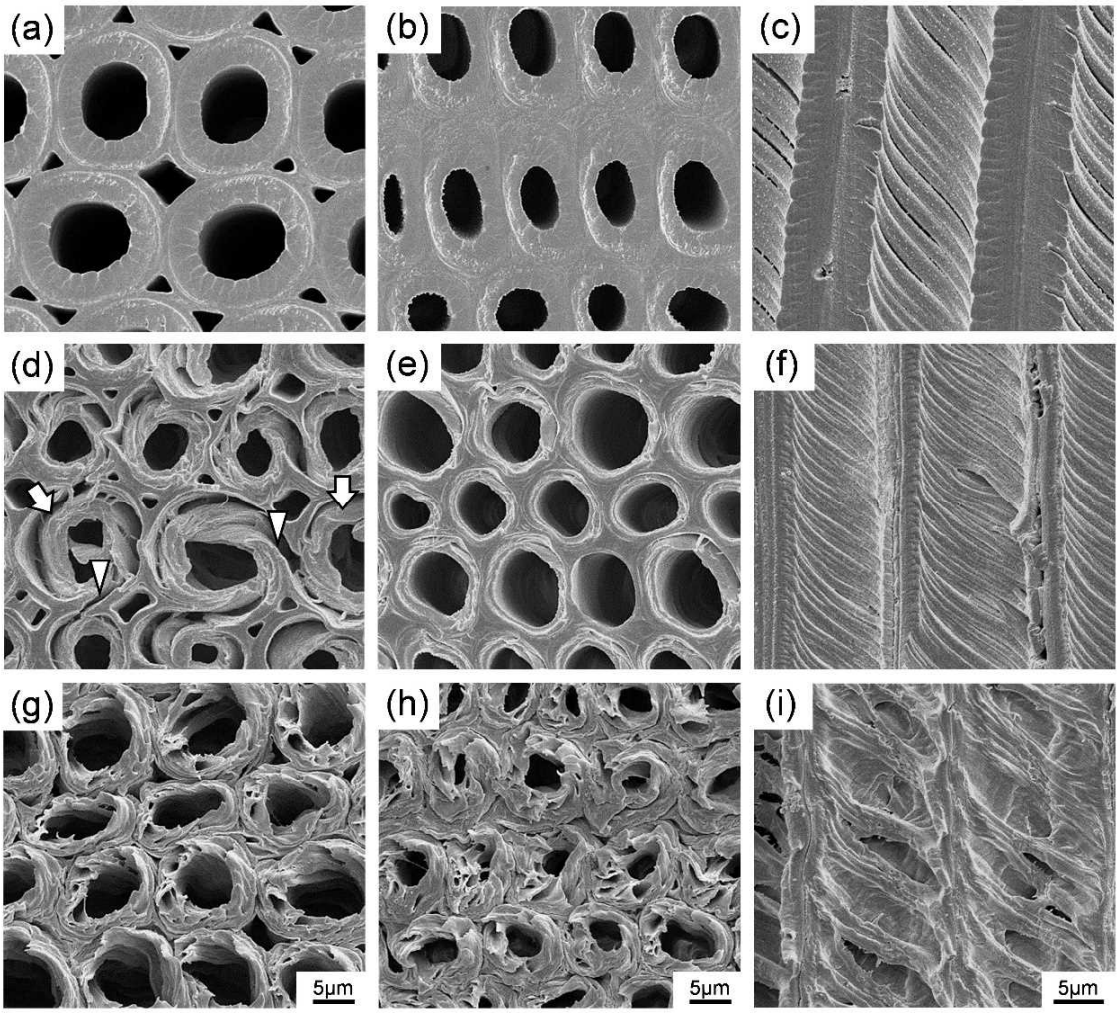

Fig. 4.4 SEM images of compression wood tracheids (a–c) before and after treatment with (d–f) [C2mim][Cl] and (g–i) [EtPy][Br] at 120°C for 72 h. (a, d, g) Transverse view of earlywood. (b, e, h) Transverse view of latewood. (c, f, i) Radial view of earlywood. Arrows, dissociated S_2; arrowheads, ruptured S_1 and CML.

walls (Fig. 4.4e). These morphological changes could also be seen in radial section (Fig. 4.4f). On the other hand, after treatment with [EtPy][Br], many pores were formed on the transverse and radial surface of the cell walls in both earlywood and latewood (Fig. 4.4g−i). It is also observed them on normal wood tracheids (Fig. 3.3) and wood fibers (Fig.3.12) treated with [EtPy][Br]. In addition, the other treatments such as steam explosion (Corrales et al. 2012), ammonia fiber expansion (Chundawat et al. 2011) and alkaline treatment (Ji et al. 2014) have been reported to result in pore formation. Therefore, the pores thought to be formed by delignification. The formation of porous structure by means of [EtPy][Br] treatment will improve accessibility of enzyme followed by development of effective bio-conversion technology such as enzymatic saccharification.

Confocal Raman microscopy analysis

To understand the chemical changes in compression wood tracheids during ionic liquids treatment at the cellular level, chemical mapping was performed to visualize the distribution of wood components using Raman mapping technique. The anatomy and chemical composition of the compression wood tissues other than tracheids are similar to those of normal wood (Hoffman and Timell 1972a, b). Thus, Raman analysis was done on only tracheids. The distribution of lignin and polysaccharides were constructed using the band regions 1585−1606 cm^{-1} and 2876−2902 cm^{-1}, respectively.

Results from the Raman mapping performed on the compression wood tracheids before and after ionic liquid treatment were described in Fig. 4.5. Before the treatment, outer S_2 layer (indicated by arrows) and CML (indicated by arrowheads) were highly lignified as with the previous reports (Wood and Goring, 1971). The lignin concentration changed slightly after [C2mim][Cl] treatment (Fig. 4.5e), but decreased significantly after [EtPy][Br] treatment except for the areas such as outer S_2 layer and CML (Fig. 4.5k). Differences in molecular structure and concentration of lignin and penetrability of ionic liquid may lead to the differences in the reactivity of ionic liquid among the morphological regions. Meanwhile, the concentration of polysaccharides decreased significantly and its signal was almost disappeared after [C2mim][Cl] treatment (Fig.

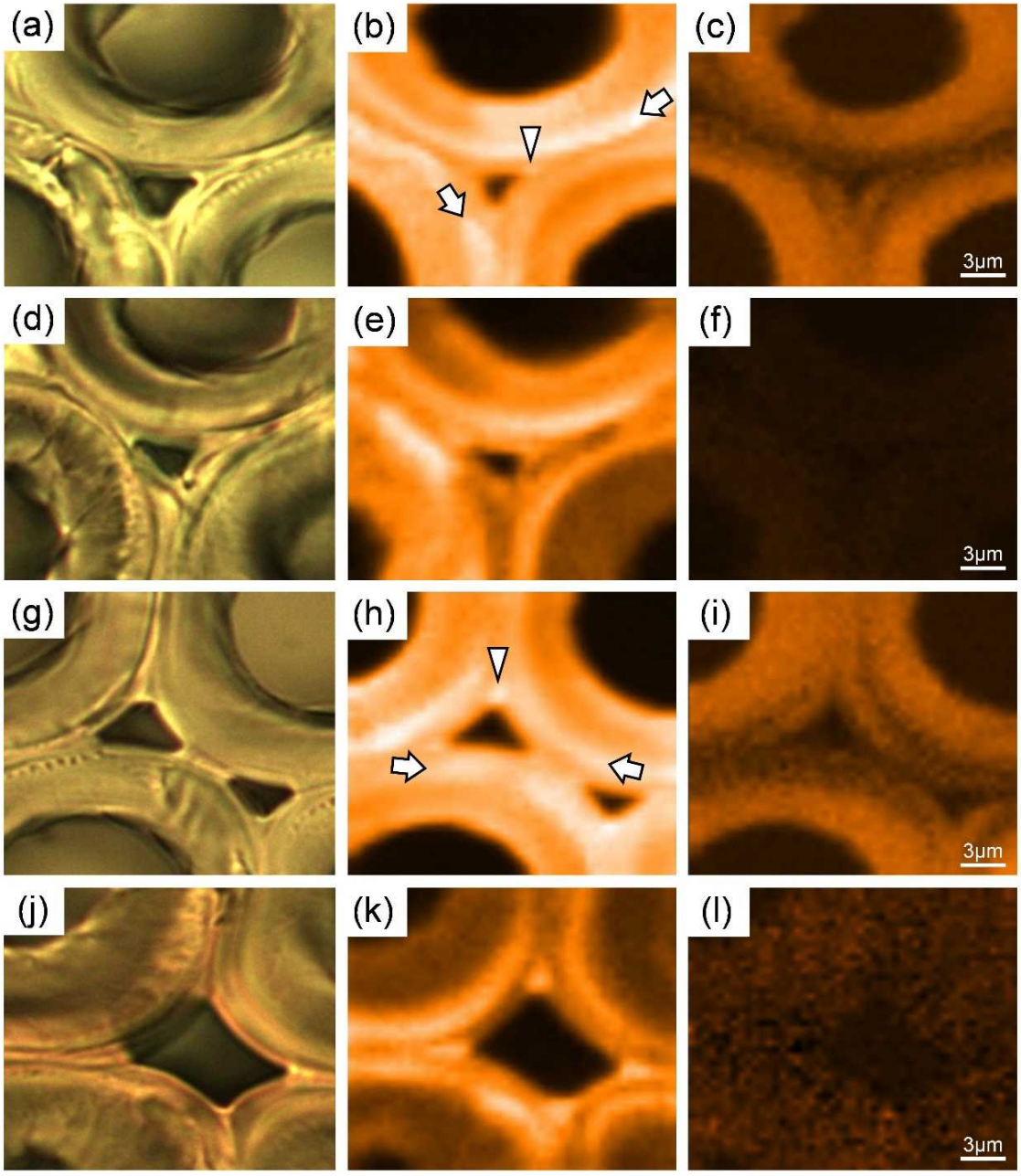

Fig. 4.5 Raman mapping on transverse sections of compression wood tracheids (a–c, g–i) before and after treatment with (d–f) [C2mim][Cl] and (j–l) [EtPy][Br] at 120°C for 72 h. (a, d, g, j) Bright field images of the measured position. (b, e, h, k) Distribution of lignin (1,585−1,606 cm^{-1}). (c, f, i, l) Distribution of polysaccharides (2,876−2,902 cm^{-1}). Bright regions represent high concentrations of specific chemical compositions, whereas dark regions represent low concentrations. Arrows, S_2(L); arrowheads, CML.

4.5f), but still have been detected after [EtPy][Br] treatment (Fig. 4.5l). These results indicate that polysaccharides in compression wood tracheids readily reacts with [C2mim][Cl] while lignin reacts with [EtPy][Br]. In addition, lignin in outer S_2 layer and CML has high recalcitrance to reactions with ionic liquids than other morphological regions.

4.3.1.2 Opposite wood

Time course bright-field micrographs clarified the deformation behavior of opposite wood tracheids during ionic liquid treatment. The opposite wood tracheids treated with [C2mim][Cl] were well ordered at 24 h but were distorted without dissociation after 72 h (Fig. 4.6). This result differed from the case of normal wood. It is reported that normal wood tracheids in latewood show significant destruction and dissociation during liquefaction process in [C2mim][Cl] (Miyafuji and Suzuki 2012). Meanwhile, in case of [EtPy][Br] treatment, no marked changes were observed in opposite wood tracheids (Fig. 4.6b) as with the result of normal wood (Fig. 3.2).

Swelling process during ionic liquid treatment was detailedly evaluated by calculating area changes in opposite wood tracheids (lower chart in Fig. 4.6). The cell wall area of opposite wood tracheids in latewood had increased by 1.8 times after 72 h of [C2mim][Cl] treatment. This value was greatly lower than that of normal wood (Miyafuji and Suzuki 2012). In addition, although the cell lumen of normal wood tracheids in latewood was mostly occluded at the early stage of the treatment (Miyafuji and Suzuki 2012), that of opposite wood tracheids was closed by only half. These differences were mainly caused by the differences in their cell wall structure. Normal wood tracheids predominantly consists of S_2 which is mostly composed of cellulose, whereas opposite wood tracheids have low amount of S_2 and thick S_3 which is highly lignified (Timell 1986b). Previous study revealed that [C2mim][Cl] reacts with cellulose rather than lignin (Miyafuji et al. 2009; Nakamura et al. 2010a). Thus, the thick S_3 has high stability to [C2mim][Cl] attack and suppressed the swelling toward the cell lumen side. These factors induced low swelling ratio of opposite wood tracheids, and they were deformed without

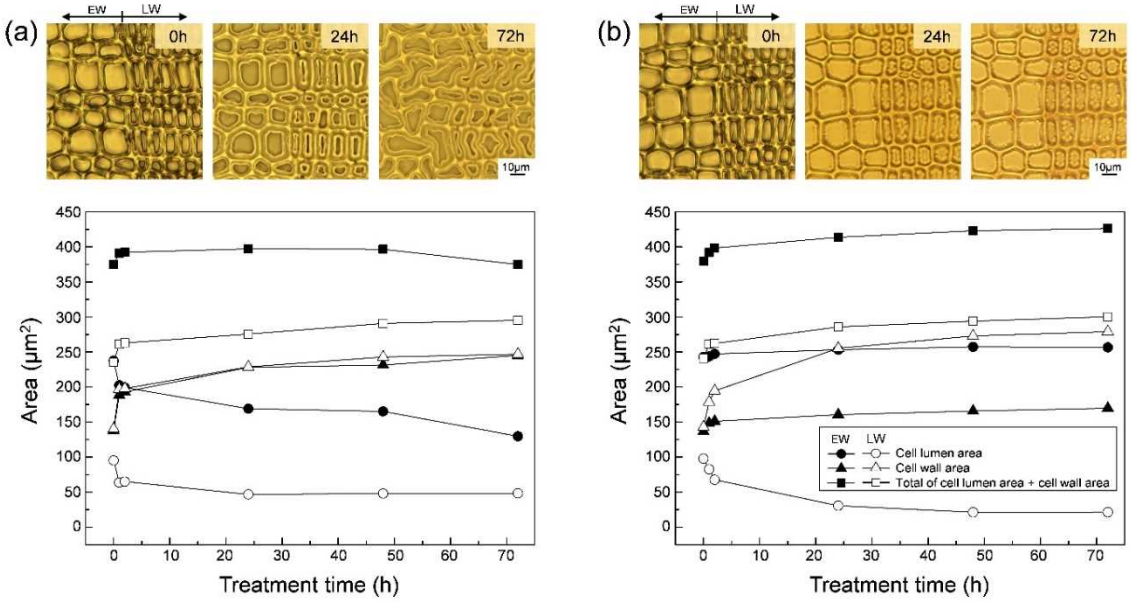

Fig. 4.6 Light microscopy images of transverse sections in opposite wood treated with (a) [C2mim][Cl] and (b) [EtPy][Br] at 120 °C for various time periods. In lower panels, changes in cell wall area, cell lumen area and total of cell lumen + cell wall area for tracheids during ionic liquid treatment are presented. *EW*: earlywood, *LW*: latewood.

dissociation. On the other hand, in [EtPy][Br] treatment, the cell wall area of opposite wood tracheids in latewood had increased by two times and the cell lumen area decreased to nearly zero after 72 h. It is reported that [EtPy][Br] prefers to react with lignin (Yokoo and Miyafuji 2014). Thus, S_3 was greatly influenced by [EtPy][Br] treatment. The liquefaction of S_3 resulted in swelling toward the cell lumen side followed by large swelling without significant morphological change.

The SEM micrographs in Fig. 4.7 show ultrastructural changes in opposite wood tracheids treated with ionic liquids. After 72 h of [C2mim][Cl] treatment, large parts of S_2 disappeared, whereas S_3 and CML which have high lignin content were preserved (Fig. 4.7b, e). Meanwhile, in [EtPy][Br] treatment, the outline of S_2 has been still remained after 72 h but the dense surface of S_2 transformed into porous and empty structure (Fig. 4.7c, f). In addition, the volume of S_3 and CML decreased significantly. With regard to torus and warts were broken by [C2mim][Cl] and [EtPy][Br], respectively (Fig. 4.7h, i), as with the results of normal wood (Miyafuji and Suzuki 2012; Fig. 3.3). These results indicate that [C2mim][Cl] and [EtPy][Br] preferentially liquefy cellulose-rich and lignin-rich regions, respectively.

4.3.2 Effect of ionic liquid treatment on morphological and topochemical features of tension wood in *Fagus crenata*

Light microscopy analysis

Fig. 4.8 shows light micrographs of transverse sections of tension wood before and after treatment with [C2mim][Cl] and [EtPy][Br]. The images took from the samples before and after treatment are of the same area. Although all the tissues were swollen after 72 h of treatment with both ionic liquids, their morphological changes were different for the types of ionic liquids. All the tissues such as wood fibers, vessels and ray parenchyma cells apart from axial parenchyma cells were significantly deformed and disintegrated after [C2mim][Cl] treatment (Fig. 4.8c): wood fibers had no trace of their original forms and gelatinous layers disappeared, ray parenchyma became corrugated shape, vessels were compressed by surrounding swollen cells, but axial parenchyma cells maintained

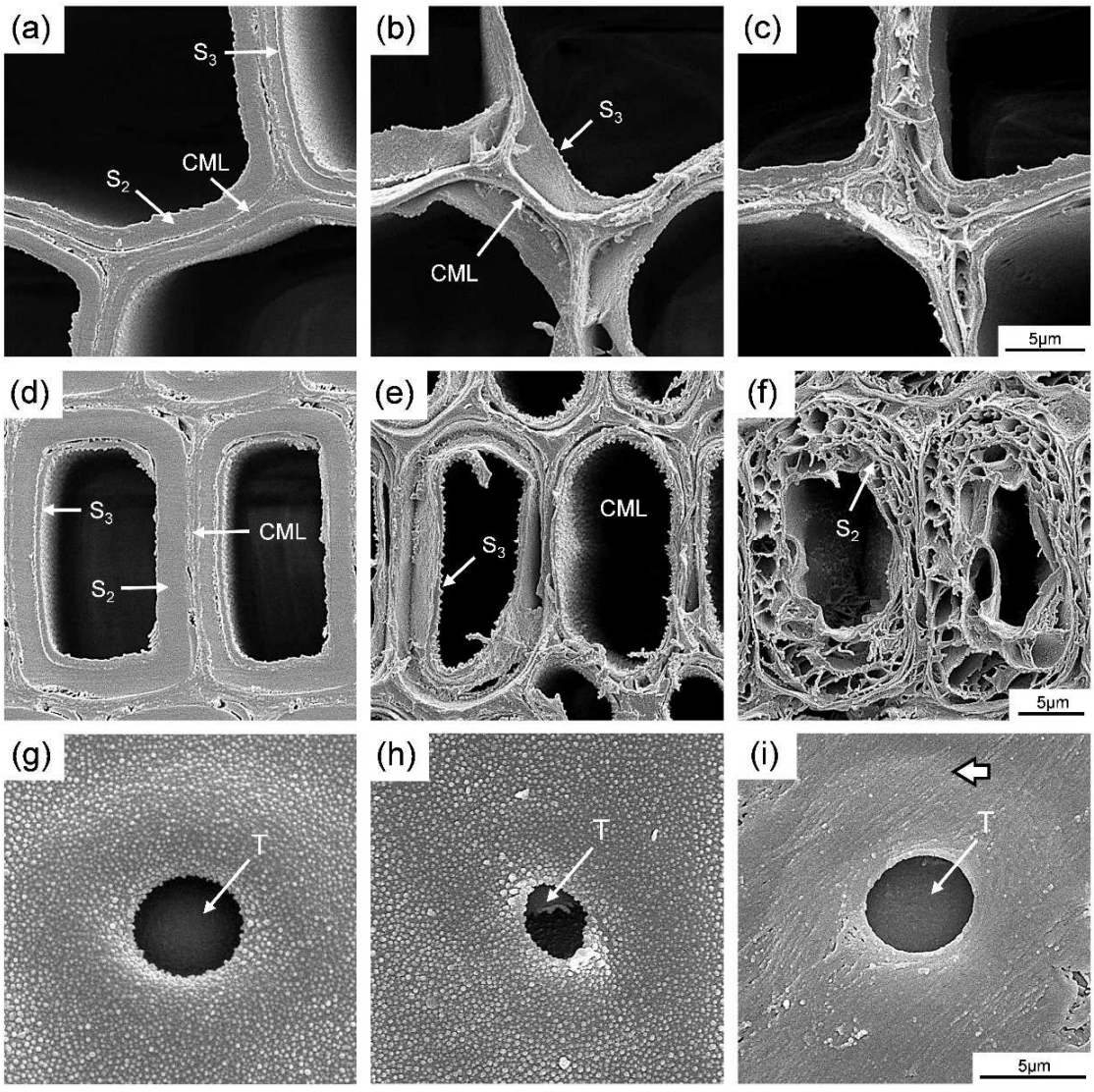

Fig. 4.7 SEM images of opposite wood tracheids (a, d, g) before and after treatment with (b, e, h) [C2mim][Cl] and (c, f, i) [EtPy][Br] at 120°C for 72 h. (a–c) Earlywood. (d–f) Latewood. (g–i)Bordered pits. *S_2*: middle layer of secondary wall, *S_3*: inner layer of secondary wall, *CML*: compound middle lamella, *T*: torus.

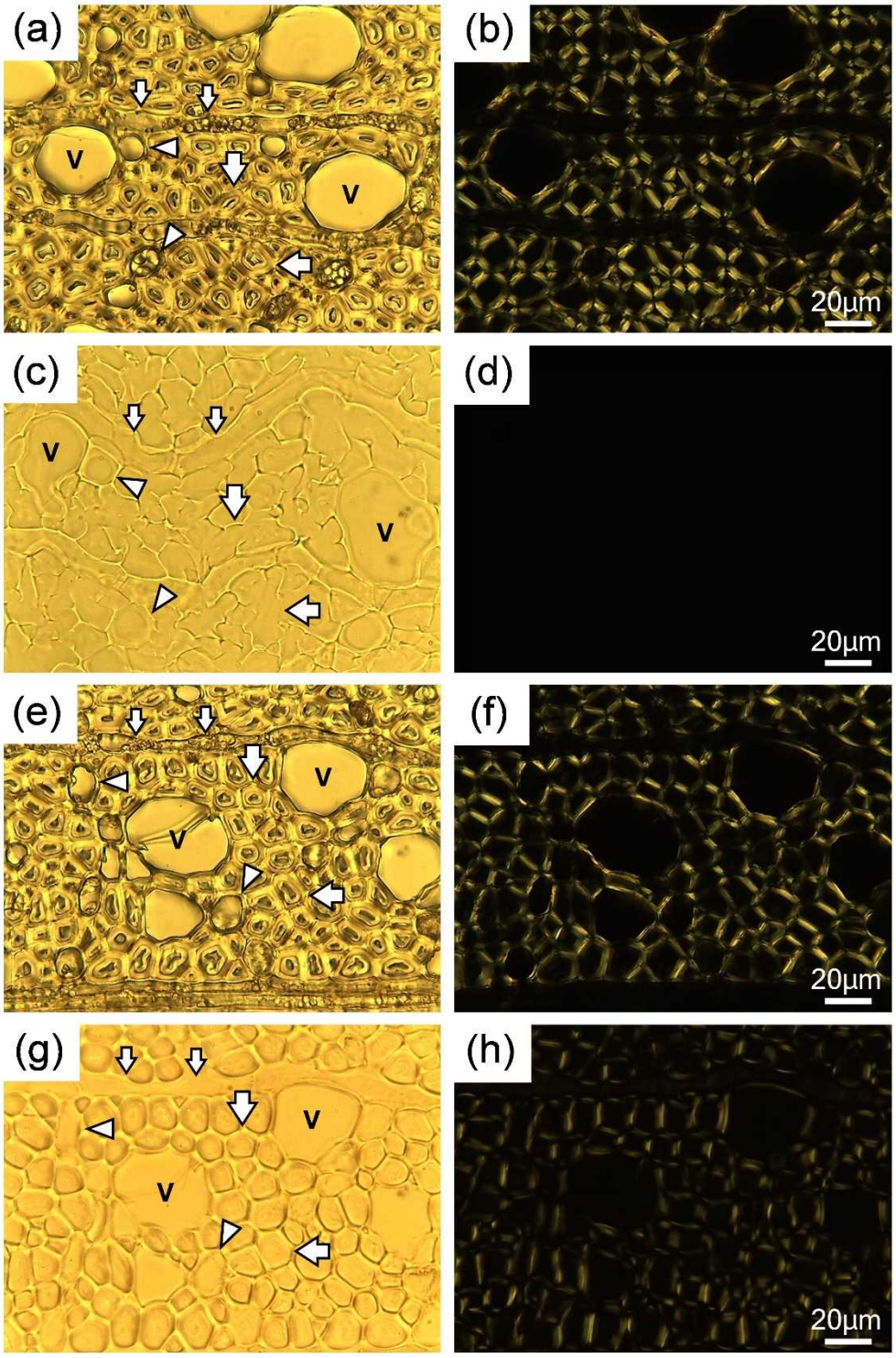

Fig. 4.8 Bright-field microscopy and polarized light microscopy images of transverse sections in tension wood (a, b, e, f) before and after treatment with (c, d) [C2mim][Cl] and (g, h) [EtPy][Br] at 120°C for 72 h. *large arrow*: gelatinous fiber, *small arrow*: ray parenchyma cell, *arrow head*: axial parenchyma cell, *V*: vessel.

their rounded shape. Meanwhile, they showed no marked changes after [EtPy][Br] treatment (Fig. 4.8g). During [C2mim][Cl] treatment, the significant distortion and disintegration of the cell walls were not observed in normal wood of *Fagus crenata* (Fig. 2.2d, f). The result in Fig. 4.8c indicates that liquefaction of tension wood in [C2mim][Cl] proceeds with destruction of the cell walls, which differs to that of normal wood. With regard to [EtPy][Br] treatment, light-microscopically, the morphological changes in tension wood were similar to those in normal wood (Fig. 3.9b).

Polarizing microscopic observation was also performed at the same regions which were observed by brighfield microscopy. In the polarization images of untreated samples, the brightness from the birefringence of crystalline cellulose was conspicuous (Fig. 4.8b, f). Although the brightness disappeared completely after 72 h of [C2mim][Cl] treatment (Fig. 4.8d), it barely changed after 72 h of [EtPy][Br] treatment (Fig. 4.8h). These results implies that the cellulose crystalline structure in tension wood is destroyed by [C2mim][Cl] treatment before the cell walls liquefy completely while it is not affected by [EtPy][Br] treatment.

In *Fagus crenata*, tension wood is mainly different from normal wood with respect to the structure of the wood fibers. Such wood fibers form gelatinous layer at inner side of the secondary wall and have been called gelatinous fibers (Côté 1968; Pilate et al. 2004). The gelatinous fibers occupy a large amount of mass in tension wood. Thus, detailed swelling behavior of gelatinous fibers during ionic liquid treatment was evaluated using image analysis software. The area changes of cell wall, cell lumen, and total of cell lumen + cell wall for gelatinous fiber during ionic liquids treatment are presented in Fig. 4.9. In both [C2mim][Cl] and [EtPy][Br] treatment, the cell lumen areas dropped rapidly to almost zero up to an hour and unchanged afterward. The cell wall area and total of cell lumen + cell wall area increased sharply in the early stages of the treatment. However, after the initial changes, they showed different behavior in each ionic liquid. The cell wall area and total of cell lumen + cell wall area increased gradually with the passage of time in [C2mim][Cl] treatment, while they showed almost no changes in [EtPy][Br] treatment after 2 h. After 72 h of [C2mim][Cl] and [EtPy][Br] treatment, the cell wall areas had increased by approximately 2 and 1.3 times, respectively. The

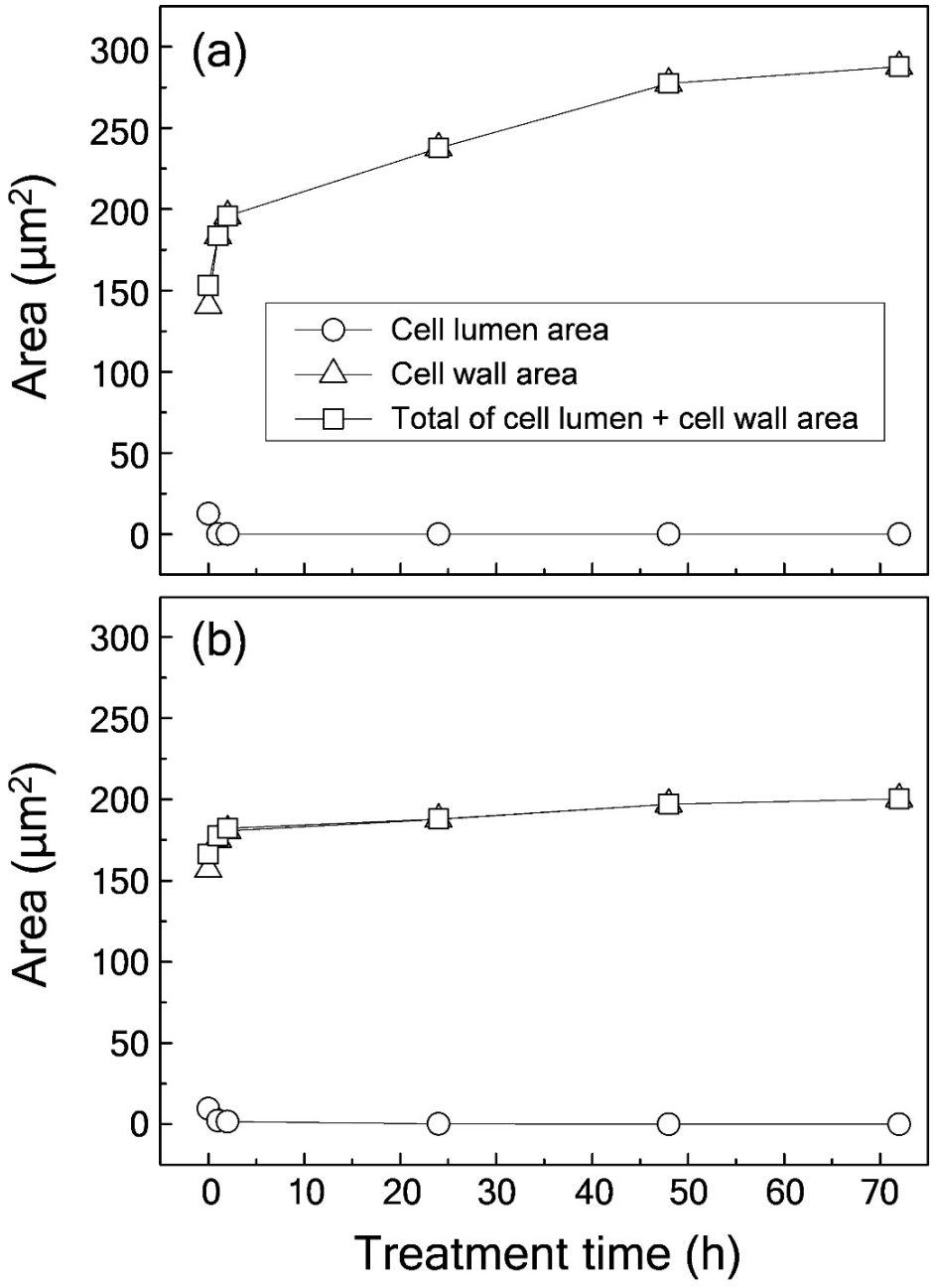

Fig. 4.9 Changes in cell wall area, cell lumen area and total of cell lumen area + cell wall area for gelatinous fiber during (a) [C2mim][Cl] and (b) [EtPy][Br] treatment at 120°C.

difference in swelling behavior is attributed to the differences in the property of the two ionic liquids. It is reported that [C2mim][Cl] is more reactive toward cellulose than lignin (Miyafuji et al. 2009; Nakamura et al. 2010), whereas [EtPy][Br] prefers to react with lignin rather than cellulose (Yokoo and Miyafuji 2014). In general, swelling of the cell walls is due principally to swelling of the bundles of cellulose microfibrils in perpendicular direction (Tsoumis 1991). Therefore, [C2mim][Cl] treatment induced large swelling of the gelatinous fibers, compared with [EtPy][Br] treatment.

Swelling ratio of fibrous cells was different between tension wood and normal wood. It is found that treatments with [C2mim][Cl] and [EtPy][Br] at 120°C for 72 h result in swelling of normal wood fibers of *Fagus crenata* up to 4 and 1.8 times, respectively (Figs. 2.3a, 3.10a). Therefore, the swelling ratio of gelatinous fibers treated with ionic liquids is smaller than that of normal wood fibers.

In the normal wood, significant swelling of wood fibers counterbalances decreasing in the cell lumen area of vessels, and the balance prevents deformation of tissues during ionic liquid treatment. Generally, in tension wood, the size and number of vessels are less than those in normal wood. While, the number of ray parenchyma in tension wood is somewhat much compared with that in normal wood (Tsoumis, 1991). As a result of the collapse of the balance due to the smallness of the size and number of vessels, significant distortion and disintegration occurred in tension wood tissues during [C2mim][Cl] treatment. In addition, many ray parenchyma surrounding gelatinous fibers is likely to result in suppression of the swelling of the gelatinous fibers.

SEM observation

Fig. 4.10 shows scanning electron micrographs of transverse sections of tension wood treated with [C2mim][Cl] and [EtPy][Br] for 72 h. After [C2mim][Cl] treatment, tissues were disordered significantly as with the results of bright-field microscopy observation (Fig. 4.10c). Although large cracks occurred at the boundary of the annual ring in normal wood (Fig. 2.5b), marked cracks were not seen in tension wood. This is probably because the swelling of gelatinous fibers in tension wood was gentle as described above. The

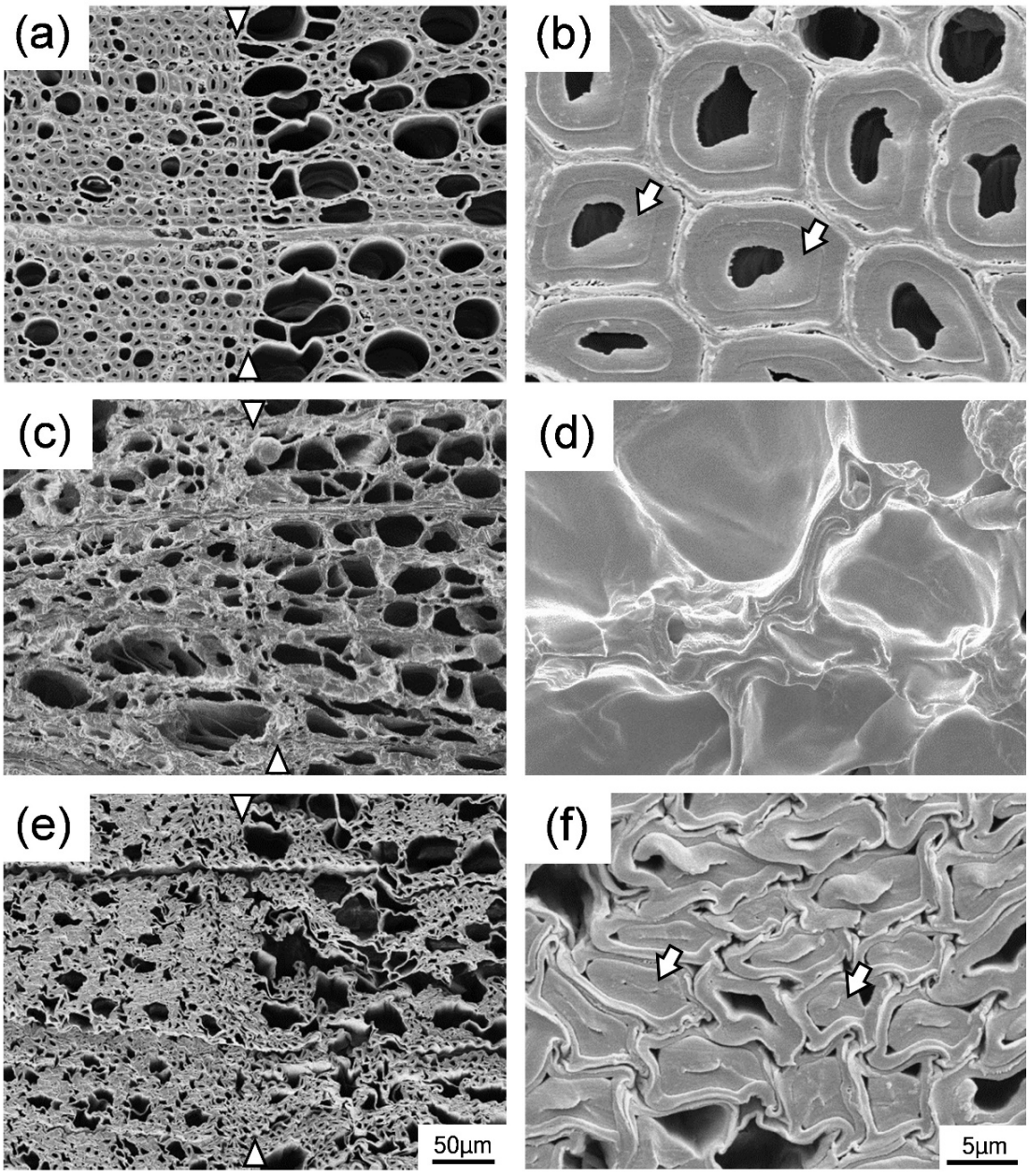

Fig. 4.10 SEM images of transverse sections in tension wood (a, b) before and after treatment with (c, d) [C2mim][Cl] and (e, f) [EtPy][Br] at 120°C for 72 h. (a, c, e) Around annual ring boundary. (b, d, f) Magnified view of gelatinous fibers. *arrow*: gelatinous layer, *arrow head*: annual ring boundary.

sample treated with [EtPy][Br] also showed no significant cracks (Fig. 4.10e).

As can be seen in enlarged view of the wood fibers in native tension wood (Fig. 4.10b), thick gelatinous layers were presented inside the secondary wall (indicated by arrows). After 72 h of [C2mim][Cl] treatment, the gelatinous fibers were collapsed, and they had no trace of their original forms (Fig. 4.10d). This morphological change is due to significant liquefaction of the cellulose-rich gelatinous layers during the treatment with [C2mim][Cl] which can preferentially react with cellulose (Miyafuji et al. 2009; Nakamura et al. 2010a). On the other hand, the gelatinous layers could still be seen after 72 h of [EtPy][Br] treatment (Fig. 4.10f). Thus [EtPy][Br] barely liquefy gelatinous layer. These results indicate that [C2mim][Cl] is a good solvent for tension wood whereas [EtPy][Br] is not very suitable for liquefaction of tension wood.

Confocal Raman microscopy analysis

The effects of ionic liquids treatment on chemical components of gelatinous layers were studied by confocal Raman microscopy. Gelatinous layers had already liquefied completely after [C2mim][Cl] treatment for 72 h. Thus, in the case of [C2mim][Cl] treatment, Raman spectra were obtained from the sample treated for 24 h.

The averaged Raman spectra for gelatinous layers treated with ionic liquids are shown in Fig. 4.11. It has been said that gelatinous layers are mostly composed of cellulose (Côté et al. 1969; Norberg and Meier 1966; Pilate et al. 2004), but obvious Raman features due to lignin molecules were seen in gelatinous layers of untreated *Fagus crenata* (Fig. 4.11a). In the gelatinous layers, the specific Raman bands of lignin were appeared at 1332, 1601, and 1658 cm^{-1}, while those of polysaccharides appeared at 350−550, 950−1200, 1378, and 2896 cm^{-1}. These bands assignment was based on previous literature (Agarwal et al. 2011; Agarwal and Ralph 1997; Edwards et al. 1997; Wiley and Atalla 1987).

After [C2mim][Cl] treatment, all the bands of polysaccharides were disappeared (Fig. 4.11b). At the same time, the lignin bands hidden in the strong polysaccharides band appeared at 2854 and 2945 cm^{-1}. However, the band intensities of lignin at 1332, 1601

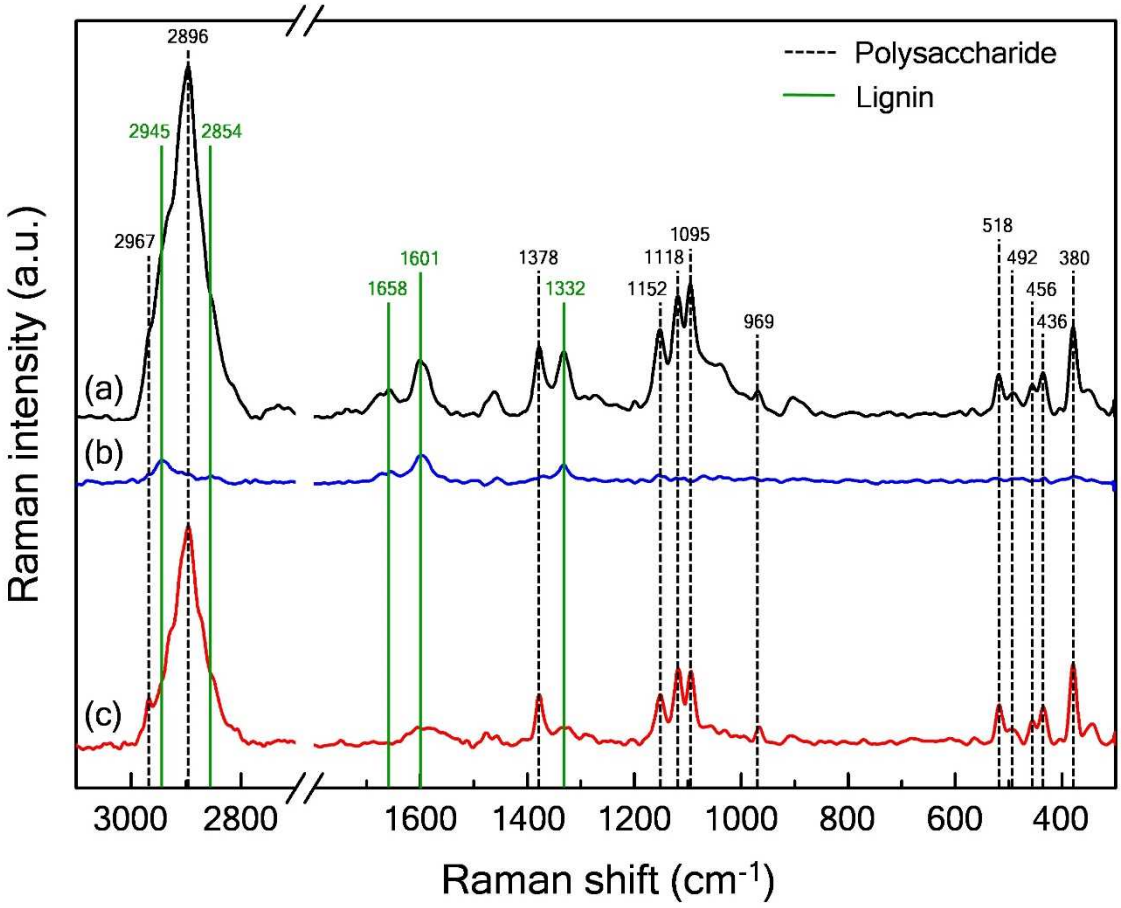

Fig. 4.11 Raman spectra for gelatinous layer (a) before and after treatment with (b) [C2mim][Cl] at 120°C for 24 h and (c) [EtPy][Br] at 120°C for 72 h. *solid lines*: lignin, *dashed lines*: polysaccharides.

and 1658 cm^{-1} decreased slightly. From these results, in gelatinous layers, polysaccharides are preferentially liquefied in [C2mim][Cl] whereas lignin can be also liquefied gradually.

On the other hand, after [EtPy][Br] treatment, most of the band intensities of polysaccharides have been still remained, and the band at 2967 cm^{-1} assigned to polysaccharides were appeared (Fig. 4.11c). With respect to the features of lignin, their band intensities were decreased significantly but were remained slightly even after 72 h of treatment. These results imply that [EtPy][Br] prefers to liquefy lignin rather than polysaccharides. However, in gelatinous layers, complete liquefaction of lignin is difficult by means of [EtPy][Br] treatment.

4.4 Conclusions

The interaction of reaction wood cell walls with ionic liquids was investigated from the morphological and topochemical point of view. Both [C2mim][Cl] and [EtPy][Br] treatments induced swelling of reaction wood cell walls. In general, during ionic liquid treatment, the swelling behaviors of compression wood, opposite wood and tension wood were gentler than that of normal wood. However, during [C2mim][Cl] treatment, the liquefaction of tension wood progressed with significant destruction of the cell walls. The crystalline structure of cellulose in both compression wood and tension wood was amorphized by [C2mim][Cl] treatment while it was slightly changed by [EtPy][Br] treatment. Raman microscopic study revealed that lignin in outer S_2 and CML of compression wood is less reactive to ionic liquid attack. In addition, [C2mim][Cl] liquefied gelatinous layers of tension wood rapidly, whereas [EtPy][Br] liquefied slowly but delignified selectively. [C2mim][Cl] has been shown to be a better solvent than [EtPy][Br] for liquefaction of tension wood, whereas [EtPy][Br] can be usable as a selective delignification solution. These novel findings will be contributed to the efficient chemical conversion of reaction wood and non-wasteful total wood utilization.

CHAPTER 5

General Conclusions

An efficient conversion technology of lignocelluloses to valuable chemicals and its energy efficient utilization may lead to some extent to a less consumption of fossil resources. Much research has been conducted on converting woody biomass into fossil resource alternatives, and ionic liquids have been vigorously studied as a novel class of solvent for the chemical conversion of woody biomass. However, fundamental study on the interaction of wood cell walls with ionic liquid have not yet been performed sufficiently. The purpose of this study is to make clear the cellular scale liquefaction mechanism of wood in ionic liquid for the development of a wood chemical processing using ionic liquid. For a better understanding of the effects of ionic liquid treatment on wood, various microscopy techniques were employed for investigating to the morphology and topochemistry of the cell walls during ionic liquid treatment.

From the results of morphology observation, it was revealed that the swelling behavior of wood cell walls varied among wood species and according to location such as earlywood and latewood. And also, the ultrastructural changes differed depending on the types of cells, pits, and ionic liquid used. The ionic liquid [C2mim][Cl] had a high capacity for cell wall swelling rather than [EtPy][Br]. In addition, the parenchyma cells showed no significant swelling and deformation during [C2mim][Cl] treatment compared with fibrous cells and vessels. The liquefaction of wood in [C2mim][Cl] predominantly proceeded in cellulose-rich tissues such as torus and pit membrane whereas that in [EtPy][Br] proceeded in lignin-rich regions such as CML and warty layer. The crystalline structure of cellulose in wood was amorphized during [C2mim][Cl] treatment while it was barely affected by [EtPy][Br].

Topochemical analyses revealed that the wood chemical components were liquefied and changed their nature with preserving tissue structures. In general, [C2mim][Cl]

prefers to react with polysaccharides in wood rather than with lignin, while [EtPy][Br] prefers to react with lignin. However, chemical changes in the cell walls differed for different layers, and lignin in CML resisted liquefaction and deterioration during ionic liquid treatment. The reactivity of polysaccharides and lignin with ionic liquid also differed depending on the types of cells, especially chemical components in parenchyma cells showed higher resistance to degradation upon [C2mim][Cl] treatment than other tissues.

The author clarified the interaction of wood with ionic liquid microscopically. Consequently, during the processing of wood liquefaction in ionic liquid, changes in the morphology and chemical compositions of wood were inhomogeneous at the cellular level. The interaction of ionic liquid with wood cell walls was quite different depending on the types of ionic liquids, wood species, tissues, and cell wall layers.

The multifaceted comprehension of the liquefaction mechanism of woody biomass in ionic liquid will be achieved by means of combining the cellular scale information obtained from this study with the knowledge of the molecular reactivity. This will assist in the utilization of ionic liquid treatment of wood to produce bio-fuels, bio-plastics, bio-based composites, and other valuable products. Furthermore, the present findings will be a sound basis for practical application of ionic liquid treatment for wood-based biorefinery.

References

Abe M, Yamada T, Ohno H (2014) Dissolution of wet wood biomass without heating. RSC Advances 4:17136-17140.

Agarwal UP (1998) Assignment of the photoyellowing-related 1675 cm^{-1} Raman/IR band to *p*-quinones and its implications to the mechanism of color reversion in mechanical pulps. Journal of Wood Chemistry and Technology 18:381-402.

Agarwal UP (1999) An overview of Raman spectroscopy as applied to lignocellulosic materials. In: Argyropoulos DS (ed) Advances in lignocellulosics characterization. TAPPI Press, Atlanta, GA, pp 201-225.

Agarwal UP (2006) Raman imaging to investigate ultrastructure and composition of plant cell walls: Distribution of lignin and cellulose in black spruce wood (*Picea mariana*). Planta 224:1141-1153.

Agarwal UP, Atalla RH (2000) Using Raman spectroscopy to identify chromophores in lignin-lignocellulosics. In: Glasser WG, Northey RA, Schultz TP (eds) Lignin: historical, biological, and materials perspectives. ACS symposium Series 742. American Chemical Society, Washington, D.C., pp 250-264.

Agarwal UP, Atalla RH (2010) Vibrational spectroscopy. In: Heitner C, Dimmel DR, Schmidt JA (eds) Lignin and lignans. Advances in Chemistry, CRC Press, Boca Raton, FL, pp 103-136.

Agarwal UP, McSweeny JD, Ralph SA (2011) FT-Raman investigation of milled wood lignins: Softwood, hardwood, and chemically modified black spruce lignins. Journal of Wood Chemistry and Technology 31:324-344.

Agarwal UP, Ralph SA (1997) FT-Raman spectroscopy of wood: Identifying contributions of lignin and carbohydrate polymers in the spectrum of black spruce (*Picea mariana*). Applied Spectroscopy 51:1648-1655.

Agarwal UP, Ralph SA (2008) Determination of ethylenic residues in wood and TMP of spruce by FT-Raman spectroscopy. Holzforschung 62:667-675.

Akim LG, Colodette JL, Argyropoulos DS (2001) Factors limiting oxygen delignification of kraft pulp. Canadian Journal of Chemistry 79:201-210.

Altaner C, Knox JP, Jarvis MC (2007) In situ detection of cell wall polysaccharides in Sitka spruce (*Picea sitchensis* (Bong.) Carrière) wood tissue. BioResources 2: 284-295.

Awano T, Takabe K, Fujita M (1998) Localization of glucuronoxylans in Japanese beech visualized by immunogold labelling. Protoplasma 202:213-222.

Baba K Sone Y, Kaku H, Misaki A, Shibuya N, Itoh T (1994) Localization of hemicelluloses in the cell walls of some woody plants using immuno-gold electron microscopy. Holzforschung 48:297-300.

Bailey AJ (1936) Lignin in Douglas fir: composition of the middle lamella. Industrial and Engineering Chemistry Analytical Edition 8:51-55.

Boutelje B (1972) Calculation of lignin concentration and porosity of cell wall regions by interference microscopy. Svensk Papperstidning 75:683-686.

Brandt A, Hallett JP, Leak DJ, Murphy RJ, Welton T (2010) The effect of the ionic liquid anion in the pretreatment of pine wood chips. Green Chemistry 4:672-679.

Bridgwater AV (2012) Review of fast pyrolysis of biomass and product upgrading. Biomass and Bioenergy 38:68-94.

Bridgwater AV, Meier D, Radlein (1999) An overview of fast pyrolysis of biomass. Organic Geochemistry 30:1479-1493.

Brownell HH, Saddler JN (1987) Steam pretreatment of lignocellulosic material for enhanced enzymatic hydrolysis. Biotechnology and Bioengineering 29:228-235.

Carlquist S (2001) Comparative wood anatomy – systematic, ecological, and evolutionary aspects of dicotyledon wood (second edition), Springer-Verlag, Berlin.

Çetinkol ÖP, Dibble DC, Cheng G, Kent MS, Knierim B, Auer M, Wemmer DE, Pelton JG, Melnichenko YB, Ralph J, Simmons BA, Holmes BM (2010) Understanding the impact of ionic liquid pretreatment on eucalyptus. Biofuels 1:33-46.

Chang VS, Holtzapple MT (2000) Fundamental factors affecting biomass enzymatic reactivity. Applied Biochemistry and Biotechnology 38:53-87.

Chang VS, Kaar WE, Burr B, Holtzapple MT (2001) Simultaneous saccharification and fermentation of lime-treated biomass. Biotechnology Letters 23:1327-1333.

Chundawat SPS, Donohoe BS, Sousa LC, Elder T, Agarwal UP, Lu F, Ralph J, Himmel

ME, Balan V, Dale BE (2011) Multi-scale visualization and characterization of lignocellulosic plant cell wall deconstruction during thermochemical pretreatment. Energy and Environmental Science 4:973-984.

Chunilall V, Bush T, Erasmus RM (2012) Investigating the lignocellulosic composition during delignification using confocal Raman spectroscopy, cross-polarization magic angle spinning carbon 13-nuclear magnetic resonance (CP/MAS ^{13}C-NMR) spectroscopy and atomic force microscopy. Cellulose Chemistry and Technology 46:269-267.

Corrales RCNR, Mendes FMT, Perrone CC, Anna C, Souza W, Abud Y, Bon EPS, Ferreira-Leitão V (2012) Structural evaluation of sugar cane bagasse steam pretreated in the presence of CO_2 and SO_2. Biotechnology for Biofuels 5:36.

Côté WAJr (1968) The structure of wood and the wood cell wall. In: Kollmann FFP, Côté WAJr (eds) Principles of Wood Science and Technology. Springer-Verlag, Berlin, pp 1-54.

Côté WAJr, Day AC, Timell TE (1969) A contribution of the ultrastructure of tension wood fibers. Wood Science and Technology 3:257-271.

Dadi AP, Schall CA, Varanasi S (2007) Mitigation of cellulose recalcitrance to enzymatic hydrolysis by ionic liquid pretreatment. Applied Biochemistry and Biotechnology 136-140:407-422.

Donaldson LA (2001) Lignification and lignin topochemistry – an ultrastructural view. Phytochemistry 57:859-873.

Donaldson LA (1985) Critial assessment of interference microscopy as a technique for measuring lignin distribution in cell walls. New Zealand Journal of Forestry Science 15:349-360.

Donaldson LA (1987) S3 lignin concentration in radiate pine tracheids. Wood Science and Technology 21:227-234.

Donohoe BS, Decker SR, Tucker MP, Himmel ME, Vinzant TB (2008) Visualization lignin coalescence and migration through maize cell walls following thermochemical pretreatment. Biotechnology and Bioengineering 101:913-925.

Earle MJ, Seddon KR (2000) Ionic liquids. Green solvents for the future. Pure and

Applied Chemistry 72:1391-1398.

Edwards HGM, Farwell DW, Webster D (1997) FT Raman microscopy of untreated natural plant fibres. Spectrochimica Acta Part A: Molecular and Biomolecular Spectroscopy 53:2383-2392.

Eriksson I, Lidbrandt O, Westermark U (1988) Lignin distribution in birch (Betula verrucosa) as determined by mercerization with SEM- and TEM-EDXA. Wood Science and Technology 22:251-257.

Fackler K, Thygesen LG (2013) Microspectroscopy as applied to the study of wood molecular structure. Wood Science and Technology 47:203-222.

Fergus BJ, Goring DAI (1970) The distribution of lignin in birch wood as determined by ultraviolet microscopy. Holzforschung 24:118-124.

Fergus BJ, Procter AR, Scott JAN, Goring DAI (1969) The distribution of lignin in spruce wood as determined by ultraviolet microscopy. Wood Science and Technology 3:117-138.

Fort DA, Remsing RC, Swatloski RP, Moyna P, Moyna G, Rogers RD (2007) Can ionic liquids dissolve wood? Processing and analysis of lignocellulosic materials with 1-*n*-butyl-3-methylimidazolium chloride. Green Chemistry 9:63-69.

Freemantle M (1998) Designer solvents – ionic liquids may boost clean technology development. Chemical & Engineering News 76 (30th March):32-37.

Fujii T, Shimizu K, Yamaguchi A (1987) Enzymatic saccharification on ultrathin sections and ultraviolet spectra of Japanese hardwoods and softwoods. Mokuzai gakkaishi 33:400-407.

Fukaya Y, Hayashi K, Wada M, Ohno H (2008) Cellulose dissolution with polar ionic liquids under mild conditions: required factors for anions. Green Chemistry 10:44-46.

Gierlinger N, Burgert I (2006) Secondary cell wall polymers studied by confocal Raman microscopy: Spatial distribution, orientation, and molecular deformation. New Zealand Journal of Forestry Science 36:60-71.

Gierlinger N, Keplinger T, Harrington M, Schwanninger M (2013) Raman imaging of lignocellulosic feedstock. In: van de Ven, T., Kadla, J. (eds) Cellulose – Biomass

conversion. InTech, Rijeka, pp 159-192.

Gierlinger N, Luss S, König C, Konnerth J, Eder M, Fratzl P (2010) Cellulose microfibril orientation of *Picea abies* and its variability at the micron-level determined by Raman imaging. Journal of Experimental Botany 61:587-595.

Gierlinger N, Schwanninger M (2006) Chemical imaging of poplar cell walls by confocal Raman microscopy. Plant Physiology 140:1246-1254.

Gierlinger N, Schwanninger M (2007) The potential of Raman microscopy and Raman imaging in plant research. Spectroscopy 21:69-89.

Goldstein IS (1980) The hydrolysis of wood. Tappi Journal 63:141-143.

Hänninen T, Kontturi E, Vuorinen T (2011) Distribution of lignin and its coniferyl alcohol and coniferyl aldehyde groups in *Picea abies* and *Pinus sylvestris* as observed by Raman imaging. Phytochemistry 72:1889-1895.

Harada H (1965) Ultrastructure of angiosperm vessels and ray parenchyma. In: Côté WA (ed) Cellular ultrastructure of woody plants. Syracuse University Press, Syracuse, pp 235-249.

Harada H, Côté WA (1985) Structure of wood. In: Higuchi T (ed) Biosynthesis and biodegradation of wood components. Academic Press, Orlando, FL, pp 1-42.

Harris JM (1977) Shrinkage and density of radiata pine compression wood in relation to its anatomy and mode of formation. New Zealand Journal of Forestry Science 7:91-106.

Hayashi N, Shimizu K, Hosoya S (1989) Pretreatment of ozone for increasing the enzymatic susceptibility of autohydrolyzed softwoods. Mokuzai Gakkaishi 35:521-529.

Henriksson G, Brännvall E, Lennholm H (2009) The trees. In: Ek M, Gellerstedt G, Henriksson G (eds) Wood chemistry and wood biotechnology. De Gruyter, Berlin, pp 13-44.

Hoffman GC, Timell TE (1972a) Polysaccharides in ray cells of normal wood of red pine (*Pinus resinosa*). Tappi 55:733-736.

Hoffman GC, Timell TE (1972b) Polysaccharides in ray cells of compression wood of red pine (*Pinus resinosa*). Tappi 55:871-873.

Honglu X, Tiejun S (2006) Wood liquefaction by ionic liquids. Holzforschung 60:509-512.

Howard RL, Abotsi E, Jansen van Rensburg EL, Howard S (2003) Lignocellulose biotechnology: Issues of bioconversion and enzyme production. African Journal of Biotechnology 2:602-619.

Jansen S, Smets E, Baas P (1998) Vestures in woody plants: A review. IAWA Journal 19:347-382.

Ji Z, Ma J, Zhang Z, Xu F, Sun R (2013) Distribution of lignin and cellulose in compression wood tracheids of *Pinus yunnanensis* determined by fluorescence microscopy and confocal Raman microscopy. Industrial Crops and Products 47:212-217.

Ji Z, Ling Z, Zhang X, Yang GH, Xu F (2014a) Impact of alkali pretreatment on the chemical component distribution and ultrastructure of poplar cell walls. BioResources 9:4159-4172.

Ji Z, Ma J, Xu F (2014b) Multi-scale visualization of dynamic changes in poplar cell walls during alkali pretreatment. Microscopy and Microanalysis 20:566-576.

Joseleau JP, Ruel K (2007) Condensed and non-condensed lignins are differentially and specifically distributed in the cell walls of softwoods, hardwoods and grasses. Cellulose Chemistry and Technology 41:487-494.

Jourez B, Riboux A, Leclercq A (2001) Anatomical characteristics of tension wood and opposite wood in young inclined stems of poplar (*Populus euramericana* cv 'Ghoy'). IAWA Journal 22:133-157.

Kanbayashi T, Miyafuji H (2013) Morphological changes of Japanese beech treated with the ionic liquid, 1-ethyl-3-methylimidazolium chloride. Journal of Wood Science 59:410-418.

Kanbayashi T, Miyafuji H (2014) Comparative study of morphological changes in hardwoods treated with the ionic liquid, 1-ethyl-3-methylimidazolium chloride. Journal of Wood Science 60:152-159.

Kanbayashi T, Miyafuji H (2015a) Raman microscopic analysis of wood after treatment with the ionic liquid, 1-ethyl-3-methylimidazolium chloride. Holzforschung 69:273-

279.

Kanbayashi T, Miyafuji H (2015b) Topochemical and morphological characterization of wood cell wall treated with the ionic liquid, 1-ethylpyridinium bromide. Planta 242:509-518.

Kanbayashi T, Miyafuji H (2016a) Raman microscopic study of Japanese beech (*Fagus crenata*) as treated with the ionic liquid, 1-ethyl-3-methylimidazolium chloride. Journal of Wood Chemistry and Technology 36:224-234.

Kanbayashi T, Miyafuji H (2016b) Microscopic investigations on woody biomass as treated with ionic liquids. In: Stanciu S (ed) Microscopy and analysis. InTech, Rijeka, In press.

Kihara M, Takayama M, Wariishi H, Tanaka H (2002) Determination of the carbonyl groups in native lignin utilizing Fourier transform Raman spectroscopy. Spectrochimica Acta Part A. Molecular and Biomolecular Spectroscopy 58:2213-2221.

Kilpeläinen I, Xie H, King A, Granstrom M, Heikkinen S, Argyropoulos DS (2007) Dissolution of wood in ionic liquids. Journal of Agricultural and Food Chemistry 55:9142-9148.

Kim JS, Awano T, Yoshinaga A, Takabe K (2010b) Immunolocalization and structural variations of xylan in differentiating earlywood tracheid cell walls of *Cryptomeria japonica*. Planta 232:817-824.

Kim JS, Awano T, Yoshinaga A, Takabe K (2010a) Immunolocalization of β-1-4-galactan and its relationship with lignin distribution in developing compression wood of *Cryptomeria japonica*. Planta 232:109-119.

Kosan B, Michels C, Meister F (2008) Dissolution and forming of cellulose with ionic liquids. Cellulose 15:59-66.

Lee SH, Doherty TV, Linhardt RJ, Dordick JS (2009) Ionic liquid-mediated selective extraction of lignin from wood leading to enhanced enzymatic cellulose hydrolysis. Biotechnology and Bioengineering 102:1368-1376.

Lehringer C, Gierlinger N, Koch G (2008) Topochemical investigation on tension wood fibres of *Acer* spp., *Fagus sylvatica* L. and *Quercus robur* L.. Holzforschung 62:255-

263.

Li B, Asikkala J, Filpponen I, Argyropoulos DS (2010) Factors affecting wood dissolution and regeneration of ionic liquids. Industrial and Engineering Chemistry Research 49:2477-2484.

Lucas M, Macdonald BA, Wagner GL, Joyce SA, Rector KD (2010) Ionic liquid pretreatment of poplar wood at room temperature: swelling and incorporation of nanoparticles. ACS Applied Materials & Interfaces 2:2198-2205.

Lucas M, Wagner GL, Nishiyama Y, Hanson L, Samayam IP, Schall CA, Langan P, Rector KD (2011) Reversible swelling of the cell wall of poplar biomass by ionic liquid at room temperature. Bioresource Technology 102:4518-4523.

Lupoi JS, Singh S, Simmons BA, Henry RJ (2014) Assessment of lignocellulosic biomass using analytical spectroscopy: an evolution to high-throughput techniques. BioEnergy Research 7:1-23.

Ma J, Zhang X, Zhou X, Xu F (2014) Revealing the changes in topochemical characteristics of poplar cell wall during hydrothermal pretreatment. BioEnergy Research 7:1358-1368.

Ma J, Zhang Z, Yang G, Mao J, Xu F (2011) Ultrastructural topochemistry of cell wall polymers in *Populus nigra* by transmission electron microscopy and Raman imaging. BioResources 6:3944-3959.

Ma J, Zhou X, Zhang X, Xu F (2013) Label-free *in situ* Raman analysis of opposite and tension wood in *Populus nigra*. BioResources 8:2222-2233.

Matsumura Y, Sudo K, Shimizu K (1977) Enzymatic hydrolysis of woods. II. Effect of grinding and alkali treatment on hydrolysis of woods by *Trichoderma viride* cellulose. Mokuzai gakkaishi 23:562-570.

Mes-Hartree M, Yu EKC, Reid ID, Saddler JN (1987) Suitability of aspenwood biologically delignified with *Pheblia tremellosus* for fermentation to ethanol or butanediol. Applied Microbiology and Biotechnology 26:120-125.

Miyafuji H (2015) Application of ionic liquids for effective use of woody biomass. Journal of Wood Science 61:343-350.

Miyafuji H, Miyata K, Saka S, Ueda F, Mori M (2009) Reaction behavior of wood in an

ionic liquid, 1-ethyl-3-methylimidazolium chloride. Journal of Wood Science 55:215-219.

Miyafuji H, Suzuki N (2011) Observation by light microscope of sugi (*Cryptomeria japonica*) treated with the ionic liquid 1-ethyl-3-methylimidazolium chloride. Journal of Wood Science 57:459-461.

Miyafuji H, Suzuki N (2012) Morphological changes in sugi (*Cryptomeria japonica*) wood after treatment with the ionic liquid, 1-ethyl-3-methylimidazolium chloride. Journal of Wood Science 58:222-230.

Miyata A, Miyafuji H (2014) Reaction behavior of cellulose in various pyridinium-based ionic liquids. Journal of Wood Science 60:438-445.

Muhammad N, Man Z, Khalil MAB (2012) Ionic liquid – a future solvent for the enhanced uses of wood biomass. European Journal of Wood and Wood Products 70:125-133.

Müller M, Burghammer M, Sugiyama J (2006) Direct investigation of the structural properties of tension wood cellulose microfibrils using microbeam X-ray fibre diffraction. Holzforchung 60:474-479.

Musha Y, Goring DAI (1975) Distribution of syringyl and guaiacyl moieties in hardwoods as indicated by ultraviolet microscopy. Wood Science and Technology 9:45-58.

Nanayakkara B, Manley-Harris M, Suckling ID, Donaldson LA (2009) Quantitative chemical indicators to assess the gradation of compression wood. Holzforschung 63:431-439.

Nakamura A, Miyafuji H, Saka S (2010a) Liquefaction behavior of Western red cedar and Japanese beech in the ionic liquid 1-ethyl-3-methylimidazolium chloride. Holzforschung 64:289-294.

Nakamura A, Miyafuji H, Saka S (2010b) Influence of reaction atmosphere on the liquefaction and depolymerization of wood in an ionic liquid, 1-ethyl-3-methylimidazolium chloride. Journal of Wood Science 56:256-261.

Norberg PH, Meier H (1966) Physical and chemical properties of the geratinous layer in wood fibres of aspen (*Populus tremula* L.). Holzforschung 20:174-178.

Oasmaa A, Solantausta Y, Arpiainen V, Kuoppala E, Sipilä K (2010) Fast pyrolysis bio-

oils from wood and agricultural residues. Energy & Fuels 24:1380-1388.

Ogawa S, Miyafuji H (2015) Reaction behavior of milled wood lignin in an ionic liquid, 1-ethyl-3-methylimidazolium chloride. Journal of Wood Science 61:285-291.

Ohno E, Miyafuji H (2013) Reaction behavior of cellulose in an ionic liquid, 1-ethyl-3-methylimidazolium chloride. Journal of Wood Science 59:221-228.

Ohno E, Miyafuji H (2014) Decomposition of cellulose in an ionic liquid, 1-ethyl-3-methylimidazolium chloride. Journal of Wood Science 60:428-437.

Panshin AJ, Zeeuw C (1970) Textbook of wood technology, vol. 1 (third edition), McGraw-Hill, New York.

Parisi F (1989) Advances in lignocellulosics hydrolysis and in the utilization of the hydrolyzates. In: Fiechter A (ed) Advances in biochemical engineering/biotechnology, Vol. 38. Springer-Verlag, Berlin, pp 53-87.

Parham RA, Gray RL (1984) Formation and structure of wood. In: Rowell RM (ed) The chemistry of solid wood, Advances in chemistry series, Vol. 207. American Chemical Society, Washington, D.C., pp 3-56.

Pettersen RC (1984) Chemical composition of wood. In: Rowell RM (ed) The chemistry of solid wood, Advances in chemistry series, Vol. 207. American Chemical Society, Washington, D.C., pp 57-126.

Pilate G, Chabbert B, Cathala B, Yoshinaga A, Leplé JC, Laurans F, Lapierre C, Ruel K (2004) Lignification and tension wood. Plant Biology and Pathology 327:889-901.

Piskorz J, Radlein D, Scott DS, Czernik S (1988) Liquid products from the fast pyrolysis of wood and cellulose. In: Bridgwater AV, Kuester JL (eds) Research in thermochemical biomass conversion. Elsevier Applied Science, London, pp 557-571.

Pohling C, Brackmann C, Duarte A, Buckup T, Enejder A, Motzkus M (2014) Chemical imaging of lignocellulosic biomass by CARS microscopy. Journal of Biophotonics 7:126-134.

Richter HG, Grosser D, Heinz I, Gasson PE (2004) IAWA list of microscopic features for softwood identification. IAWA Journal 25:1-70.

Ritter GJ (1925) Distribution of lignin in wood: microscopical study of changes in wood structure upon subjection to standard methods of isolating cellulose and lignin.

Industrial and engineering chemistry 17:1194-1197.

Röder T, Koch G, Sixta H (2004) Application of confocal Raman spectroscopy for the topochemical distribution of lignin and cellulose in plant cell walls of beech wood (*Fagus sylvatica* L.) compared to UV microspectrophotometry. Holzforschung 58:480-482.

Rogers RD, Seddon KR (2003) Ionic liquids – Solvents of the future? Science 302:792-793.

Ruelle J (2014) Morphology, anatomy and ultrastructure of reaction wood. In: Gardiner B, Barnett J, Saranpää P, Gril J (eds) The Biology of reaction wood. Springer-Verlag, Berlin, pp 13-35.

Saka S, Goring DAI (1988) The distribution of lignin in white birch wood as determined by bromination with TEM-EDXA. Holzforschung 42:149-153.

Saka S, Thomas RJ (1982a) Evaluation of the quantitative assay of lignin distribution by SEM-EDXA-technique. Wood Science and Technology 16:1-18.

Saka S, Thomas RJ (1982b) A study of lignification in loblolly pine tracheids by the SEM-EDXA technique. Wood Science and Technology 16:167-179.

Saka S, Whiting P, Fukazawa K, Goring DAI (1982) Comparative studies on lignin distribution by UV microscopy and bromination combined with EDXA. Wood Science and Technology 16:269-277.

Sannigrahi P, Ragauskas AJ, Tuskan GA (2010) Poplar as a feedstock for biofuels: A review of compositional characteristics. Biofuels Bioproducts Biorefining 4:209-226.

Schenzel K, Almlöf H, Germgård U (2009) Quantitative analysis of the transformation process of cellulose I → cellulose II using NIR FT Raman spectroscopy and chemometric methods. Cellulose 16:407-415.

Schenzel K, Fischer S (2001) NIR FT Raman spectroscopy – a rapid analytical tool for detecting the transformation of cellulose polymorphs. Cellulose 8:49-57.

Schmidt M, Schwartzberg AM, Perera PN, Weber-Bargioni A, Carroll A, Sarkar P, Bosneaga E, Urban JJ, Song J, Balakshin MY, Capanema EA, Auer M, Adams PD, Chiang VL, James Schuck P (2009) Label-free in situ imaging of lignification in the

cell wall of low lignin transgenic Populus trichocarpa. Planta 230:589-597.

Scott JAN, Goring DAI (1970) Lignin concentration in the S3 layer of softwoods. Cellulose Chemistry and Technology 4:83-93.

Scott JAN, Procter AR, Fergus BJ, Goring DAI (1969) The application of ultraviolet microscopy to the distribution of lignin in wood description and validity of the technique. Wood Science and Technology 3:73-92.

Seddon KR (1997) Ionic liquids for clean technology. Journal of Chemical Technology and Biotechnology 68: 351-356.

Selig MJ, Viamajala S, Decker SR, Tucker MP, Himmel ME, Vinzant TB (2007) Deposition of lignin droplets produced during dilute acid pretreatment of maize stems retards enzymatic hydrolysis of cellulose. Biotechnology Progress 23:1333-1339.

Séné CFB, McCann MC, Wilson RH, Grinter R (1994) Fourier-transform Raman and Fourier-transform infrared spectroscopy: an investigation of five higher plant cell walls and their components. Plant Physiology 106:1623-1631.

Sheldon R (2001) Catalytic reactions in ionic liquids. Chemical Communications 23:2399-2407.

Smith E, Dent G (2005) Introduction, basic theory and principles. In: Smith E, Dent G (eds) Modern Raman spectroscopy – a practical approach. John Wiley & Sons Ltd., Chichester, pp 1-21.

Sudo K, Matsumura Y, Shimizu K (1976) Enzymatic hydrolysis of woods. I. Effect of delignification on hydrolysis of woods by *Trichoderma viride* cellulose. Mokuzai Gakkaishi 22:670-676.

Sugimoto T, Magara K, Hosoya S, Oosawa S, Shimoda T, Nishibori K (2009) Ozone pretreatment of lignocellulosic materials for ethanol production: Improvement of enzymatic susceptibility of softwood. Holzforschung 63:537-543.

Sun L, Simmons BA, Singh S (2011) Understanding tissue specific compositions of bioenergy feedstocks through hyperspectral Raman imaging. Biotechnology and Bioengineering 108:286-295.

Sun N, Rahman M, Qin Y, Maxim ML, Rodriguez H, Rogers RD (2009) Complete

dissolution and partial delignification of wood in the ionic liquid 1-ethyl-3-methylimidazolium acetate. Green Chemistry 11:646-655.

Swatloski RP, Spear SK, Holbrey JD, Rogers RD (2002) Dissolution of cellulose with ionic liquids. Journal of the American Chemical Society 124:4974-4975.

Synytsya A, Čopíková J, Matějka P, Machovič V (2003) Fourier transform Raman and infrared spectroscopy of pectins. Carbohydrate Polymer 54:97-106.

Taherzadeh MJ, Eklund R, Gustafsson L, Niklasson C, Liden G (1997) Characterization and fermentation of dilute-acid hydrolyzates from wood. Industrial & Engineering Chemistry Research 36:4659-4665.

Takayama M, Johjima T, Yamanaka T, Wariishi H, Tanaka H (1997) Fourier transform Raman assignment of guaiacyl and syringyl marker bands for lignin determination. Spectrochimica Acta Part A: Molecular and Biomolecular Spectroscopy 53:1621-1628.

Terashima N, Fukushima K (1988) Heterogeneity in formation of lignin – XI: An autoradiographic study of the heterogeneous formation and structure of pine lignin. Wood Science and Technology 22:259-270.

Timell T E (1969) The chemical composition of tension wood. Svensk Papperstidning 72:173-181.

Timell TE (1982) Recent progress in the chemistry and topochemistry of compression wood. Wood Science and Technology 16:83-122.

Timell TE (1986a) Compression wood in gymnosperms, vol. 1, Springer-Verlag, Berlin.

Timell TE (1986b) Compression wood in gymnosperms, vol. 3, Springer-Verlag, Berlin.

Tirumalai VC, Agarwal UP, Obst JR (1996) Heterogeneity of lignin concentration in cell corner middle lamella of white birch and black spruce. Wood Science and Technology 30:99-104.

Torr KM, Love KT, Çetinkol ÖP, Donaldson LA, George A, Holmes BM, Simmons BA (2012) The impact of ionic liquid pretreatment on the chemistry and enzymatic digestibility of *Pinus radiata* compression wood. Green Chemistry 14:778-787.

Tsoumis G (1991) Science and technology of wood. Van Nostrand Reinhold, New York.

Tsubaki S, Azuma J (2011) Application of microwave technology for utilization of

recalcitrant biomass. In: Grundas S (ed) Advances in induction and microwave heating of mineral and organic materials, InTech, Rijeka, pp 697-722.

Viell J, Marquardt W (2011) Disintegration and dissolution kinetics of wood chips in ionic liquids. Holzforschung 65:519-525.

Walker JCF (1993) Basic wood chemistry and cell wall ultrastructure. In: Walker JCF (ed) Primary wood processing – principles and practice, Chapman & Hall, London, pp 23-67.

Wardrop AB, Dadswell HE (1950) The nature of reaction wood II. The cell wall organization of compression wood tracheids. Australian Journal of Biological Sciences 3:1-13.

Wardrop AB, Dadswell HE (1952) The cell wall structure of xylem parenchyma. Australian Journal of Scientific Research Series B 5:223-236.

Watanabe Y, Sano Y, Asada T, Funada R (2006) Histochemical study of the chemical composition of vestured pits in two species of Eucalyptus. IAWA Journal 27:33-43.

Westermark U, Lidbrandt O, Eriksson I (1988) Lignin distribution in spruce (*Picea abies*) determined by mercerization with SEM-EDXA technique. Wood Science and Technology 22:243-250.

Whiting P, Goring DAI (1982) Chemical characterization of tissue fractions from the middle lamella and secondary wall of black spruce tracheids. Wood Science and Technology 16:261-267.

Wiley JH, Atalla RH (1987) Band assignments in the Raman spectra of celluloses. Carbohydrate Research 160:113-129.

Wilkes JS, Zaworotko MJ (1992) Air and water stable 1-ethyl-3-methylimidazolium based ionic liquids. Journal of the Chemical Society, Chemical Communications 13:965-967.

Wimmer R, Johansson M (2014) Effects of reaction wood on the performance of wood and wood-based products. In: Gardiner B, Barnett J, Saranpää P, Gril J (eds) The Biology of reaction wood. Springer-Verlag, Berlin, pp 225-248.

Wood JR, Goring DAI (1971) The distribution of lignin in stem wood and branch wood of Douglas fir. Pulp and Paper Magazine of Canada 72:T95-T102.

Xu C, Etcheverry T (2008) Hydro-liquefaction of woody biomass in sub- and super-critical ethanol with iron-based catalysts. Fuel 87:335-345.

Xu F, Sun RC, Lu Q, Jones GL (2006) Comparative study of anatomy and lignin distribution in normal and tension wood of *Salix gordejecii*. Wood Science and Technology 40:358-370.

Yamazaki J, Minami E, Saka S (2006) Liquefaction of beech wood in various supercritical alcohols. Journal of Wood Science 52:527-532.

Yokoo T, Miyafuji H (2014) Reaction behavior of wood in an ionic liquid, 1-ethylpyridinium bromide. Journal of Wood Science 60:339-345.

Yoshida K, Kusaki J, Ehara K, Saka S (2005) Characterization of low molecular weight organic acids from beech wood treated in supercritical water. Applied Biochemistry and Biotechnology 121-124:795-806.

Zhang H, Wu J, Zhang J, He J (2005) 1-Allyl-3-methylimidazolium chloride room temperature ionic liquid: A new and powerful nonderivatizing solvent for cellulose. Macromolecules 38:8272-8277.

Zhang X, Ma J, Ji Z, Yang GH, Zhou X, Xu F (2014) Using confocal Raman microscopy to real-time monitor poplar cell wall swelling and dissolution during ionic liquid pretreatment. Microscopy Research and Technique 77:609-618.

Zhang Z, Ma J, Ji Z, Xu F (2012) Comparison of anatomy and composition distribution between normal and compression wood of *Pinus bungeana* Zucc. Revealed by microscopic imaging techniques. Microscopy and Microanalysis 18:1459-1466.

Zhao X, Cheng K, Liu D (2009) Organosolv pretreatment of lignocellulosic biomass for enzymatic hydrolysis. Applied Microbiology and Biotechnology 82:815-827.

Zhao Y, Wang Y, Zhu JY, Ragauskas A, Deng Y (2008) Enhanced enzymatic hydrolysis of spruce by alkaline pretreatment at low temperature. Biotechnology and Bioengineering 99:1320-1328.

Zhou X, Ma J, Ji Z, Zhang X, Ramaswamy S, Xu F, Sun R (2014) Dilute acid pretreatment differentially affects the compositional and architectural features of *Pinus bungeana* Zucc. Compression and opposite wood tracheid walls. Industrial Crops and Products 62:196-203.

Zhu JY, Pan XJ (2010) Woody biomass pretreatment for cellulosic ethanol production: Technology and energy consumption evaluation. Bioresource Technology 101:4992-5002.

Zhu S, Wu Y, Chen Q, Yu Z, Wang C, Jin S, Ding Y, Wu G (2006) Dissolution of cellulose with ionic liquids and its application: a mini-review. Green Chemistry 9:325-327.

Zobel B (1981) Wood quality from fast-grown plantations. Tappi 64:71-74.

Acknowledgements

First of all, I would like to express my heartfelt appreciation to my supervisor, Professor Hisashi Miyafuji, Graduate School of Life and Environmental Sciences, Kyoto Prefectural University, whose enormous supports and insightful comments were invaluable during the course of my Ph.D. work. His guidance help me in all the time of research and writing of this thesis.

My sincere thanks also go to Assistant Professor Nobuhiko Kasuya, Graduate School of Life and Environmental Sciences, Kyoto Prefectural University, for his valuable discussion and hard questions for this study. Thank you also for his assistance with collecting of wood samples.

I am also thankful to Professor Toshinari Kawada and Professor Yuzo Furuta, Graduate School of Life and Environmental Sciences, Kyoto Prefectural University, for their valuable suggestion for this thesis.

I wish to offer my special thanks to Special-appointment Associate Professor Takashi Hosoya and Special-appointment Assistant Professor Koichi Yoshioka, Graduate School of Life and Environmental Sciences, Kyoto Prefectural University, who gave me kind advice and warm encouragement.

I would like to show my deepest appreciation to the friendship of all the members in Laboratory of Forest Resource Circulatory System. And also, I express my gratitude towards Dr. Yuka Miyoshi, Forestry and Forest Products Research Institute, Ms. Yuki Tashiro, Mr. Tomoaki Kiryu, and other members in Laboratory of Biomaterials Science, for having meaningful time.

I am very grateful to Dr. Shiro Miyake, Advanced Science, Technology & Management Research Institute of KYOTO and Dr. Jun Wada and Dr. Naohiro Tomari, Kyoto Municipal Institute of Industrial Technology and Culture, for assistance with the confocal Raman microscopic analyses.

For financial support I thank the Kyoto Prefectural University (KPU) Academic Promotion Fund, Ayako Ueda Academic Promotion Fund, and a Grant-in-Aid for JSPS (the Japan Society for the Promotion of Science) Research Fellows (No. 15J05592).

Finally, I especially thank my wife for her support and encouragement during the entire period of this work. My deepest gratitude is also due to my parent, grandparent, and brother. I wish to dedicate this thesis to all of them.